Middle East Journal of Science

www.dergipark.org.tr/mejs

MEJS

VOLUME 7
ISSUE 2

DECEMBER
2021

E-ISSN
2618-6136

Email (for orders and customer services enquiries): bilgumus@gmail.com

Visit our home page on www.dergipark.org.tr/mejs

(Prof.Dr., İstanbul Medeniyet University, Faculty of Medicine, Dep. of Biophysics, Turkey)
sdasdag@gmail.com
Tamraz H. Tamrazov
Field: Biological Sciences
(Assoc.Prof.Dr., Department of Plant Physiology and Biotechnology, Research Institute of Crop Husbandry, Ministry of Agriculture of the Republic of Azerbaijan)
tamraz.tamrazov@mail.ru
Yusuf Zeren
Field: Mathematics, Topology
(Assoc.Prof.Dr., Yıldız Technical University, Faculty of Science and Letters, Dep. of Mathematics, TURKEY) yzeren@yildiz.edu.tr
Z. Gökay KAYNAK
Field: Nuclear Physics
(Retired Prof.Dr., Uludag University, Faculty of Science, Dep. of Physics, Turkey)
kaynak@uludag.edu.tr

CONTENTS

Research Articles

Middle East Journal of Science

https://dergipark.org.tr/mejs

MEJS

e-ISSN:2618-6136

Research Article

THREE MSA TOOLS ANALYSIS IN DNA AND PROTEIN DATASETS

***Fırat Aşır**[1] **Tuğcan Korak**[2] **Özgür Öztürk**[3]

[1]Department of Histology and Embryology, Medical School, Dicle University, Diyarbakır, Turkey
[2]Department of Medical Biology and Genetics, Medical School, Kocaeli University, Kocaeli, Turkey
[3]Pharmaceutical Biotechnology, Center for System-based Drug Research, Department of Pharmacy, Ludwig Maximilian University of Munich, Germany

* Corresponding author; firatasir@gmail.com

Abstract: *Multiple sequence alignment (MSA) is the alignment of three or more sequences of DNA, RNA, and protein. MSA is used to construct phylogenetic trees and to compare evolutionary relationships between sequences analyzing similarities and dissimilarities. A variety of multiple sequence alignment tools are available, each using different methods and parameters to align sequences. In this article three MSA tools; CLUSTALW, SAGA, and MAFFT* ***were*** *used to analyze five datasets BALiBASE_R9, DIRMBASE, SABmark, DNABali, and ProteinBali. The* ***results*** *showed that MAFFT may be more useful to align DNA and protein sequences than the other two tools.*

Keywords*: multiple sequence alignment, MAFFT, SAGA, CLUSTALW*

Received: August 17, 2021 Accepted: November 25, 2021

1. Introduction

Multiple sequence alignment (MSA) refers to the alignment of more than two DNA, RNA, or amino acid sequences to determine structural, functional, and evolutionary relationships among organisms and also to predict secondary and tertiary protein structure [1-5]. MSA may offer functional and conserved regions in a whole sequence family and illustrate evolutional history or comparison of the sequences by considering re-arrangements, insertions, deletions, or mutations [6, 7]. MSA is also adapted to next-generation sequencing methods for structural and functional comparisons [8].

Over the past decade, various MSA algorithms or strategies have been developed to perform convenient alignment of different datasets. One of them is CLUSTALW that uses progressive alignment. It starts to align the most similar sequences and then continues with less similar ones in order to obtain global alignment. It is the third generation of CLUSTAL software and has improvements on down or up weighting to similar and divergent sequences, respectively. In addition, amino acid substitution matrices are altered in accordance with the divergence of aligned sequences. Moreover, residue-specific and locally reduced gap penalties in hydrophilic sites promote new gaps in possible loop sites [9]. Sequence alignment by genetic algorithm (SAGA) is an MSA software that uses an automatic scheduling scheme to manage the usage of various operators in order to combine or mutate alignments among generations. It produces alignments in a similar manner to evolution and provides a gradual

development of fitness of the alignment populations through objective function which measures multiple alignment quality. Objective function score and comparison with reference alignments based on sequences of the known tertiary structure are the strengths of the SAGA [10]. Moreover, Multiple Alignment using Fast Fourier Transform (MAFFT) is another software that applies progressive and iterative approaches with several modifications. It provides fast recognition of homologous regions by the Fast Fourier transform algorithm and increases alignment accuracy of distantly related sequences or sequences that have large insertions, and decreases CPU time by the simplified scoring system. Although both use the progressive method MAFFT uses less CPU time than CLUSTALW with similar accuracy [11]. Besides these software, there are also various MSA approaches such as Clustal Omega [12], MUMMALS [13], ProbCons [14], T-Coffee [15], DIALIGN [16], MUSCLE [5], PROMALS3D [17], Kalign [18], M-Coffee [19], Align-M [20], PRANK [21, 22], 3DCoffee [23], Expresso [24] and HAlign [25] etc. Each of them has its own advantages and disadvantages to optimize sequence alignments, align distantly related sequences and minimize the computational time [11].

Choosing the best tool for MSA requires consideration of several aspects based on the study's scope [2]. Thus, analyzing the performance of the MSA tools with different datasets is essential to illustrate or facilitate software selection in further studies. In this study, CLUSTALW, SAGA, and MAFFT were compared by consistency, the column with gap and sum of pair scores with BAliBASE, SABmark, DIRMBASE, ProteinBali, and DNABali datasets.

2. Materials and Methods

Reference data (aligned data, data with dashes) were acquired from benchmarks BAliBASE (Version 3.0 R9), SABmark (Version 1.63), DIRMBASE (Version 1.0), and the manually constructed ProteinBali and DNABali datasets. All datasets are compatible with the following three MSA tools; CLUSTALW (Version 2.1), SAGA (Version 0.95), and MAFFT (Version 6). The reference data in this study were randomly picked up from datasets to evaluate the performance of MSA tools.

BAliBASE benchmark includes sequences that are specifically designed for MSA. It contains high-quality manually refined reference alignments by considering 3D superpositions and distinctive reference datasets with different properties. [26]. Box10, 22, 32 were acquired from BAliBASE benchmark. ProteinBali was randomly constructed from a different subset of BAliBASE benchmark and includes the following protein sequences: box46, box50, box56. DNABali (Reference Protein-Coding DNA Alignments Databases: http://dna.cs.byu.edu/mdsas/download.shtml) was randomly designed from BAliBASE benchmark and consists of the following DNA sequences: RV61_sushi_ref6, RV64_kringle_1_ref6, and RV70_photo_ref7. DIRMBASE offers locally related DNA sequences including highly conserved motifs generated by a random model of sequence evolution [27]. dna-400-30-4-0, r1-dna-400-30-4-1, r1-dna-400-30-4-2, r1-dna-400-30-4-3 and r1-dna-400-30-4-4 were selected from DIRMBASE. SABmark dataset offers MSA of protein sequences with low homology [28, 29,]. D1a6m__-d1ash, d1ash__-d1dlwa, d1dlwa_-d1ew6a, d1ew6a_-d1gtea1, d1gtea1-d1gvha1 were selected from SABmark.

In order to perform MSA tools, reference data were converted to FASTA format using Jalview software. Unaligned (undashed) data were converted from Multiple Sequence Format (MSF) to FASTA format by using Jalview (only those that were not FASTA format). Each data was individually uploaded to SAGA, CLUSTALW, and MAFFT. For SAGA and DNABali (DNA datasets), data were converted

into protein sequences, then uploaded to tools. In each software, some parameters were changed in order to obtain the highest scores. Input parameters were adjusted according to the dataset either DNA or protein. Results were recorded in FASTA format (if available), otherwise in clustal.aln format. Clustal.aln formats were converted to FASTA format by Jalview. Firstly, reference data, then FASTA formatted data was uploaded to SuiteMSA. For each individual data, consistency, the sum of pair scores, and column score with gaps were recorded. Scores attained from Suit MSA were arranged in a table according to datasets and tools (Figure 1). Regarding all scores, tables and graphs were constructed for each individual dataset by SAGA, CLUSTALW, and MAFFT. Mean values of data were considered in the comparison of tools.

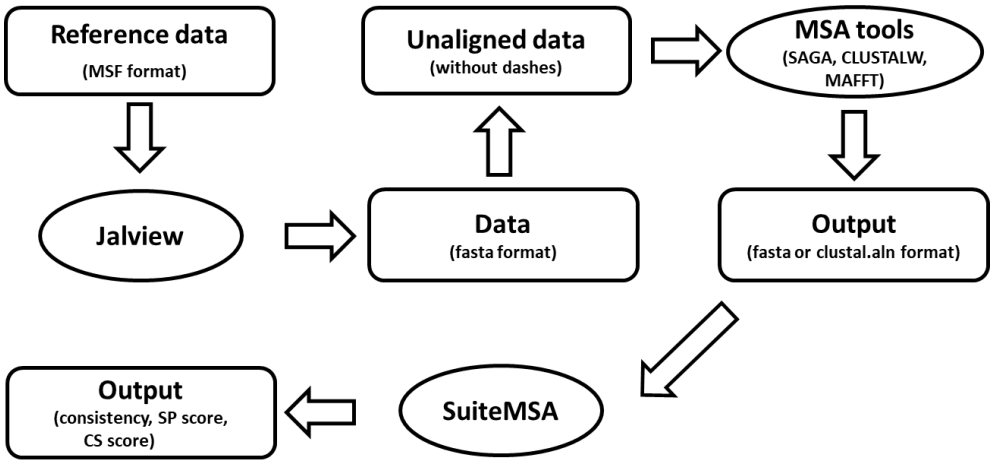

Figure 1: A roadmap of data conversion and processing for sequences to be aligned with MSA tools. Rectangles stand for data, the circle represents software.

3. Results

For each dataset, scores from SUITMSA were recorded and a graph corresponding to each data was constructed regarding CLSUTALW, MAFFT, and SAGA. Table 1 shows all data exploited in this study. From BALiBASE benchmark, box10, box22, and box32 protein data were used and their all scores from each MSA tools were recorded. From DIRMBASE benchmark, dna0, dna1, dna2, and dna3 nucleotide data were used and SuitMSA comparator results were shown. In SABmark, randomly five pairwise sequences (d1h97a_-d1irdb_, d1irdb_-d1itha_, d1itha_-d1jboa_, d1jboa_-d1ngka_, d1ngka_-d1qlab1_) were chosen and labeled as 7-8, 8-9, 9-10, 10-11 and 11-12. DNABali and ProteinBali datasets were chosen as same way in SABmark.

Table 1. Show all five datasets (BALiBASE, DIRMBASE, SABmark, DNABali, and ProteinBali) and three tools (CLUSTALW, MAFFT, and SAGA) and scores of tools according to each data set.

		CLUSTALW			MAFFT			SAGA		
Data set	**Individual data**	**Const (%)**	**SOP**	**CS w gap**	**Const (%)**	**SOP**	**CS w gap**	**Const (%)**	**SOP**	**CS w gap**
BAliBASE	Box10	15.416	0.411	0.044	6.282	0.538	0.064	9.081	0.515	0.071
	Box22	11.377	0.405	0.003	14.379	0.509	0.095	10.256	0.494	0.062
	Box32	19.981	0.392	0.187	21.978	0.462	0.213	17.325	0.433	0.184
	mean	**15.591**	**0.403**	**0.078**	**14.213**	**0.503**	**0.124**	**12.221**	**0.481**	**0.106**
DIRMBASE	Dna0	1.502	0.016	0.000	3.953	0.233	0.000	1.590	0.043	0.011
	Dna1	1.059	0.021	0.000	6.877	0.123	0.023	2.602	0.034	0.007
	Dna2	1.302	0.030	0.000	19.908	0.438	0.202	1.294	0.125	0.010
	Dna3	0.866	0.003	0.000	6.212	0.076	0.030	2.143	0.037	0.012
	mean	**1.182**	**0.018**	**0.000**	**9.238**	**0.218**	**0.064**	**1.907**	**0.060**	**0.010**
SABmark	7_8	38.667	0.419	0.378	52.469	0.581	0.573	63.432	0.681	0.676
	8_9	67.114	0.689	0.674	63.758	0.674	0.659	65.126	0.734	0.748
	9_10	13.58	0.206	0.149	44.809	0.451	0.383	46.123	0.487	0.409
	10_11	9.877	0.000	0.000	8.287	0.000	0.000	12.019	0.000	0.000
	11_12	10.145	0.000	0.000	18.71	0.000	0.000	16.540	0.000	0.000
	mean	**27.877**	**0.263**	**0.240**	**37.607**	**0.341**	**0.323**	**40.648**	**0.380**	**0.367**
DNABali	Kringle	2.864	0.247	0.000	4.057	0.233	0.000	2.150	0.205	0.000
	Photo	21.460	0.774	0.0172	27.556	0.832	0.254	5.551	0.583	0.059
	Sushi	38.669	0.093	0.000	38.834	0.097	0.000	30.942	0.037	0.000
	mean	**20.998**	**0.371**	**0.006**	**23.482**	**0.387**	**0.085**	**12.881**	**0.275**	**0.020**
ProteinBali	Box46	5.087	0.356	0.000	5.089	0.514	0.000	4.023	0.624	0.000
	Box50	20.186	0.678	0.193	54.381	0.828	0.503	35.984	0.184	0.346
	Box56	3.423	0.512	0.024	26.277	0.619	0.236	16.671	0.503	0.190
	mean	**9.565**	**0.515**	**0.072**	**28.582**	**0.654**	**0.246**	**18.893**	**0.437**	**0.179**

Const: Consistency; SOP: sum of pair scores. CS w gap stands for column score with gaps

3.1. BALIBASE Results

Mean consistency scores of CLUSTALW (15.591%) were better than MAFFT's (14.213%) and SAGA's scores (12.221**%**) (Figure 2a). For any tool, the sum of pair cores was close to each other, meaning that individual data differences were not reflected in the sum of pair scores thus putting tools at the forefront rather than data in scoring (Figure 2b). MAFFT performed the best column scores (Figure 2c).

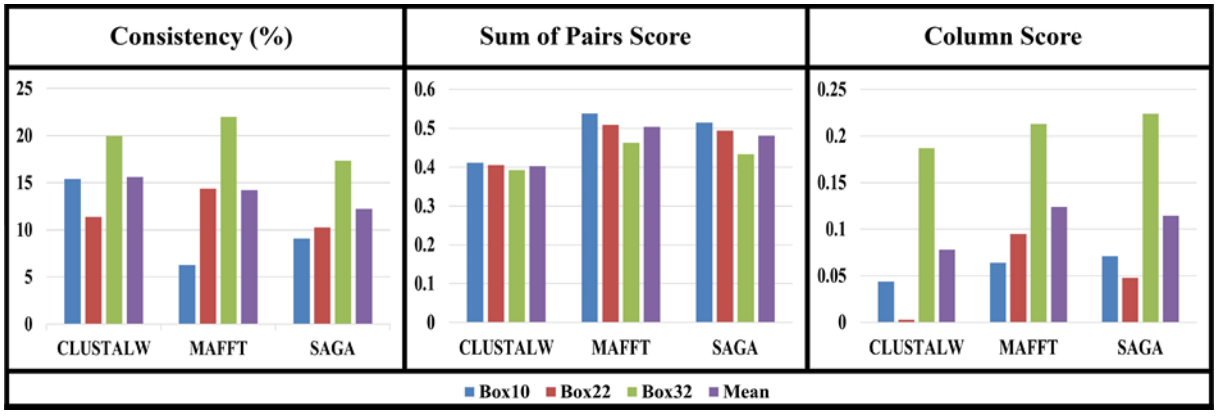

Figure 2. Graphical representation of a) consistency, b) sum of pairs score, c) column score with gaps of BALIBASE data with CLUSTALW, MAFFT, and SAGA.

3.2. DIRMBASE Results

Figure 3a shows the consistency (%) of individual DIRMBASE datasets and means by CLUSTALW, MAFFT, and SAGA. MAFFT resulted in the highest consistency score (7.238%). Figure 3b shows the sum of pair scores of three MSA tools. CLUSTALW rendered the lowest score, while MAFFT performed the highest score as in consistency. Column scores with all tools were very close to zero but MAFFT got a relatively better score than the other two tools (Figure 3c).

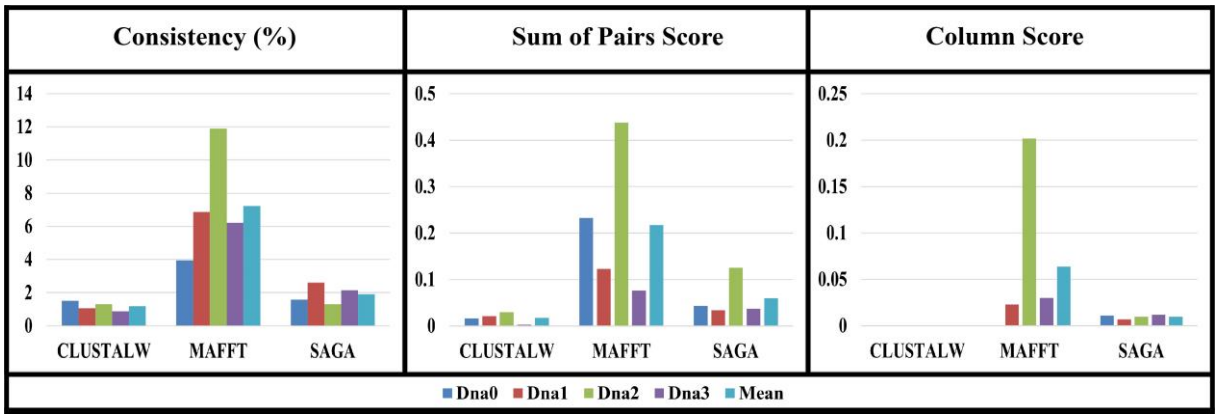

Figure 3. Graphical representation of a) consistency, b) sum of pairs score, c) column score with gaps results of DIRMBASE data with CLUSTALW, MAFFT and SAGA.

3.3. SABmark Results

Higher scores were recorded in SABmark dataset than scores in BALiBASE and DIRMBASE. Although higher than scores of CLUSTALW, consistency scores of SAGA and MAFFT were close to each other (Figure 4a). Figure 4b shows the sum of pair scores with three MSA tools. SAGA and MAFFT resulted in higher scores than CLUSTALW. SAGA's score was slightly higher than MAFFT's score, making SAGA the best tool according to the sum of pair scores. Among tools, SAGA and MAFFT recorded similar results which were higher than that of CLUSTALW (Figure 4c).

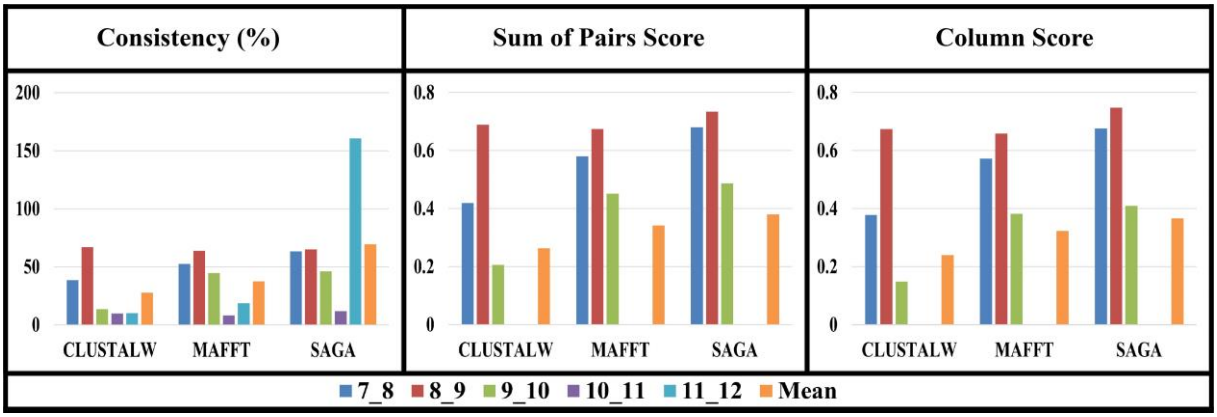

Figure 4. Graphical representation of a) consistency, b) sum of pairs score, c) column score with gaps results of SABmark data with CLUSTALW, MAFFT and SAGA.

3.4. DNABali Results

Figure 5a shows consistent results for three MSA tools based on DNABali dataset. The highest mean consistency score was recorded by MAFFT while SAGA performed the lowest score. Figure 5b shows the sum of the pair score of individual data by tools. SAGA got the lowest sum of pair scores while MAFFT rendered the highest score. MAFFT generated the highest column sores with a gap, which was not statistically significant (Figure 5c).

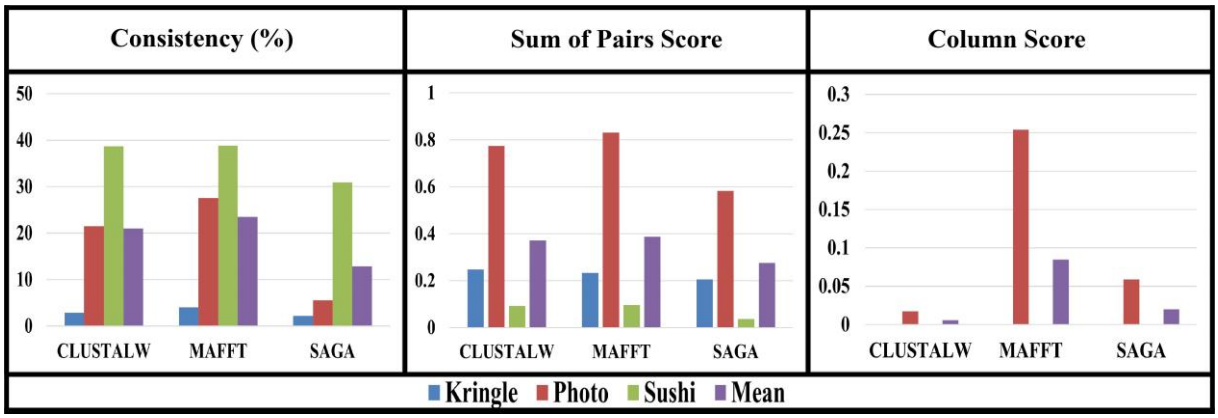

Figure 5. Graphical representation of a) consistency, b) sum of pairs score, c) column score with gaps results of DNABali data with CLUSTALW, MAFFT and SAGA.

3.5. PROTEINBali Results

Figure 6a shows consistent results for three MSA tools based on PROTEINBali dataset. The highest mean consistency score was recorded with MAFFT while the score of ClustalW was the lowest value. Regarding the sum of pair scores, MAFFT generated the highest mean value among others while SAGA resulted in the lowest value (Figure 6b). The highest score was recorded with MAFFT while the lowest score was recorded with ClustalW (Figure 6c).

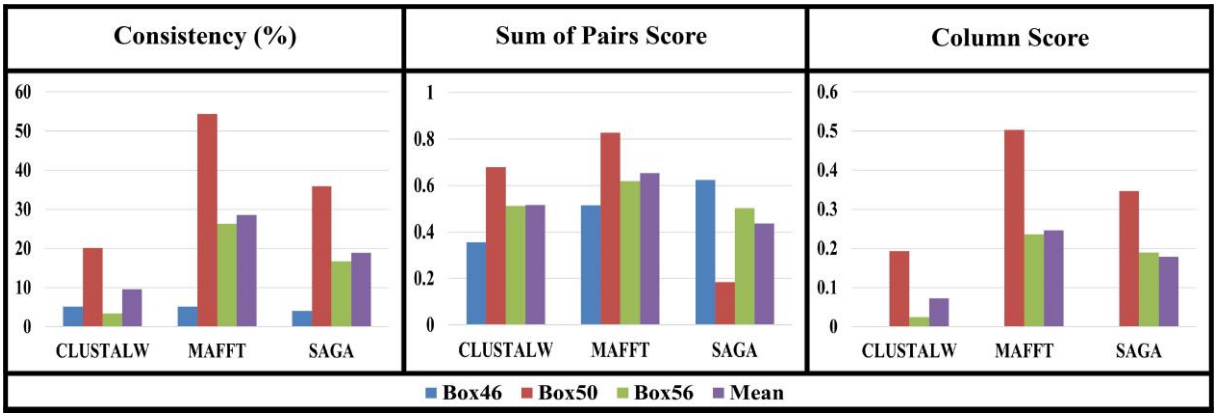

Figure 6. Graphical representation of a) consistency, b) sum of pairs score, c) column score with gaps results of PROTEINBali data with CLUSTALW, MAFFT and SAGA.

We constructed Table 2 to show each tool's performance by consistency (%), SP score, and CS score with each dataset. MAFFT performed best scores in most cases.

Table 2. Arrangement of MSA tools by consistency, SP and CS scores from best to worst performance.

	Consistency (%)			SP score			CS score		
BALIBASE	CLUSTALW (15.591)	MAFFT (14.213)	SAGA (12.221)	MAFFT (0.503)	SAGA (0.481)	CLUSTALW (0.403)	MAFFT (0.124)	SAGA (0.106)	CLUSTALW (0.078)
DIRMBASE	MAFFT (9.238)	SAGA (1.907)	CLUSTALW (1.182)	MAFFT (0.218)	SAGA (0.060)	CLUSTALW (0.018)	MAFFT (0.064)	SAGA (0.010)	CLUSTALW (0.000)
SABmark	SAGA (40.648)	MAFFT (37.607)	CLUSTALW (27.877)	SAGA (0.380)	MAFFT (0.341)	CLUSTALW (0.263)	SAGA (0.367)	MAFFT (0.323)	CLUSTALW (0.240)
DNABali	MAFFT (23.482)	CLUSTALW (20.998)	SAGA (12.881)	MAFFT (0.387)	CLUSTALW (0.371)	SAGA (0.275)	MAFFT (0.085)	SAGA (0.020)	CLUSTALW (0.006)
ProteinBali	MAFFT (28.582)	SAGA (18.893)	CLUSTALW (9.565)	MAFFT (0.654)	CLUSTALW (0.515)	SAGA (0.437)	MAFFT (0.246)	SAGA (0.179)	CLUSTALW (0.072)

4. Discussion

Multiple sequence alignment (MSA) is an algorithm used for identifying shared regions of homology, determination of the consensus sequence, predicting the secondary and tertiary structures, and constructing a phylogenetic tree in mathematics and bioinformatics [28]. MSA algorithms align three or more sequences of DNA, RNA, or protein with different ways such as dynamic programming, progressive alignment construction, iterative methods, hidden Markov models, and genetic algorithms and simulated annealing techniques [29]. MSA tools consume a lot of CPU time to give the best results, and the processing time can increase quadratically depending on the length and number of sequences. Due to increasing biological data, the performance of MSA algorithms is gaining importance. In multiple alignments, consistency, the sum of pair score (PS), and column score (CS) are popular parameters used to analyze the performance of MSA tools [30, 31]. These scores are useful when reference alignment of the same sequences is available. Consistency shows the percentage of identical columns in the test alignments and the columns of reference alignments [32]. The SP score is generated by comparing identically aligned residue pairs in the test and the reference alignments. SP score is calculated based on the test alignments and a determinant parameter to analyze the performance of the tool in the sequence alignment. The SP score equals score 1 when test alignment is identical to reference alignment while zero score means no identity between alignments. CS calculates scores the fraction of identically aligned positions. 2.3 CS score is calculated according to the individual comparison of columns and the calculated score then is divided into the number of columns analyzed. Of these, SP scores is a determinant of tool quality, while other scores are supporting SP score [33, 34].

In our study, consistency, SP score, and CS score were recorded to evaluate the quality and reliability of three MSA tools. We analyzed CLUSTALW, MAFFT and SAGA performance on five datasets from benchmarks BALiBASE (protein-based), DIRMBASE (nucleotide-based), SABmark (protein-based) and manually constructed DNABali (nucleotide-based) and ProteinBali (protein-based) (Table 1). BALIBASE is manually constructed and known to include a high-quality sequence of proteins with linear motifs (protein interaction sites, cell compartment targeting signals, post-translational modification sites, or cleavage sites). BALIBASE includes protein families sequences that are disordered and hard to align by conventional multiple sequence alignment algorithms [35]. MAFFT resulted in higher performance in SP and CS scores than CLUSTALW and SAGA, while CLUSTALW was best in consistency for BALIBASE dataset, however, consistency of MAFFT was close to CLUSTALW's consistency (Table 1 and 2, Figure 2). DIRMBASE is a database that contains highly

conserved motives and locally related sequences and is used for local alignments [36]. In DRIMBASE dataset, MAFFT outperformed the other tools by far for each parameter (Table 1 and 2, Figure 3). All tools got their highest score in consistency, SP score, and CS scores in SABmark dataset (Table 1 and 2, Figure 4). The reason for that is SABmark includes sequences with up to 50% similarity because over this region makes programs perform better since it is easy to align [37]. Also, pairwise alignment was opted for SABmark dataset, this improved scores for all tools. SAGA got higher performance than CLUSTALW and MAFFT in consistency, SP and CS scores in SABmark dataset, but there was no big gap between SAGA's and MAFFT's performances. For DNABali and ProteinBali dataset, MAFFT was far better than other tools for each parameter (Table 1 and 2, Figure 5 and 6, respectively).

By analyzing the performance of tools with consistency, we observed that MAFFT got the highest performance in 3 out of 5 datasets, while SAGA and CLUSTALW resulted in once. For the SP scores, which is a very important indicator for the effectiveness of an MSA **tool**, MAFFT performed the higher score than CLUSTALW and SAGA 4 out of 5 datasets. Likewise, CS score also revealed that MAFFT's performance was better than other tools in the 4 datasets. We have analyzed three popular MSA tools in five different datasets ~~with different~~. We conclude that MAFFT was better than CLUSTALW and SAGA to align multiple sequences of DNA and protein families.

5. Conclusion

Our results showed that MAFFT seems to be a better tool for both DNA and protein sequence**s** alignment than CLUSTALW and SAGA. To get the best alignment, the type of sequence and the tool specific to data should be picked up, otherwise, it may give false or non-optimal results. Tool requirements and parameters should not be ignored during multiple alignments.

5.1. Supplementary information about tools

CLUSTALW and its parameters:

Online webserver: http://www.genome.jp/tools/clustalw/

For protein data, protein parameter with BLOSUM matrix, for nucleotide data DNA parameter with IUB matrix was selected. The slow/accurate option was used to get more accurate results. Gap open penalty and gap extension value were adjusted to 30.00 and 6.00, relatively. For additional options, -OUTORDER=INPUT was used. Output format was selected as FASTA. The remaining setting was set to default.

MAFFT and its parameters:

Online webserver: https://www.ebi.ac.uk/Tools/msa/mafft/

For protein data, protein parameter with BLOSUM62 matrix, for nucleotide data nucleic acid parameter with none matrix was selected. Gap open penalty and gap extension values were adjusted to 3.00 and 0.5, respectively. Maximum iteration number was set to 100, FFT was local pair, ORDER was input, output was FASTA format. Rest was adjusted as default.

SAGA and its parameters:

Online webserver: http://rsdb.csie.ncu.edu.tw/tools/msa.htm

For protein data, protein and nucleic acid (as converted to protein sequence) parameter with PAM250 matrix (SAGA runs only for protein) has opted. Gap open penalty and gap extension value was adjusted to 8.00 and 12, relatively. Output was saga_aln. Settings remaining are left to default.

In order to convert DNA sequences to protein sequences at default settings. We use http://web.expasy.org/translate/

For SuiteMSA, we download SuiteMSA package (v1.3.22B) [zip file]
http://bioinfolab.unl.edu/~canderson/SuiteMSA/

Acknowledgment

We would like to thank Jens ALLMER for the conceptualization and permission for this study to be published. This study has not received any funding.

Conflict of interest:

The authors declare no conflict of interest.

The Declaration of Ethics Committee Approval

The author declares that this document does not require an ethics committee approval or any special permission. Our study does not cause any harm to the environment.

Authors' Contributions:

All authors read and approved the final manuscript. All authors mentioned in the paper have significantly contributed to the research:

F.A.: Conceptualization, Investigation, Software, Validation, Visualization, Project administration, Supervision, Writing – review and editing (%35)

T.K.: Conceptualization, Investigation, Methodology, Visualization, Writing – original draft, Writing – review, and editing (%35)

Ö.Ö.: Investigation, Methodology, Validation, Visualization, Data curation Visualization, Writing – original draft, Writing – review and editing (%30)

References

[1] Notredame, C. "Recent Evolutions of Multiple Sequence Alignment Algorithms", *PLOS Computational Biology*, 3(8), e123, 2007.

[2] Edgar, R.C., Batzoglou, S. "Multiple sequence alignment", *Current opinion in structural biology*, 16(3), 368-373, 2006.

[3] Moretti, S., et al. "The M-Coffee web server: a meta-method for computing multiple sequence alignments by combining alternative alignment methods", *Nucleic Acids Research*, 35(Web Server issue), W645-8, 2007.

[4] Chowdhury, B., Garai, G. "A review on multiple sequence alignment from the perspective of genetic algorithm", *Genomics*, 109(5), 419-431, 2017.

[5] Edgar, R.C. "MUSCLE: a multiple sequence alignment method with reduced time and space complexity", *BMC Bioinformatics*, 5, 113-31, 2004.

[6] Kumar, S., Filipski, A. "Multiple sequence alignment: in pursuit of homologous DNA positions", *Genome Research*, 17(2), 127-35, 2007.

[7] Chatzou, M., et al. "Multiple sequence alignment modeling: methods and applications", *Briefings in Bioinformatics,* 17(6), 1009-1023, 2016.

[8] Bawono, P., et al. "Multiple Sequence Alignment", *Methods Mol Biol*, 1525, 167-189, 2017.

[9] Thompson, J.D. et al. "CLUSTAL W: improving the sensitivity of progressive multiple sequence alignment through sequence weighting, position-specific gap penalties and weight matrix choice", *Nucleic Acids Research*, 22(22), 4673-80, 1994.

[10] Notredame, C, Higgins, D.G. "SAGA: Sequence Alignment by Genetic Algorithm", *Nucleic Acids Research*, 24(8), 1515-1524, 1996.

[11] Katoh, K., et al. "MAFFT: a novel method for rapid multiple sequence alignment based on fast Fourier transform", *Nucleic Acids Research*, 30(14), 3059-66, 2002.

[12] Sievers, F., et al. "Fast, scalable generation of high-quality protein multiple sequence alignments using Clustal Omega", *Molecular Systems Biology*, 7, 539-44, 2011.

[13] Pei, J., Grishin, N.V. "MUMMALS: multiple sequence alignment improved by using hidden Markov models with local structural information", *Nucleic Acids Research*, 34(16), 4364-4374, 2006.

[14] Do, C.B., et al. "ProbCons: Probabilistic consistency-based multiple sequence alignment", *Genome Research*, 15(2), 330-40, 2005.

[15] Notredame, C., et al. "T-Coffee: A novel method for fast and accurate multiple sequence alignment", *Journal of Molecular Biology*, 302(1), 205-17, 2000.

[16] Morgenstern, B., et al. "DIALIGN: finding local similarities by multiple sequence alignment", *Bioinformatics*, 14(3), 290-4, 1998.

[17] Pei, J., et al. "PROMALS3D: a tool for multiple protein sequence and structure alignments", *Nucleic Acids Research*, 36(7), 2295-300, 2008.

[18] Lassmann, T., Sonnhammer, E.L.L. "Kalign – an accurate and fast multiple sequence alignment algorithm", *BMC Bioinformatics*, 6(1), 298-306, 2005.

[19] Wallace, I.M., et al. "M-Coffee: combining multiple sequence alignment methods with T-Coffee", *Nucleic acids research*, 34(6), 1692-1699, 2006.

[20] Van Walle, I., et al. "Align-m--a new algorithm for multiple alignment of highly divergent sequences", *Bioinformatics*, 20(9), 1428-35, 2004.

[21] Löytynoja, A., Goldman, N. "Phylogeny-aware gap placement prevents errors in sequence alignment and evolutionary analysis", *Science*, 320(5883), 1632-5, 2008.

[22] Löytynoja, A., Goldman, N. "An algorithm for progressive multiple alignment of sequences with insertions", *Proceedings of the National Academy of Sciences of the United States of America*, 102(30), 10557-62, 2005.

[23] O'Sullivan, O., et al. "3DCoffee: Combining Protein Sequences and Structures within Multiple Sequence Alignments", *Journal of Molecular Biology*, 340(2), 385-395, 2004.

[24] Armougom, F., et al. "Expresso: automatic incorporation of structural information in multiple sequence alignments using 3D-Coffee", *Nucleic acids research*, 34(Web Server issue), W604-W608, 2006.

[25] Zou, Q., et al. "HAlign: Fast multiple similar DNA/RNA sequence alignment based on the centre star strategy", *Bioinformatics*, 31(15), 2475-81, 2015

[26] Pais, F.S., Ruy, P.C., Oliveira, G. and Coimbra, R.S. "Assessing the efficiency of multiple sequence alignment programs", *Algorithms for Molecular Biology*, 9(1), 4-11, 2014.

[27] Subramanian, A.R., et al. "DIALIGN-TX: greedy and progressive approaches for segment-based multiple sequence alignment", *Algorithms for Molecular Biology*, 3, 6-16, 2008.

[28] Carillo, H., Lipman, D.J. "The multiple sequence alignment problem in biology", *SIAM Journal on Applied Mathematics*, 48, 1073–1082, 1988.

[29] Daugelaite, J., et al. "An Overview of Multiple Sequence Alignments and Cloud Computing in Bioinformatics", *ISRN Biomathematics*, 2013, 615-630, 2013.

[30] Hogeweg, P., Hesper, B. "The alignment of sets of sequences and the construction of phyletic trees: an integrated method", *Journal of Molecular Evolution*, 20, 175–18, 1984.

[31] Karplus, K., Hu, B.R. "Evaluation of protein multiple alignments by SAM-T99 using the BAliBASE multiple alignment test set", *Bioinformatics*, 17, 713–720, 2001.

[32] Lassmann, T., Sonnhammer, E.L.L. "Quality assessment of multiple alignment programs". *FEBS Letters*, 529, 126–130, 2002.

[33] Pais, F.S., et al. "Assessing the efficiency of multiple sequence alignment programs", *Algorithms for Molecular Biology*, 9(1), 4, 2014.

[34] Anderson, C.L., et al. "SuiteMSA: visual tools for multiple sequence alignment comparison and molecular sequence simulation", *BMC Bioinformatics*, 12(1), 184, 2011.

[35] Bahr, A., et al. "BAliBASE (Benchmark Alignment dataBASE): enhancements for repeats, transmembrane sequences and circular permutations", *Nucleic Acids Research*, 29 (1), 323-6, 2001.

[36] Menke, M., et al. "Matt: local flexibility aids protein multiple structure alignment", *PLOS Computational Biology*, 4(1), e10, 2008.

[37] Van Walle, I., et al. "SABmark--a benchmark for sequence alignment that covers the entire known fold space", *Bioinformatics*, 21(7), 1267-1268, 2005.

Middle East Journal of Science

https://dergipark.org.tr/mejs
e-ISSN:2618-6136

MEJS

Research Article

INVESTIGATION OF Pd@*g*-C_3N_4/TiO_2 NANOPARTICLES AS PHOTOCATALYST IN THE DEGRADATION OF METHYLENE BLUE UNDER VISIBLE LIGHT IRRADIATION

***Halil İbrahim ÖNAL*[1]** ***[*]Feyyaz DURAP*[2]**

[1]Dicle University, Science Faculty, Department of Chemistry, 21280-Diyarbakır, Turkey
[2]Dicle University, Science Faculty, Department of Chemistry, 21280-Diyarbakır, Turkey
[*]Corresponding author: fdurap@dicle.edu.tr

Abstract: *In the present study, the efficiency of Pd@g-C_3N_4/TiO_2 NPs as photocatalysts on the degradation of organic pollutant methylene blue (MB) dye under visible light has been investigated. A traditional one-step impregnation-reduction method was used for the preparation of photocatalysts. Pd@g-C_3N_4/TiO_2 NPs were characterized by several techniques such as FT-IR, DR/UV-Vis, SEM-EDX, TEM, P-XRD, and XPS analyses. The photocatalytic performance of Pd@g-C_3N_4/TiO_2 NPs was evaluated for the degradation of MB dye under visible light irradiation. Among different loadings of Pd (0.3, 0.5, and 0.7 %), the 0.5% loading Pd@g-C_3N_4/TiO_2 NPs showed the highest catalytic activity. The results revealed an enhancement in the visible light photocatalytic activity of g-C_3N_4/TiO_2 when it was coupled with Pd in the composite. Compared with pure g-C_3N_4/TiO_2, the Pd@ g-C_3N_4/TiO_2 hybrid photocatalyst exhibited enhanced visible-light photoactivity, which was approximately three times higher than that of pure g-C_3N_4/TiO_2.*

Keywords: *Pd, g-C_3N_4/TiO_2, Methylene Blue, Photocatalyst, Nanoparticle.*

Received: October 1, 2021 Accepted: December 20,2021

1. Introduction

One of the main factors for serious environmental problems is the release of several hazardous organic dyes from textile industries in wastewater, which is concerned with human health and the environment due to the toxicity and the carcinogenic effect of these dyes [1]. In this context, we can list the process generally used to remove these toxic dyes from water as adsorption [2], chemical precipitation [3], sedimentation [4], biological membranes [5], ion exchange [6], and electrochemical [7]. However, these methods have several disadvantages such as they usually proceed slowly, require expensive equipment and require further elimination [8]. Photocatalytic methods can increase the use of solar energy and reduce pollutants in wastewater [9]. This issue is important both in terms of environmental protection and shows the importance of using a photocatalyst in terms of economy and time. In recent years, nano-sized semiconductors such as TiO_2 [10, 11, 12], ZnO [13], Fe_2O_3 [14] and CdS [15] have yielded successful results in dye removal, which shows that they exhibit high photocatalytic reactivity.

Graphitic carbon nitride (*g*-C_3N_4) is a photocatalytic support material that has recently attracted attention with its advantageous stable physicochemical properties (absorption at 400-450 nm and narrow energy band gap) but it has disadvantages such as high recombination rate, which reduces its catalytic activity. [16,17,18,19]. Furthermore, number of reports have shown that TiO_2 exhibits robust photocatalytic activity, although its absorption efficiency for visible light is greatly limited due to its

wide band gap (3.2 eV) [20, 21, 22, 23]. Among the developed photocatalytic systems, *g*-C_3N_4/TiO_2 composites with a high specific surface area and special heterostructure were prominent in this pursuit due to their easy synthesis, stronger visible light activity and higher electron transfer rate [24, 25, 26, 27]. Moreover, it has been proven that the noble metal palladium (Pd) can effectively improve the visible light absorption rate of composite materials, as it has abundant vacant orbitals that effectively promote electron transfer in composite materials. [28, 29, 30, 31].

In this respect, we prepared Pd@*g*-C_3N_4-TiO_2 nano heterostructured catalysts using a conventional one-step impregnation-reduction method. The results showed that these catalyst systems present excellent photocatalytic performance for methylene blue (MB) degradation under visible light, which demonstrates a promising strategic approach in the field of photocatalysis. The newly prepared Pd@*g*-C_3N_4/TiO_2 NPs were characterized by FT-IR, DR/UV-Vis, SEM-EDX, TEM, P-XRD, and XPS analyses.

2. Materials and Methods

2.1. Materials

Palladium Nitrate ($Pd(NO_3)_2$).$2H_2O$ (99%), Titanium (IV) oxide (anatase, nanopowder <25 nm particle size (99,7%), tetramethylthionine chloride (Methylene Blue; MB; $C_{16}H_{18}ClN_3SH_2O$), sodium borohydrate ($NaBH_4$), Ethanol (C_2H_5OH), Methanol (CH_3OH) were purchased from Sigma Aldrich® and Urea (CH_4N_2O) were purchased from Merck. All glassware and magnetic stir sticks were washed with acetone, rinsed profusely with ethanol and furnace dried.

2.2. Synthesis of g-C_3N_4 and g-C_3N_4/TiO_2 Composite

The *g*-C_3N_4 (CN)[32] and g-C_3N_4/TiO_2[33] composite was prepared by using well-established procedures of which the details were given in recent publications.

2.3. Preparation of Pd@g-C_3N_4/TiO_2

The Pd@*g*-C_3N_4/TiO_2 catalyst was synthesized by conventional impregnation-reduction steps [34]. For this, 5.0 mL of an aqueous solution containing $Pd(NO_3)$ (2.50 mg, 9.38 μmol Pd) and *g*-C_3N_4/TiO_2 (0.2g) was stirred for 2 hours. A fresh 1.0 mL aqueous solution of $NaBH_4$ (5.43 mg, 0.14 mmol) was then added dropwise to this mixture and stirred under ambient conditions for half an hour. The final product was washed with copious amounts of water and ethanol (2x20 mL), filtered on filter paper and dried in an oven at 353 K. As a result, the Pd@*g*-C_3N_4/TiO_2 catalyst was obtained as gray color powder.

2.4. Characterization Methods

P-XRD patterns were obtained with a Rigaku Ultima-III X-ray diffractometer at 40 kV and 35 mA using Cu Ka radiation (k = 1.54059 A). For TEM analysis, diluted suspensions of the samples were prepared and the solvent was dried after dropping onto the carbon TEM grid. SEM analyses were performed on Zeiss Sigma 300. XPS patterns were performed on a Specs-Flex XPS with a photoelectron take-off angle of 45^0. The FT-IR spectra of the samples were taken on a Cary 630 FTIR spectrometer. DR/UV–Vis analyses were performed using Shimadzu UV-3600 Plus device.

2.5. Photocatalytic Tests

The photocatalytic degradation efficiency of the prepared photocatalyst was assessed by using methylene blue dye under UV-Vis light irradiation. A 300W Tungsten halogen lamp was used as a visible light source in this photocatalytic system. An experiment was carried out by adding 10 mg of the prepared catalysts to 30 mL of methylene blue aqueous solutions (7 μg/mL) in a cooling water-jacketed Pyrex glass reactor vessel. The solution was stirred in the dark (30 min) to reach an adsorption-desorption equilibrium between the MB and the catalyst surface. A certain amount of sample (2mL) was taken from the reactor vessel and the catalyst was removed by centrifugation (4000 rpm, 6 minutes). Changes in MB concentrations in solution were analyzed using a Cary 100 Bio UV–Vis spectrophotometer at maximum absorption (λ =664 nm) at room temperature.

The photodegradation efficiency (η) and the apparent pseudo-first-order rate constant (kapp) were determined by the following equation:

$$\eta = \frac{C_0 - C}{C_0}\ x100 \quad (1)$$

$$ln\frac{C_0}{C} = k_{app}t \quad (2)$$

C_0 in the equation is the initial concentration and C is the methylene blue concentration as a function of irradiation time t.

3. Results and Discussion

3.1. The Preparation and Characterization of Pd@*g*-C_3N_4/TiO_2 Nanocomposite

Before the preparation of Pd@g-C_3N_4/TiO_2 catalyst, first g-C_3N_4 and then g-C_3N_4/TiO_2 support materials were prepared by using a modified version of the method given in the literature[40]. The g-C_3N_4/TiO_2 support material was evidenced by FT-IR spectroscopy. FT-IR data were collected for the TiO_2, *g*-C_3N_4, and *g*-C_3N_4/TiO_2 structures as seen in Figure 1. The presence of g-C_3N_4 and *g*-C_3N_4/TiO_2 nanocomposites has been observed through FT-IR spectroscopy. Strong peaks observed at 1238, 1328, and 1573 cm^{-1} for pure g-C_3N_4 are attributed to the typical stretching vibration of C-N heterocycles and a sharp peak at 806 cm^{-1} is related to the characteristic stretching vibration of triazine units. The broad peak in the range 3100-3300 cm^{-1} is assigned to the stretching vibration of N-H bonds of amines (-NH_2 and =NH)[35,36]. The wide absorption peak at 400-700 cm^{-1} corresponds to the Ti-O stretching and Ti-O-Ti bridging stretching vibrations of pure TiO_2 [37, 38]. In addition, the peaks corresponding to bending and stretching vibrations of the O-H group were observed at 1630 and 3500 cm^{-1}. The spectrum of Pd@*g*-C_3N_4-TiO_2 catalyst was similar to that of *g*-C_3N_4-TiO_2 composite and also showed all the peaks of g-C_3N_4 and TiO_2.

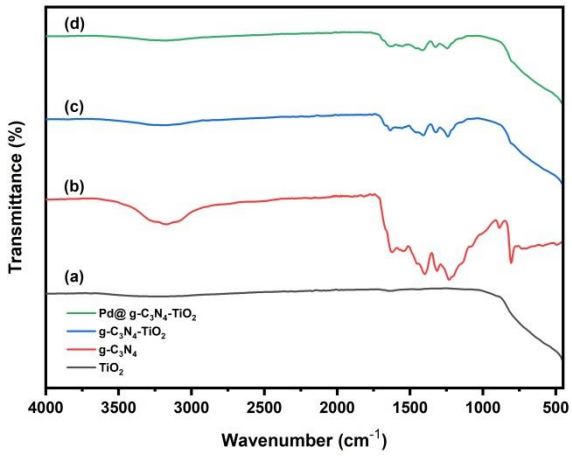

Figure 1. FT-IR spectra of TiO_2 (a), g-C_3N_4 (b), g-C_3N_4/TiO_2 (c) Pd@*g*-C_3N_4-TiO_2 (d).

In order to determine the optical properties of the Pd@*g*-C_3N_4/TiO_2 nanocatalyst, the UV-Vis diffuse reflectance spectral analysis of TiO_2, *g*-C_3N_4, and *g*-C_3N_4/TiO_2 was carried out, and the results are shown in Figure 2. As seen in Figure 2, the absorption sharp edges of TiO_2, *g*-C_3N_4, and *g*-C_3N_4/TiO_2 composite were found to be around 391, 425, and 412 nm, respectively. In addition, band gap values (Eg) of pure TiO_2, pure g-C_3N_4, and g-C_3N_4/TiO_2 composite were determined as ~ 3.08, 2.81, and 2.84 eV, respectively. In conclusion, the *g*-C_3N_4/TiO_2 nanocomposite exhibited enhanced absorption in the visible region compared to TiO_2 due to the synergistic effect between TiO_2 and g-C_3N_4. It can be seen that the bandgap of TiO_2 decreases with the addition of *g*-C_3N_4. [39].

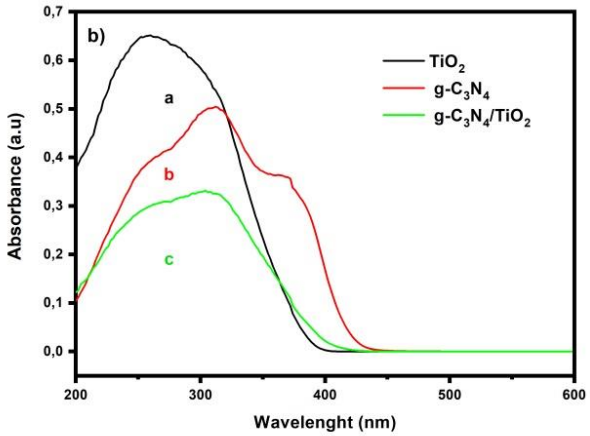

Figure 2. UV–Vis Diffuse Reflectance spectra of TiO_2 (a), *g*-C_3N_4 (b), and *g*-C_3N_4/TiO_2 composite (c)

Afterward, Pd@*g*-C_3N_4/TiO_2 nanocatalyst was simply and reproducibly prepared by following the procedure [40], Pd@*g*-C_3N_4/TiO_2 nanocatalyst was obtained as powders and characterized by P-XRD, XPS, SEM-EDX, and TEM.

The XRD patterns for fresh *g*-C_3N_4/TiO_2 composite and Pd@*g*-C_3N_4/TiO_2 photocatalyst samples are shown as a pattern in Figure 3. All the samples show the diffraction peaks of TiO_2 with 2θ values which depict the anatase phase of TiO_2 (JCPDS card No. 21–1272) and rutile phase (JCPDS card No. 21-1276) as shown in Figure 3. The one diffraction peak of *g*-C_3N_4 overlapped with the peak of the rutile phase at 27.5° (110) planes. Moreover, the diffraction peaks of Pd can only be observed

when the loading of Pd is 5% or more than 5 wt% with 2θ values of 40.2° (111), 48.0° (200), and 68.8° (220) that corresponds to the presence of Pd (JCPDS 05-0681)[41,42].

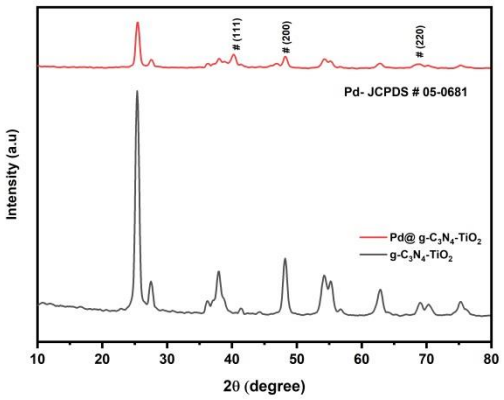

Figure 3. XRD patterns of *g*-C_3N_4/TiO_2 composite and Pd@*g*-C_3N_4/TiO_2 photocatalyst.

The surface elemental composition of the Pd@*g*-C_3N_4/TiO_2 nanocatalyst was investigated by using XPS analysis. The XPS spectrum of Pd@*g*-C_3N_4/TiO_2 taken as a survey scan is depicted in Figure 4. As seen in this spectrum, obtained signals disclose that the surface composition consists of Ti, Pd, N, C, and O.

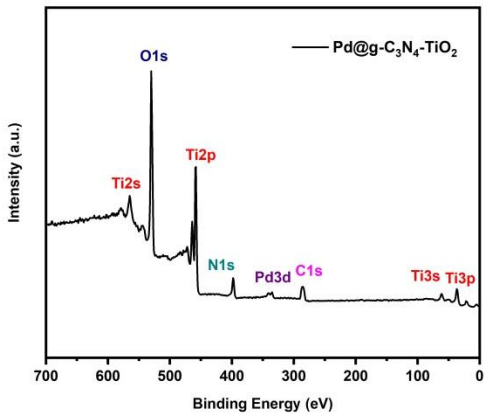

Figure 4. (a) Survey scan XPS spectrum of Pd@g-C_3N_4/TiO_2

The morphology and nanostructure of samples (*g*-C_3N_4, TiO_2, *g*-C_3N_4/TiO_2, and Pd@*g*-C_3N_4/TiO_2) are studied by SEM-EDX (Figure 5a-d) and TEM (Figure 5f-g). In SEM image of g-C_3N_4, the nanosheet structure (Figure 5b). Pure TiO_2 presents spherical-like large cauliflower-shaped particles that are non-agglomerate. Figure 5c-d shows the image of *g*-C_3N_4/TiO_2 and Pd@*g*-C_3N_4/TiO_2, respectively. Compositional analysis of prepared Pd@*g*-C_3N_4/TiO_2 catalysts was done using Energy Dispersive X-Ray Analysis (EDX). EDX results of Pd@*g*-C_3N_4/TiO_2 successfully revealed the presence of C, N, Ti, O, and Pd in the synthesized sample (Figure 5e). A transmission electron microscopy (TEM) image of the Pd@*g*-C_3N_4/TiO_2 (Figure 5f-g) nanocatalyst indicated that the presence of Pd NPs in the range of 0.04–2.5 nm with a mean diameter of 1.0 nm.

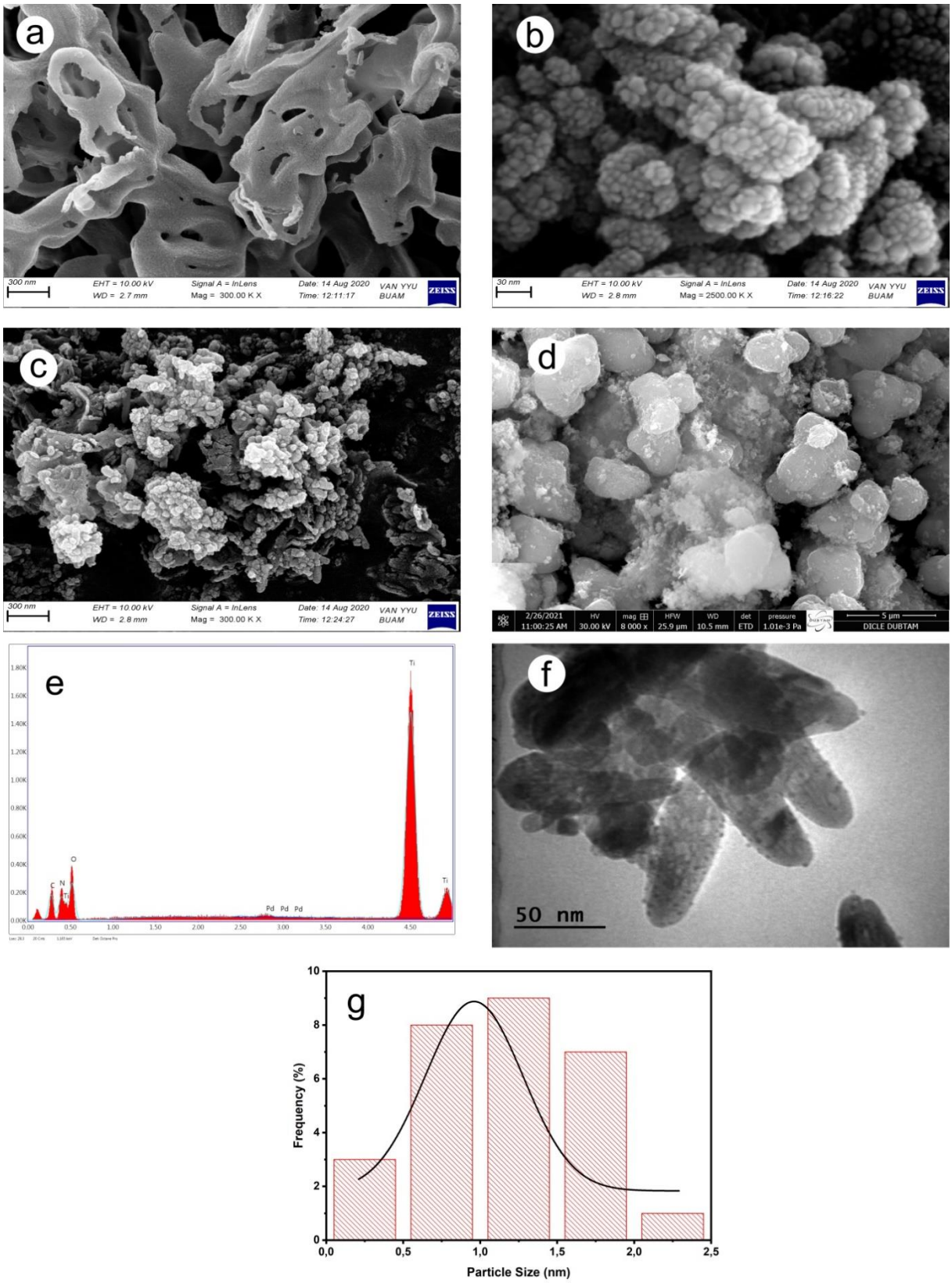

Figure 5. SEM image of a) *g*-C_3N_4 b) TiO_2 c) *g*-C_3N_4/TiO_2 and d) Pd@*g*-C_3N_4/TiO_2 e) SEM-EDX figure of Pd@*g*-C_3N_4/TiO_2 photocatalyst f) TEM image of Pd@*g*-C_3N_4/TiO_2 photocatalyst and g) size histogram of Pd NPs

3.2. Photocatalytic Activities for Methylene Blue (MB) Degradation under Visible Light Irradiation

The photocatalytic performance of Pd@*g*-C_3N_4/TiO_2 and *g*-C_3N_4/TiO_2 was assessed by determining the degradation degree of MB solution (30 mL, 7 µg/mL) under the irradiation of visible light using 0.3 %, 0.5 %, and 0.7%wt Pd (10 mg catalyst) and water as a sole solvent. As shown in Figure 6a, significant decreases in the absorption peak at 664 nm are observed in these samples, indicating that the concentration of MB in the solution is decreased. However, the Pd@g-C_3N_4/TiO_2 nanocatalyst tends to have a much faster peak descent compared to the *g*-C_3N_4/TiO_2 composite. When the *g*-C_3N_4/TiO_2 composite was used as the photocatalyst, it took 90 minutes for MB to completely degrade (Fig. 6a-b), whereas when the 0.5% wt charged Pd@*g*-C_3N_4/TiO_2 nanocatalyst was used, MB took 40 minutes to completely degrade. Also, for all these photocatalysts, the tendency of the absorption peak of MB to be blue-shifted with increasing irradiation time implies a change in the molecular structure of MB. As a result, compared with *g*-C_3N_4/TiO_2, the as-prepared Pd@*g*-C_3N_4/TiO_2 photocatalysts (0.3, 0.5, or 0.7 % wt Pd loading) showed enhanced photocatalytic performance on the degradation of MB under visible light irradiation (λ>400nm). Furthermore, to understand the reaction kinetics of the photocatalytic degradation of MB (Fig. 6b-c), the rate constant k was calculated from the equation $\ln(C_0/C_t) = kt$, and the process followed the first-order reaction. Here, C_0 and C_t are the concentrations of the MB solution at times 0 and t, respectively. The rate constant obtained from the degradation of methylene blue, as seen in Figure 6e, indicates that the reaction proceeds via pseudo-first-order kinetics. Under the irradiation of visible light, the first-order rate constants for MB degradation could be ranked as k(0.5% Pd@*g*-C_3N_4-TiO_2) >k(0.7% Pd@*g*-C_3N_4-TiO_2)> k(0.3% Pd@*g*-C_3N_4-TiO_2)> k(*g*-C_3N_4-TiO_2)(Fig. 6d). Among all catalysts, 0.5%Pd@*g*-C_3N_4-TiO_2 catalyst exhibits the highest k value. The rate constant (k) of the (0.5% Pd@*g*-C_3N_4-TiO_2) photocatalyst was approximately three times higher than that of pure *g*-C_3N_4-TiO_2. As a result, a larger k value means higher utilization efficiency of visible light, resulting in better degradation performance. In addition, the following reactions are predicted to occur during the visible light assisted photodegradation of MB dye [43].

$$\text{Catalyst} + h\nu \rightarrow h^+_{VB} + e^-_{CB} \quad (3)$$

$$h^+ + H_2O(ads) \rightarrow \bullet OH\ (ads) + H^+(ads) \quad (4)$$

$$O_2 + 2e^- \rightarrow (\bullet O^{2-})\ (ads) \quad (5)$$

$$\bullet O^{2-}\ (ads) + H^+ \leftrightarrow \bullet HO_2(ads) \quad (6)$$

$$\bullet HO_2(ads) \rightarrow H_2O_2(ads) + O_2 \quad (7)$$

$$H_2O_2(ads) \rightarrow 2\ \bullet OH\ (ads) \quad (8)$$

$$\bullet HO + MB \rightarrow CO_2 + H_2O \quad (9)$$

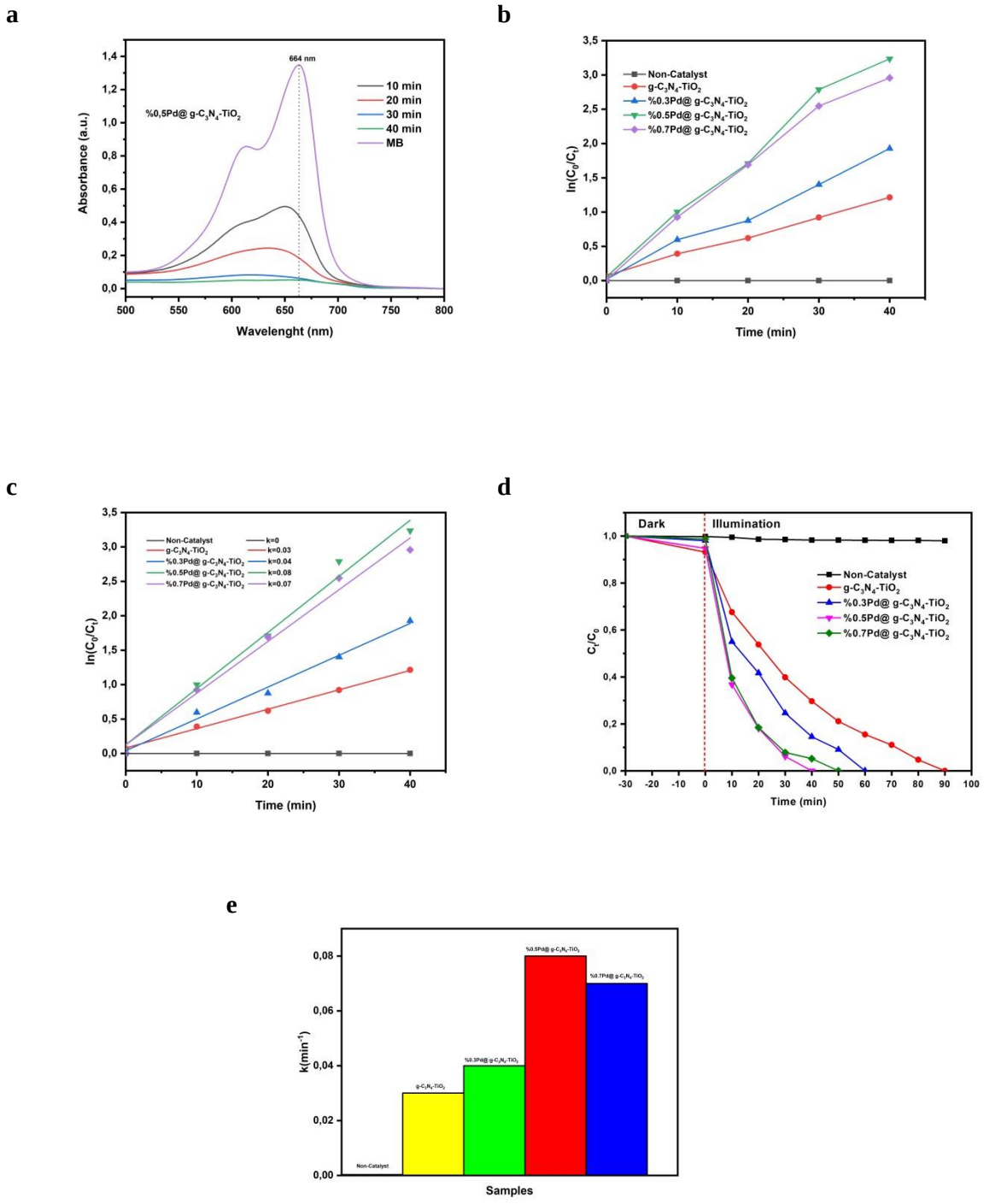

Figure 6. The degradation of MB by different photocatalysts (a) change of absorbance of MB solution (b) correlation between $\ln(C_0/C)$ with time t, (c) linear transform $\ln(C_0/C_t)$ of the kinetic curves of MB degradation d) correlation between C/C_0 with time t, e) apparent pseudo-first-order rate constant k with different catalysts.

4. Conclusions

In conclusion, we designed and successfully prepared new Pd nanoparticles, which are uniformly deposited on *g*-C_3N_4-TiO_2 through a facile method by the conventional impregnation and subsequent reduction steps. Pd@*g*-C_3N_4-TiO_2 nanocatalysts revealed a particle size of approximately 1.0 nm ±0.33 nm. We also demonstrated the characterization and use of the highly active 0.5 % wt loading Pd@*g*-C_3N_4-TiO_2 nanocatalyst for the degradation of methylene blue under visible light irradiation. The apparent rate constant for 0.5 % wt loading Pd@*g*-C_3N_4-TiO_2 is approximately three times higher than that of pure *g*-C_3N_4-TiO_2. Hence, the Pd@*g*-C_3N_4-TiO_2 as a visible light-driven photocatalyst is a promising material for the photodegradation of methylene blue in wastewater.

Acknowledgment

We would like to thank gratefully Dicle University Research Fund (*DUBAP Project No:* FEN.19.012) Diyarbakır, Turkey, for the financial support.

Ethical statement

The authors declare that this document does not require an ethics committee approval or any special permission. Our study does not cause any harm to the environment.

Declaration of Competing Interest

The authors declare no potential conflicts of interest related to the research, authorship, and publication of this article.

Authors' Contributions:

F. D: Conceptualization, Methodology, Formal analysis, Writing - Original draft preparation (50 %)

H.İ.Ö: Conceptualization, Methodology, Resources, Investigation, Writing (50 %)

All authors read and approved the final manuscript.

The compliance to Research and Publication Ethics

This work was carried out by obeying research and ethics rules.

References

[1] Akpan, U. G., Hameed, B.H., "Parameters affecting the photocatalytic degradation of dyes using TiO_2-based photocatalysts: A review", *Journal of Hazardous Materials,* 170, 520-529, 2009.

[2] Luo, X., Zhang, L., "High effective adsorption of organic dyes on magnetic cellulose beads entrapping activated carbon", *Journal of Hazardous Materials,* 171, 340-347, 2009.

[3] Zhu, M.X., Lee, L., Wang, H.H., Wang, Z., *Journal of Hazardous Materials,* 149, 735-741, 2007.

[4] Weber, E.J., Adams, R.L., *Environmental Science Technology*, 29, 1163-1170, 1995.

[5] Bruggen, B.V.D., Vandecastelee, C., Gestel T.V., Doyen W., Leysen R., *Environmental Progress,* 22, 46-56, 2003.

[6] Raghu, S., Basha, C.A., "Chemical or electrochemical techniques, followed by ion exchange, for recycle of textile dye wastewater" *Journal of Hazardous Materials,* 149, 324-330, 2007.

[7] Brillas, E., Martinez, C.A., "Decontamination of wastewaters containing synthetic organic dyes by electrochemical methods. An updated review", *Applied Catalysis B: Environmental,* 166-167, 603-643, 2015.

[8] Correira, V.M., Stephanson, T., Judd, S.J., "Characterisation of Textile Wastewaters-A Review", *Environmental Technology,* 15, 917-929, 1994.

[9] Qiu, J.H., Feng, Y., Zhang, X.F., Zhang, X.G., Jia, M.M., Yao, J.F., "Facile stir-dried preparation of g-C_3N_4/TiO_2 homogeneous composites with enhanced photocatalytic activity", *RSC Advances*, 7, 10668-10674, 2017.

[10] Wang, G.H., Xu, L., Zhang, J., Yin, T.T., Han, D., "Enhanced photocatalytic activity of powders (P25) via calcination treatment", *International Journal of Photoenergy*, 2012, 265760, 2012.

[11] Li, J.L., Jia, S.Q., Sui, G.Z., Du, L.J., Li, B.X., "Preparation of hollow Nd/TiO_2 sub-microspheres with enhanced visible-light photocatalytic activity", *RSC Advances*, 7, 34857-34865, 2017.

[12] Konstantinou, I.K., Albanis, T.A., "TiO_2-assisted photocatalytic degradation of azo dyes in aqueous solution: kinetic and mechanistic investigations: A review", *Applied Catalysis B: Environmental*, 49, 1-14, 2004.

[13] Teh, C.Y., Wu, T.Y., Juan, J.C., "An application of ultrasound technology in synthesis of titania-based photocatalyst for degrading pollutant", *Chemical Engineering Journal*, 317, 586-612, 2017.

[14] Teh, C.Y., Wu, T.Y., Juan, J.C., "Facile sonochemical synthesis of N,Cl-codoped TiO2: Synthesis effects, mechanism and photocatalytic performance", *Catalysis Today*, 256, 365-374, 2015.

[15] Ullah, R., Dutta, J.,"Photocatalytic degradation of organic dyes with manganese-doped ZnO nanoparticles", *Journal of Hazardous Materials*, 156,194-200, 2008.

[16] Zhang, G., Gao, Y., Zhang, Y., Guo, Y., "Fe_2O_3-Pillared Rectorite as an Efficient and Stable Fenton-Like Heterogeneous Catalyst for Photodegradation of Organic Contaminants", *Environmental Science Technology*, 44, 6384-6389, 2010.

[17] Li, X., Zhu, J., Li, H., "Comparative study on the mechanism in photocatalytic degradation of different-type organic dyes on SnS_2 and CdS", *Applied Catalysis B: Environmental*, B 123, 174-181, 2012.

[18] Gong, D.G., Highfield, J.G., Ng, S.Z.E., Tang, Y.X., Ho, W.C.J., Tay, Q.L., Chen, Z., "Poly Tristriazines as visible light sensitizers in Titania-based composite photocatalysts: Promotion of Melon development from urea over acid Titanates", *ACS Sustainable Chemistry & Engineering*, 2, 149–157, 2014.

[19] Wang, X., Maeda, K., Thomas, A., Takanabe, K., Xin, G., Carlsson, J.M., Domen, K., Antonietti, M., "A metal-free polymeric photocatalyst for hydrogen production from water under visible light", *Nature Materials.* 8, 76–80, 2009.

[20] Li, Y.N., Wang, M.Q., Bao, S.J., Lu, S.Y., Xu, M.W., Long, D.B., Pu, S.H.. "Tuning and thermal exfoliation graphene-like carbon nitride nanosheets for superior photocatalytic activity", *Ceramics International*, 42, 18521-18528, 2016.

[21] Chen, Y., Wang, X.C., "Template-free synthesis of hollow g-C_3N_4 polymer with vesicle structure for enhanced photocatalytic water splitting", *The Journal of Physical Chemistry C*, 122, 3786-3793, 2018.

[22] Li, J.L., Liu, T., Sui, G.Z., Zhen, D.S., "Photocatalytic performance of a Nd-SiO_2-TiO_2 nanocomposite for degradation of Rhodamine B dye wastewater", *Journal Nanoscience And Nanotechnology*, 15, 1408-1415, 2015.

[23] Wang, J., Wang, G.H., Wei, X.H., Liu, G., Li, J., "ZnO nanoparticles implanted in TiO_2 macrochannels as an effective direct Z-scheme heterojunction photocatalyst for degradation of RhB", *Applied Surface Science*, 456, 666-675, 2018.

[24] Zhou, W., Li, W., Wang, J.Q., Qu, Y., Yang, Y., Xie, Y., Zhang, K.F., Wang, L., Fu, H.G., Zhao, D.Y., "Ordered mesoporous black TiO_2 as highly efficient hydrogen evolution photocatalyst", *Journal of the American Chemical Society*, 136, 9280-9283, 2014.

[25] Thompson, T.L., Yates, J.T., "Surface science studies of the photoactivation of TiO_2-New photochemical processes", *Chemical Reviews*., 38, 4428-4453, 2006.

[26] Tong, Z.W., Yang, D., Xiao, T.X., Tian, Y., Jiang, Z.Y., "Biomimetic fabrication of g-C_3N_4/TiO_2 nanosheets with enhanced photocatalytic activity toward organic pollutant degradation", *Chemical Engineering. Journal*, 260, 117-125, 2015.

[27] Lu, N., Wang, C.Y., Sun, B., Gao, Z.M., Su, Y., "Fabrication of TiO_2-doped single layer graphitic-C_3N_4 and its visible-light photocatalytic activity", *Separation And Purification Technology*., 286, 226-232, 2017.

[28] Tan, Y.G., Shu, Z., Zhou, J., Li, T.T., Wang, W.B., Zhao, Z.L., "One-step synthesis of nanostructured g-C_3N_4/TiO_2 composite for highly enhanced visible-light photocatalytic H_2 evolution", *Application Catalyst B-environmental*., 230, 260–268, 2018.

[29] Li, J.L., Du, L.J., Jia, S.Q., Sui, G.Z., Zhang, Y. L., Zhuang, Y., Li, B.X., Xing, Z.Y.. "Synthesis and photocatalytic properties of visible light-responsive, three-dimensional, flower-like La–TiO_2/g-C_3N_4 heterojunction composites", *RSC Advances*, 8, 29645-29653, 2018.

[30] Das, T. K., Banerjee, S., Vishwanadh, B., Joshi, R., Sudarsan, V., "On the nature of interaction between Pd nanoparticles and C_3N_4 support", *Solid State Sciences*, 83, 70–75, 2018.

[31] Ming Lei, Zhiying Wang, Lihua Zhu, Wenshan Nie, Heqing Tang, "Complete debromination of 2,2′,4,4′-tetrabromodiphenyl ether by visible-light photocatalysis on g-C_3N_4 supported Pd", *Applied Catalysis B: Environmental*, 261, 118-236, 2020.

[32] Hosseini S. M., Ghiaci M., Farrokhpour H., "The adsorption of small size Pd clusters on a g-C_3N_4 quantum dot: DFT and TD-DFT study", *Materials Research Express*, 6(10), 105079, 2019.

[33] Guo Y., Xiao L., Zhang M., Li Q., Yang J., "An oxygen-vacancy-rich Z-scheme g-C_3N_4/Pd/TiO_2 heterostructure for enhanced visible light photocatalytic performance, *Applied Surface Science*, 440, 432–439, 2018.

[34] R.A. Senthil, J. Theerthagiri, A. Selvi, J. Madhavan, "Synthesis and characterization of low-cost g-C_3N_4/TiO_2 composite with enhanced photocatalytic performance under visible-light irradiation", *Optical Materials*, 64, 533-539, 2017.

[35] R.A. Senthil, J. Theerthagiri, A. Selvi, J. Madhavan, "Synthesis and characterization of low-cost g-C_3N_4/TiO_2 composite with enhanced photocatalytic performance under visible-light irradiation", *Optical Materials*, 64, 533-539, 2017.

[36] Çelebi, M., Yurderi, M., Bulut A., Kaya, M., Zahmakıran, M., "Palladium nanoparticles supported on amine-functionalized SiO_2 for the catalytic hexavalent chromium reduction" *Applied Catalysis B: Environmental*, 180, 53-64, 2016.

[37] Yan, H., Yan, H., "TiO_2–g-C_3N_4 composite materials for photocatalytic H_2 evolution under visible light irradiation", *Journal of Alloys and Compounds*, 509, 26- 29, 2011.

[38] Sabri, N.A., Nawi, M.A., Nawawi, W.I., "Porous immobilized C coated N doped TiO_2 containing in-situ generated polyenes for enhanced visible-light photocatalytic activity", *Optical Materials*, 48, 258-266, 2015.

[39] Zhang, Q., Meng, G., Wu, J., Li, D., Liu, Z., "Study on enhanced photocatalytic activity of magnetically recoverable Fe_3O_4@C@TiO_2 nanocomposites with core-shell nanostructure", *Optical Materials*, 46, 52-58, 2015.

[40] R.A. Senthil, J. Theerthagiri, A. Selvi, J. Madhavan, "Synthesis and characterization of low-cost g-C_3N_4/TiO_2 composite with enhanced photocatalytic performance under visible-light irradiation", *Optical Materials*, 64, 533-539, 2017.

[41] Yu Y., Zhao Y., Huang T., Liu H., "Shape-controlled synthesis of palladium nanocrystals by microwave irradiation", *Pure Applied Chemistry*, 81, 2377-2385, 2009.

[42] Ghorbani S., Parnian R., Soleimani E. "Pd nanoparticles supported on pyrazolone-functionalized hollow mesoporous silica as an excellent heterogeneous nanocatalyst for the selective oxidation of benzyl alcohol", *Journal of Organometallic Chemistry*, 952, 122025, 2021.

[43] Rauf, M. A., & Ashraf, S. S., "Fundamental principles and application of heterogeneous photocatalytic degradation of dyes in solution", *Chemical engineering journal*, 151 (1-3), 10-18, 2009.

Middle East Journal of Science

https://dergipark.org.tr/mejs **MEJS**

e-ISSN:2618-6136

Research article

BIOSENSOR PROPERTIES OF PLASMONIC SILVER NANOPARTICLES PRODUCED BY THE PLD MECHANISM

***Ilhan CANDAN*[1,2*]** ***Serap YİĞİT GEZGİN*[3]** ***Yasemin GÜNDOĞDU*[4]**
***Hadice BUDAK GUMGUM*[1,2]**

[1] Dicle University, Faculty of Science, Department of Physics, 21280, Diyarbakir, Turkey
[2] Dicle University, Institute of Science and Technology, Department of Physics, 21280, Diyarbakir, Turkey
[3] Department of Physics, Faculty of Science, University of Selcuk, 42031 Selcuklu, Konya, Turkey
[4] Department of Electric and Energy, Kadınhanı Faik İçil Vocational High School, University of Selçuk, 42031 Selçuklu, Konya, Turkey
*Corresponding author: ilhan.candan@dicle.edu.tr

Abstract: *Plasmonic metal nanoparticles (NPs), such as Ag, Au, Cu NPs, attract great interest due to their notable applications in biological, and chemical sensing. Researchers have studied the plasmonic metal NPs which have exceptional optical properties in a large spectral region. Metal NPs form a unique surface plasmon resonance (SPR) peak that is in the electromagnetic spectrum's visible part. The peak of SPR firmly depends on the NP's size, shape, dielectric constant, and medium that the particle is in. Light interacts with nanoparticles that are smaller than the wavelength of incident light in localized surface resonance. That leads Localised Surface Plasmon Resonance (LSPR) in which an oscillating local plasma around the NP with a certain frequency form. The LSPR detection is the most common method for wavelength shift measurement. Since analyte absorption causes a significant change on the value of local dielectric constant, the LSPR peak shifts. It is known that biological molecules such as proteins and antibodies can sensitively be detected while they affect the local dielectric environment. Therefore, Ag or Au based metal NPs can be used as a sensor with the help of LSPR wavelength shift technique. Among the metal NPs, Ag has a relatively higher refractive index sensitivity. Moreover, Ag NPs generate measurements that are more precise since they have a shaper LSPR peak. In our work, we produce plasmonic Ag NPs with various sizes and spherical shapes by making use of the Pulsed Laser Deposition (PLD) mechanism. Subsequently, we have investigate the LSPR peaks of these NPs via the UV-Vis spectroscopy. Additionally, biosensor properties of plasmonic Ag NPs are investigated by binding Protein A molecules to surface of the NPs. It is significant to mention here that we obtain an LSPR wavelength shift, which has a value around 100 nm/RIU.*

Keywords: *Plasmonic nanoparticles; Silver nanoparticles; LSPR; PLD, Plasmonic sensor*

Received: October 21, 2021 Accepted: December 22, 2021

1. Introduction

Nanoparticles (NPs), which attract attention with their small-scale dimensions, strong absorption coefficients, large surface area/volume ratios, find a lot of importance in analytical chemistry [1, 2]. Analytical techniques built on NPs not only take vital roles in the detection widespread significance in in the fields of pharmaceutical, clinical, food safety, and environmental because of their simple structures, wide linear ranges, and high sensitivity. Therefore, metal nanostructures are of great interest, both fundamentally and technologically, due to their unique functionality and properties in contrast to their large counterparts. In addition to this, optical features of the NPs have important aspects. Many

metal structures such as nanoscale gold and silver perform great absorption in the visible spectrum compared to their bulk structures. The standard absorption peaks of Au and Ag elements are around 520 and 400 nm, respectively. The nanoscale metal particles' optical properties varies by numerous parameters such as their size [3], shapes [4], metal composition [5], and environment of the nanoparticles [6-10]. In many research areas, the metal NPs play significant roles. For instance, the effects of quantum restrictions on electronic, magnetic, and other related features can be investigated by making use of an experimental model of the NPs [11, 12]. Additionally, the metal NPs are additionally employed in various fields such as catalysis [13], photography [14], biological labelling [15], photonics [16], optoelectronics [17], information storage [18], as well as the surface enhanced Raman scattering (SERS) [19, 20]. It is generally known that the metal NPs may be produced via several methods such as electrochemical techniques, organometallic precursors' decomposition, and metal salts' reduction or vapour deposition in the presence of stabilizers, especially the Laser Ablation (LA) and the Pulsed Laser Deposition (PLD). In these techniques, the nanoparticle size and density can be adjusted to the desired scale by easily controlling the parameters (for example laser fluency, wavelength, pulse number, pulse duration, pressure of background gas and distance from substrate to target, substrate temperature) of PLD system. Thanks to these distinctive features of PLD, the movement of LSPR peaks of plasmonic nanoparticles in the short or long wavelength direction of the solar spectrum can be easily achieved.

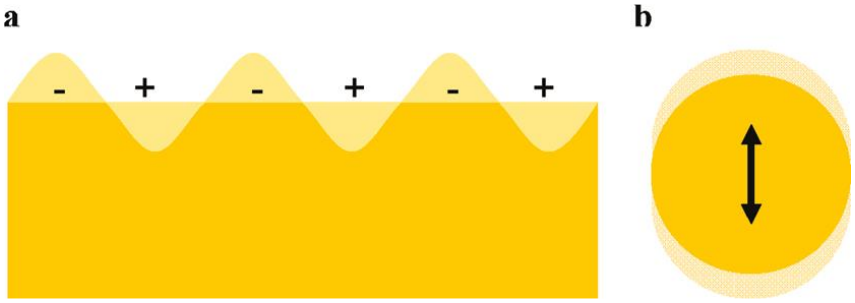

Figure 1. Illustrations of a) surface plasmons and b) a localized surface plasmon[21].

The plasmonic metal NPs' optical properties are very important because of the SPR phenomenon. The SPR corresponds to oscillation frequency of the conduction electrons in results of the electromagnetic radiation's electric field. As shown in Figure 1, surface plasmons are produced by oscillations of free electrons within the metal as result of electromagnetic waves that are trapped in the interface between metal and dielectric parts. The Mie theory explains this phenomenon successfully via the Maxwell equation [22]. The SPR peak is generated by considering material's negative real and positive imaginary dielectric constants. On the other hand, the SPR is a harmonic oscillation of electrons in the surface of metal NP and stimulated by electromagnetic field in the optical region. Consequently, the resulting signal is considerably strengthened.

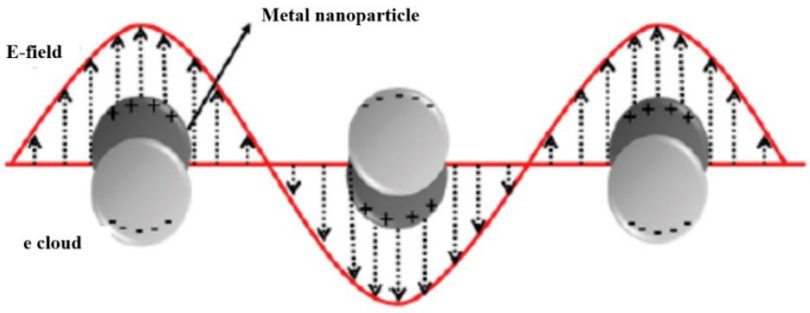

Figure 2. Schematic representation of plasmon oscillations demonstrating the relative displacement between the cloud of electron and nuclei.

Light interacts with smaller nanoparticles compared to the wavelength of incident light in the localized surface plasmon. As shown in Figure 2, the results in the formation of a local plasma around the nanoparticle, which has, a frequency named as the localized surface plasmon resonance (LSPR). As a matter of fact, the LSPR is similar to the SPR and has a high sensitivity when changes occur in the local dielectric environment [23]. The LSPR wavelength shifts are generally detected through changes occurring in the local environment, and an angularly resolved sensing is possible for the LSPR mechanism [24].

The way how metal NPs interact with electromagnetic radiation is explained quite well by Mie's scattering theory utilizing Maxwell's equations. It mainly expresses the optical extinction for the metal NPs that has a smaller radius compared to the incident radiation's wavelength ($2r << \lambda$) [25]

The biosensors, development is very significant for the analysis and detection of numerous chemicals, toxic substances, as well as biologically crucial compounds, which are used in the environmental monitoring, clinical, food safety and safety. Recently, for the development of biosensors, the SPR has been utilized [26, 27]. The interaction of unlabelled biomolecules can be detected by the SPR biosensors; thus, they can be used to detect unlabelled biomolecules. For this reason, the SPR biosensors are widely used in interaction studies and in receptors, carbohydrates, proteins, cells, different forms of bacteria, clinical diagnosis, military defence. Due to its good detection sensitivity, outstanding features such as unlabelled and detection in the real-time, the SPR biosensors are employed in various applications, for instance, bacteria, pesticides, allergens, and viruses' detection. Varying on the target sample's size, four distinct test formats have been developed for the SPR-based biosensors, which are used in the direct testing, competitive testing, sandwich testing and inhibition testing mechanisms [28-31].

In this paper, plasmonic Ag nanoparticles were produced by using the PLD method. The produced plasmonic Ag nanoparticles' LSPR peak are measured by the UV-Vis spectrometer. The LSPR peaks of 12600 and 14400 laser pulse Ag NPs were found to be at 680 and 700 nm, respectively. The morphological of the Ag NP thin films were investigated by Scanning Electron Microscopy (SEM) method and composition of the thin films were analysed by the Energy Dispersive Spectroscopy (EDX) technique. Shape of the produced Ag NPs were measured to be sphere and the size of that was found to be ranging from one to few hundreds nm. Additionally, biosensor properties of Ag NPs were investigated by binding protein A to NPs' surface.

2. Materials and Methods

2.1. Experimental Setup

The PLD system was used to produce silver nanoparticles. Nd:YAG laser (Continuum, Minilite II) system was operated and had pulsed mode with duration of 5 ns and repetition rate of 10 Hz at 1064 nm. The laser system has a capability of producing second, third, and fourth harmonics for 1064 nm, which are 532, 355, and 266 nm, respectively. In this work, 1064 nm fundamental wavelength had been employed. A neutral density filter was used to control laser pulse power that was measured before focusing lens as shown in Figure 3a. A glass microscope slide was used as a substrate to deposit Ag NP on. To clean the glass microscope slide, firstly, soap foam was applied, and then, it was bathed in isopropyl alcohol and acetone for 15 minutes each step. After that, the substrates were placed in an ultrasonic bath to further the cleaning process. Lastly, a nitrogen gas flow was used to dry the substrates. In our experiment, we utilized commercially available silver sputtering target with high purity (99.99%, Plasmaterials, USA). In order to avoid any damaging effect, the target and substrate were located on two independently rotating holders. As each laser pulse hit different part in the target, a homogeneous coating was achieved after laser ablation process as illustrated in Figure 3b.

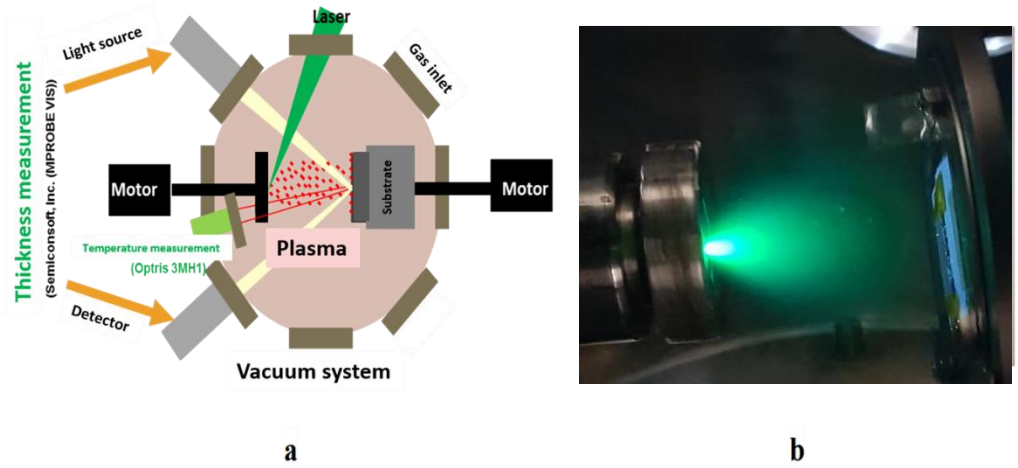

Figure 3. a) Schematic view of the PLD system designed and manufactured locally by the Laser spectroscopy group of Selcuk University, b) Plasma of the ablated Ag target material, using the PLD system.

5 cm fixed distance was applied between the target and substrate parts. Subsequently, Laser deposition process was carried out at room temperature for all films. The energy of laser was set to 35 mJ per pulse and the laser beam was focused on Ag target using a lens having 50 cm focal length. The laser beam's angle was fixed to be 45^0 on the target surface. The experiments were carried out in ultra-high vacuum which was around 5×10^{-7} mbar. The silver sputtering target was ablated by applying 12600 and 14400 laser pulses for different nanoparticle production. The produced Ag nanoparticle morphologies was analysed by the SEM measurement and the EDX spectrum was taken to investigate the element composition of the thin film. The Ag nanoparticles' absorption spectra were determined by utilizing a UV-Vis spectrometer (V-670 Jasco, USA). For investigating sensor properties of the produced plasmonic nanoparticles, the protein A (Sigma-Aldrich) solution of 1 ppm was used. Ultra-pure water was used as a solvent. Plasmonic Ag nanoparticles' LSPR peak shifts were measured by the UV-Vis spectrometer.

3. Results and Discussion

Plasmonic Ag NP thin films were produced by the PLD. The produced Ag NPs were investigated by the UV-Vis spectrum and the result is shown in Figure 4. As seen from the figure, two LSPR peaks of Ag NPs appear for 12600 and 14400 laser pulses, which are positioned at 680 and 700 nm, respectively. The LSPR peaks of Ag NPs are 680 and 700 nm for 21 and 24 minutes. Both peaks are in the visible part of the electromagnetic spectrum. With the increase in the number of laser pulses, the LSPR peak shifted slightly to the longer wavelength region and their absorption intensity increased.

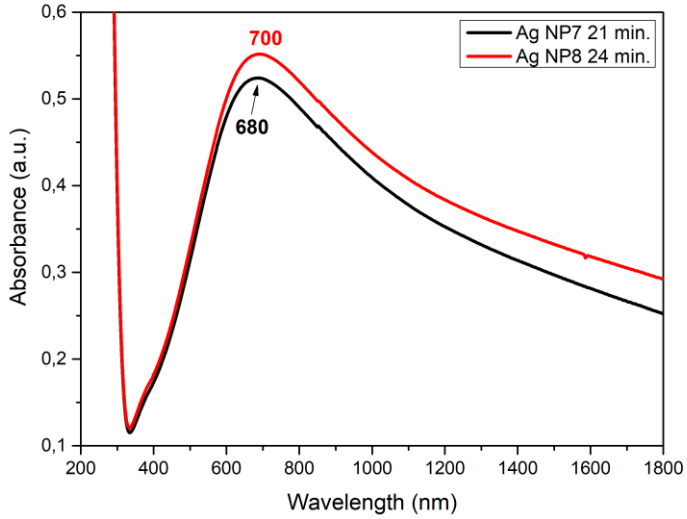

Figure 4. UV-Vis spectrum of plasmonic Ag NP produced by PLD for deposition times of 21 (12600 laser pulses) and 24 minutes (14400 laser pulses).

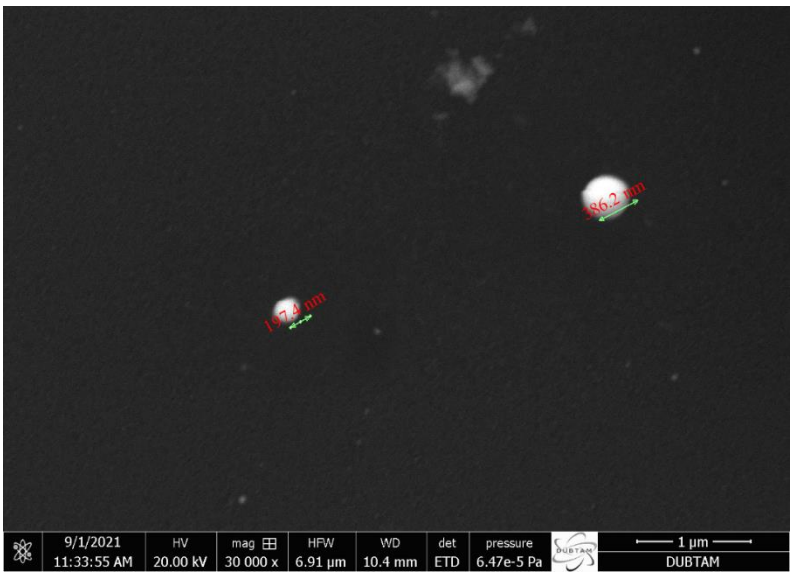

Figure 5. SEM image of Ag NP produced by PLD for 21 minutes (12600 laser pulses).

The SEM images of Ag NPs produced by the PLD for 12600 laser pulses are shown in Figure 5. Shapes of the produced NPs are spherical and sizes of them are 197.4 and 386.2 as seen in Figure 5. It should be noted that the imaged NPs are merely chosen for the purpose of illustration. There may be Ag NPs of different sizes in the other parts of the thin film as they are out of focus in the SEM image.

On the other hand, Figure 6 illustrates the SEM image of Ag NPs produced by the PLD for 14400 laser pulses. The shape of these NPs is spherical as well. The size of the NP illustrated in the figure is around 398 nm. Inset picture is the same Ag NP with size of 398 nm. It can be concluded that the NPs produced for 14400 laser pulses are larger than those of produced for 12600 laser pulses. Because, with the increase in the number of laser pulses, the rate of deposition is increased. The increase in the number of Ag nanoparticles deposited on top of each other and side-by-side at high laser pulse, number caused the particle size to increase.

Figure 6. SEM image of Ag NP produced by PLD for 24 minutes (14400 laser pulses).

The size of the plasmonic nanoparticles can be calculated by the following equation:

$$d = \frac{ln\left(\frac{\lambda_{spr} - \lambda_o}{L_1}\right)}{L_2} \quad (1)$$

where, $\lambda_o = 400$ nm; $L_1 = 6.53$ nm; $L_2 = 0.0216\, nm^{-1}$ [32]. Using Eq (1), the nanoparticle size was theoretically calculated to be 174 nm for LSPR peak of 680 nm, while it was obtained 177 nm to the LSPR peak in 700 nm. As in the morphological structure, while the number of laser pulses increased, the particle size expanded with the increase of the long wavelength of the LSPR peak.

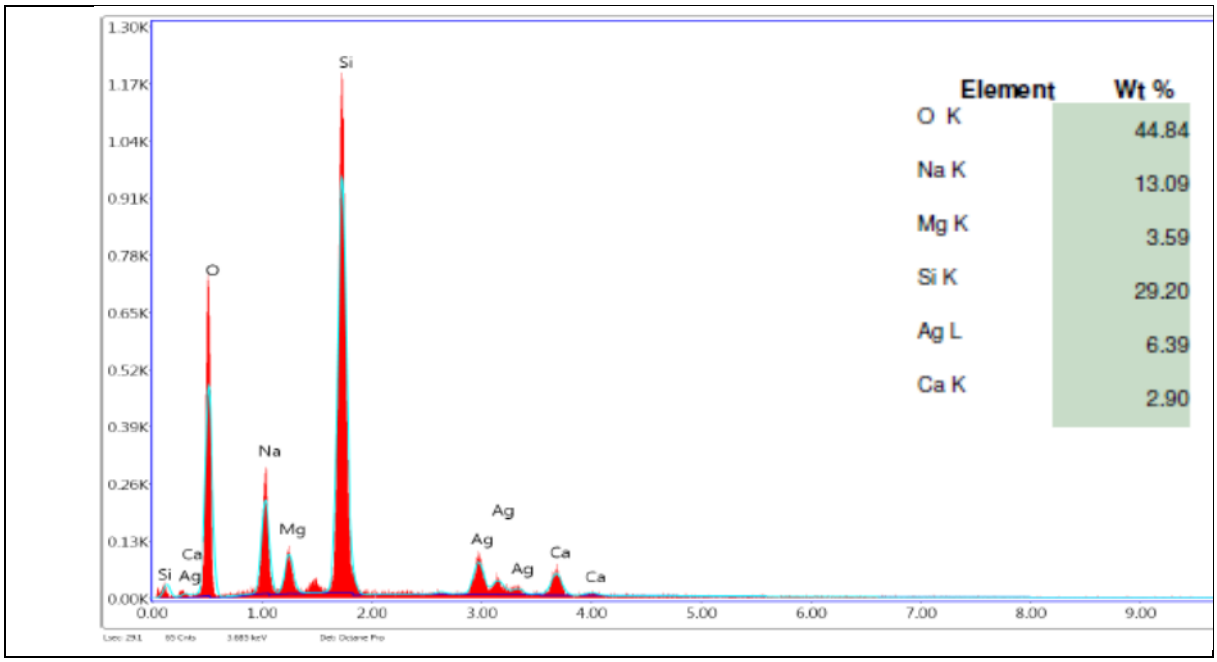

Figure 7. EDX spectrum of the Ag NPs produced for 12600 laser pulses.

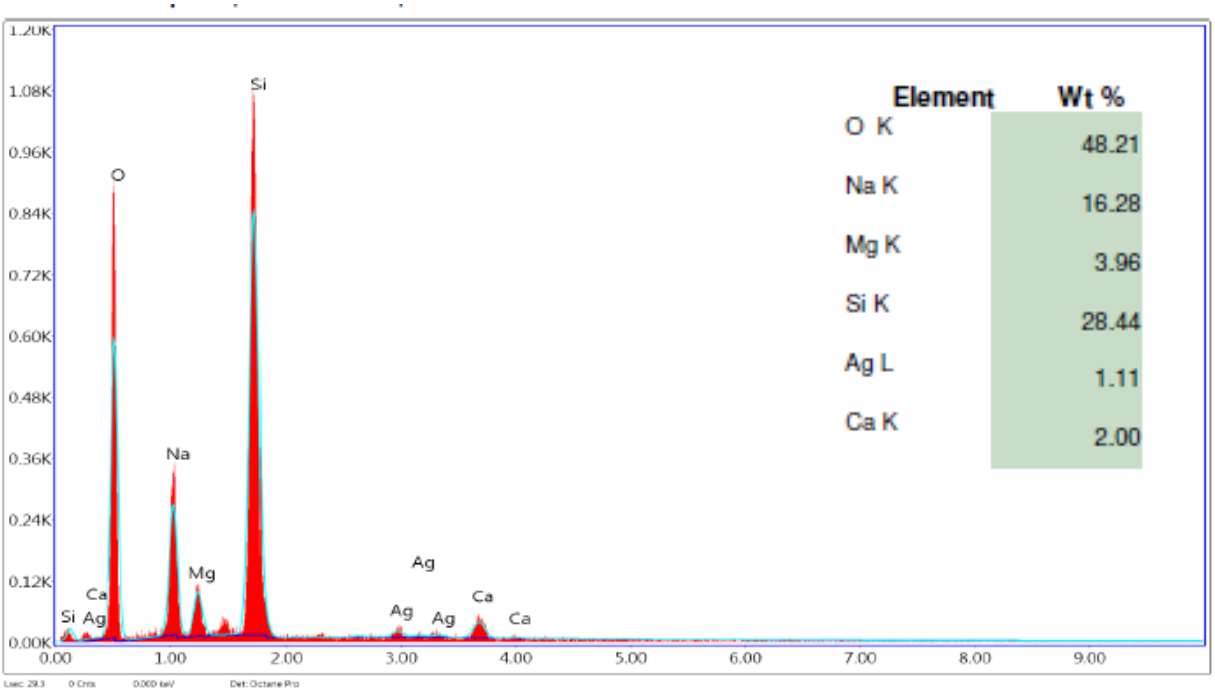

Figure 8. EDX spectrum of Ag NP for 24 minutes (14400 laser pulses).

The contents of the elements in the thin films are including Ag, Si, O, Na, Ca, Na, and Mg. Ag content proves that we have used the Ag target for the experiment as well as the other contents as we deposited the NPs on the glass microscopic slides. The wt % of the elements are given in the inset of Figure 7.

The EDX spectrum of Ag NPs produced for 14400 laser pulses are demonstrated in Figure 8. The contents of the thin film are composed of Ag, Si, O, Na, Ca, Na, and Mg. The Ag NPs are deposited in the glass microscope slides and the EDX findings agree with the experimental set up.

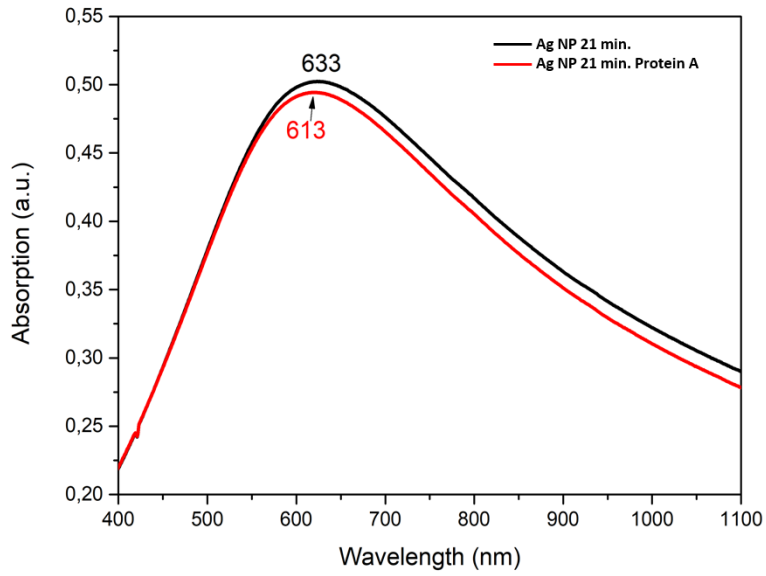

Figure 9. The UV-Vis spectrum of Ag and protein A binding NP produced by the PLD for 21 minutes (12600 laser pulses). The Ag NP with protein A is blue shifted for 20 nm.

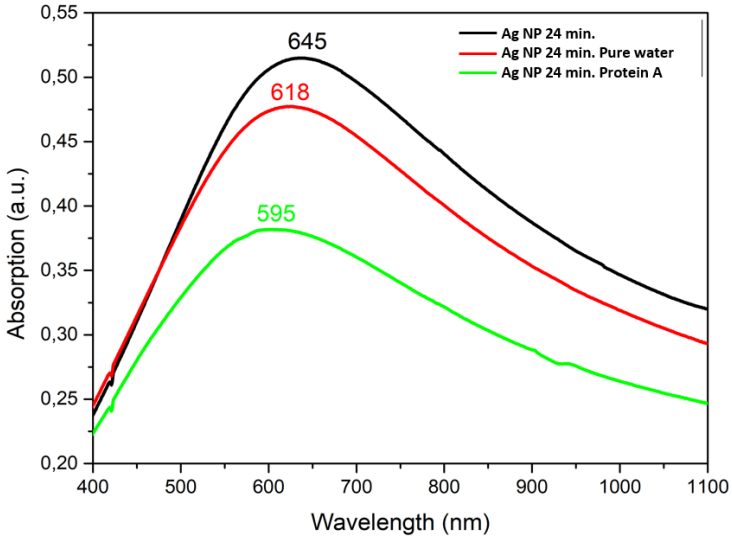

Figure 10. The UV-Vis spectrum of Ag, pure water and protein A binding NPs produced by the PLD for 24 minutes (14400 laser pulses). The pure water, and protein A binding NPs are blue shifted for 27 and 50 nm, respectively.

Figure 9 illustrates the UV-Vis spectrum of Ag and protein A binding NP produced by the PLD for 12600 laser pulses. The Ag NP with protein A is blue shifted for 20 nm. This suggests that the protein A molecules are bonded to the surface of the Ag NPs in the produced thin films. In addition of the LSPR peak shift of the Ag NPs with protein A, the full width at half maximum (FWHM) of the peak is measured to be changed. This may infer that the figure of merit for the produced Ag NP is suitable for a potential sensor.

The UV-Vis spectrum of pure Ag, Ag with pure water and Ag with protein A is shown in Figure 10. As Ag NPs are bounded by protein A, the LSPR peak blue-shift is around 50 nm. Ag NPs with pure water also shifts to blue side of the spectrum by 27 nm compared to the pure Ag NPs. In terms of refractive index unit (RIU), this corresponds to a wavelength shift around 100 nm/RIU.

4. Conclusion

Ag NPs with different sizes and spherical shapes were produced by the PLD method. The produced Ag NPs were investigated by the UV-Vis spectrometer. The plasmonic LSPR peaks of Ag NPs were found to be positioned at 680 and 700 nm for deposition of 12600 and 14400 laser pulses, respectively. The morphology of Ag NPs was determined by the SEM images and it is found that the Ag NPs produced for 12400 laser pulses are relatively smaller than those of Ag NPs produced for 14400 laser pulses. When duration of deposition increases, the size of produced NPs increases. The EDX spectrum of both Ag NPs produced for 12600 and 14400 laser pulses are containing the expected elements of Ag and the ones that include in the composition of glass microscope slides. The wavelength shift of the LSPR peaks is examined by binding Ag NPs' surface by pure water and protein A. The resulting blue-shifts are 27 and 50 nm for 12600 and 14400 laser pulses, respectively. These results suggest that the produced Ag NPs could be employed as sensors for different biomolecules in the future experiments.

Acknowledgements

This work was supported by Dicle University Scientific Research Projects Coordinatorship under Project No FEN.20.006.

Ethical Statements

The author declares that this document does not require an ethics committee approval or any special permission. Our study does not cause any harm to the environment.

Conflict of interest

Authors declare no conflict of interest.

Authors Contributions

IC, SYG and YG carried out the experiments and wrote the manuscript. HBG supervised the project. All authors discussed the results and contributed to the final manuscript.

References

[1] C.-T. Liu, and A.-N. Tang, "Applications of nanoparticles in elemental speciation," *Analytical Letters,* 48(7), 1031-1043, 2015.

[2] N. Li, D. Liu, and H. Cui, "Metal-nanoparticle-involved chemiluminescence and its applications in bioassays," *Analytical and bioanalytical chemistry,* 406(23), 5561-5571, 2014.

[3] C. L. Haynes, and R. P. Van Duyne, "Nanosphere lithography: a versatile nanofabrication tool for studies of size-dependent nanoparticle optics," ACS Publications, 2001.

[4] A. R. Tao, S. Habas, and P. Yang, "Shape control of colloidal metal nanocrystals," *small,* 4(3), 310-325, 2008.

[5] E. Ringe, B. Sharma, A.-I. Henry *et al.*, "Single nanoparticle plasmonics," *Physical Chemistry Chemical Physics,* 15(12), 4110-4129, 2013.

[6] A. Powell, M. Wincott, A. Watt *et al.*, "Controlling the optical scattering of plasmonic nanoparticles using a thin dielectric layer," *Journal of Applied Physics,* 113(18), 184311, 2013.

[7] A. L. González, C. Noguez, and A. S. Barnard, "Mapping the structural and optical properties of anisotropic gold nanoparticles," *Journal of Materials Chemistry C,* 1(18), 3150-3157, 2013.

[8] T. Ahmad, I. A. Wani, J. Ahmed *et al.*, "Effect of gold ion concentration on size and properties of gold nanoparticles in TritonX-100 based inverse microemulsions," *Applied Nanoscience,* 4(4), 491-498, 2014.

[9] W. A. Murray, B. Auguié, and W. L. Barnes, "Sensitivity of localized surface plasmon resonances to bulk and local changes in the optical environment," *The Journal of Physical Chemistry C,* 113(13), 5120-5125, 2009.

[10] M. M. Miller, and A. A. Lazarides, "Sensitivity of metal nanoparticle surface plasmon resonance to the dielectric environment," *The Journal of Physical Chemistry B,* 109(46), 21556-21565, 2005.

[11] A. C. Templeton, W. P. Wuelfing, and R. W. Murray, "Monolayer-protected cluster molecules," *Accounts of chemical research,* 33(1), 27-36, 2000.

[12] M. A. El-Sayed, "Some interesting properties of metals confined in time and nanometer space of different shapes," *Accounts of chemical research,* 34(4), 257-264, 2001.

[13] L. N. Lewis, "Chemical catalysis by colloids and clusters," *Chemical Reviews,* 93(8), 2693-2730, 1993.

[14] T. Tani, Silver nanoparticles: from silver halide photography to plasmonics: Oxford University Press, USA, 2015.

[15] S. R. Nicewarner-Pena, R. G. Freeman, B. D. Reiss *et al.*, "Submicrometer metallic barcodes," *Science*, 294(5540), 137-141, 2001.

[16] S. A. Maier, M. L. Brongersma, P. G. Kik *et al.*, "Plasmonics—a route to nanoscale optical devices," *Advanced materials*, 13(19), 1501-1505, 2001.

[17] P. V. Kamat, "Photophysical, photochemical and photocatalytic aspects of metal nanoparticles," ACS Publications, 2002.

[18] C. Murray, S. Sun, H. Doyle *et al.*, "Monodisperse 3d transition-metal (Co, Ni, Fe) nanoparticles and their assembly intonanoparticle superlattices," *Mrs Bulletin*, 26(12), 985-991, 2001.

[19] S. Nie, and S. R. Emory, "Probing single molecules and single nanoparticles by surface-enhanced Raman scattering," *science*, 275(5303), 1102-1106, 1997.

[20] L. A. Dick, A. D. McFarland, C. L. Haynes *et al.*, "Metal film over nanosphere (MFON) electrodes for surface-enhanced Raman spectroscopy (SERS): Improvements in surface nanostructure stability and suppression of irreversible loss," *The Journal of Physical Chemistry B*, 106(4), 853-860, 2002.

[21] K. M. Mayer, and J. H. Hafner, "Localized surface plasmon resonance sensors," *Chemical reviews*, 111(6), 3828-3857, 2011.

[22] C. W. Hsu, B. G. DeLacy, S. G. Johnson *et al.*, "Theoretical criteria for scattering dark states in nanostructured particles," *Nano letters*, 14(5), 2783-2788, 2014.

[23] T. R. Jensen, M. L. Duval, K. L. Kelly *et al.*, "Nanosphere lithography: effect of the external dielectric medium on the surface plasmon resonance spectrum of a periodic array of silver nanoparticles," *The Journal of Physical Chemistry B*, 103(45), 9846-9853, 1999.

[24] K. Hamamoto, R. Micheletto, M. Oyama *et al.*, "An original planar multireflection system for sensing using the local surface plasmon resonance of gold nanospheres," *Journal of Optics A: Pure and Applied Optics*, 8(3), 268, 2006.

[25] G. Mie, "Articles on the optical characteristics of turbid tubes, especially colloidal metal solutions," *Ann. Phys*, 25(3), 377-445, 1908.

[26] I. Abdulhalim, M. Zourob, and A. Lakhtakia, "Surface plasmon resonance for biosensing: a mini-review," *Electromagnetics*, 28(3), 214-242, 2008.

[27] D. R. Shankaran, K. V. Gobi, and N. Miura, "Recent advancements in surface plasmon resonance immunosensors for detection of small molecules of biomedical, food and environmental interest," *Sensors and Actuators B: Chemical*, 121(1), 158-177, 2007.

[28] F. S. R. R. Teles, "Biosensors and rapid diagnostic tests on the frontier between analytical and clinical chemistry for biomolecular diagnosis of dengue disease: A review," *Analytica chimica acta*, 687(1), 28-42, 2011.

[29] P. Leonard, S. Hearty, J. Brennan *et al.*, "Advances in biosensors for detection of pathogens in food and water," *Enzyme and Microbial Technology*, 32(1), 3-13, 2003.

[30] A. Olaru, C. Bala, N. Jaffrezic-Renault *et al.*, "Surface plasmon resonance (SPR) biosensors in pharmaceutical analysis," *Critical reviews in analytical chemistry*, 45(2), 97-105, 2015.

[31] R. G. Smith, N. D'Souza, and S. Nicklin, "A review of biosensors and biologically-inspired systems for explosives detection," *Analyst*, 133(5), 571-584, 2008.

[32] W. Haiss, N. T. Thanh, J. Aveyard *et al.*, "Determination of size and concentration of gold nanoparticles from UV− Vis spectra," *Analytical chemistry*, 79(11), 4215-4221, 2007.

Middle East Journal of Science

https://dergipark.org.tr/mejs **MEJS**

e-ISSN:2618-6136

Research Article

TIME SERIES OUTLIER ANALYSIS FOR MODEL, DATA AND HUMAN-INDUCED RISKS IN COVID-19 SYMPTOMS DETECTION

Ahmet Kaya [1] ***Rojan Gümüş*** [2] ***Ömer Aydın**** [3]

[1] Ege University, Tire Kutsan Vocational School, Tire, İzmir, Turkey
[2] Dicle University, Ataturk Vocational School of Health Services, Diyarbakır, Turkey
[3]Manisa Celal Bayar University, Faculty of Engineering, Department of Electrical and Electronics Engineering, Manisa, Turkey
* Corresponding author; omer.aydin@cbu.edu.tr

Abstract: *Information systems are important references aiming to support the decisions of decision-makers. Information reliability depends on the accuracy and efficacy of data and models. Therefore, some risks may emerge in information systems concerning models, data, and humans. It is important to identify and extract outliers in decision support systems developed for the health information systems such as the detection system of Covid-19 symptoms. In this study, the risks that are important in decision making in Covid-19 symptom detection were determined by the statistical time series (ARMA) approach. Potential solutions are proposed in this way. Moreover, outliers are detected by software developed by using the Box-Jenkins model, and the reliability and accuracy of data are increased by using estimated data instead of outliers. In the implementation of this study, time-series-based data obtained from laboratory examinations of Covid-19 test devices can be used. With the method revealed here, outliers originating from healthcare workers or test apparatus can be detected and more accurate results can be obtained by replacing these outliers with estimated values.*

Keywords: *Covid-19, Health information systems, time series, outlier analysis, ARMA*

Received: July 12, 2021 Accepted: October 26, 2021

1. Introduction

Health institutions are very important centers where financial values and risks must be managed effectively because, for all health institutions, it is essential to employ qualified personnel, purchase expensive equipment and machinery and use full-fledged buildings. In addition, it is particularly important to manage information systems accurately and use them effectively. A transformation is realized on the way from data to information and such transformation is implemented by information systems [1]. Thus, useful and meaningful outputs can be achieved by transforming so-called raw data into information [2]. Transformation into the required strategic information after a line of transactions such as preparation, processing, and communication of raw information is realized thanks to the information systems [3]. It is obvious that information systems also have a strategic role for organizations. Information systems are highly important in the development of products, services, and qualifications needed by organizations to gain an advantage over their rivals [4].

Strategic information systems are described as instruments using development, practice, transformation, and communication of organizational strategies [5]. Thus, information systems are a set of associated elements generated to enable control and coordination in the organization and collect, process, store and disseminate data to be used in decision-making [6].

Information system, on the other hand, is a series of organized transactions that support decision-making and provide control. An information system has a 7-phase hierarchical structure that contributes to the decision-making process. This structure is as described below [7]:

(1) Data collection (through observation or measurement),
(2) Data organization,
(3) Data processing,
(4) Outputs,
(5) Transformation from outputs into information,
(6) Presentation to the decision-maker,
(7) Decision-making (contributed by the expertise of decision-maker).

As physicians manage and supervise diagnosis, treatment, and control processes of a disease, they are often required to make accurate and effective decisions. The Decision-making process aims to encourage versatile thinking and transform uncertain environments into relatively stable environments. On the other hand, it is necessary to take into consideration the conditions of patients who will be positively or negatively affected by the decisions made, as well as the potential gains, losses, and risks. Decisions taken by physicians have a broad area of impact. These decisions are virtually managerial and each decision results in an array of changes and costs. Changes are generally directed toward increasing the competitive edge and efficiency and can be used to create new areas of health investment [8].

Health institutions are significant tools in the transition from conventional therapy methods to modern therapy [9]. These institutions have developed a major reliance on information and communication technologies from the past to the present [10]. This reliance is undoubtedly out of necessity. The most significant tools of information technologies are information systems. Data entered into information systems must be protected to maintain the reliability and efficacy of these information systems. Such protection is called security. In fact, data entered into health information systems are data regarding patients and, thus, they must be given the utmost care and consideration [10]. While electronic data enable health care organizations to identify areas of strength and weakness within their own operational environments, sometimes unintended negative consequences can occur even among the highest-functioning healthcare systems [11]. Data concerning a patient contain clues used in the diagnosis and treatment of the disease and are of vital importance to the patient. If such clues cannot be protected or become biased due to human or instrument-induced errors, then a physician who makes decisions based upon such data may be mistaken. As a result, diagnosis and treatment decisions will be erroneous as well. In such cases, serious vital risks occur for the patient. The physician and health institution may also inevitably encounter problematic processes.

Such errors not only put the patient's life in danger, but they also cause irreparable loss of prestige for health institutions that need to be managed in a serious manner. Furthermore, the hospital is faced with numerous question marks, and the health institution and physician encounter a series of material and immaterial sanctions. In addition, this kind of news is presented to large populations via mass communication tools, media devices, and social media platforms. It is apparent that the diagnostic decisions of physicians who are significant elements of health institutions have a broad area of influence. Prior to making decisions bearing very significant material and vital risks for both health institutions and physicians, and most importantly for the patients, data utilized in disease diagnosis and treatment must be subjected to a series of control processes before their entry into the information systems [12].

Information that is acquired from information systems and contributes to the decision-making process may contain models, data, and human-induced outliers. However accurately the information system and the physician works, such errors may result in biases in information generation and cause physicians who are in the decision-making position to make wrong decisions. Data that provide a basis for models, thus for information, maybe misentered by individuals, or if data is obtained via measurement and weighing instruments, misuse of such instruments may cause a bias on data. Also, data is by its nature acquired in different ways than expected, which is explained as an expression of an unforeseen outlier [13].

In this study, a method is proposed for verifying the accuracy of data used in health information systems. Statistical time series (ARMA) approach and Box-Jenkins model were used in the method. The method was applied to data known as Box-Jenkins A series and outliers were detected and eliminated.

This study uses time series analysis in health information systems. Despite the fact that the method was used in different kinds of fields, no studies, projects, or reports using the method on health data are available in the literature. In this regard, it is considered that the present study will serve as a source for this type of study.

2. Literature Review

Time series is a highly effective forecasting and analysis tool in statistics and various other disciplines in recent years, in relation to the analysis of datasets obtained in equal and unequal time intervals. Datasets obtained at equal time intervals are defined as discrete time series, and datasets obtained at unequal time intervals are defined as continuous time series. Detection of outliers in time series is known as outlier analysis. Outliers in time series were first studied by Fox in 1972 [15]. Fox developed a method called the likelihood ratio test to detect outliers (effects) in autoregressive (AR) models and defined the outliers detected with this method as first and second-type outliers. Fox also conducted studies on the power functions of outliers. Henceforth, many researchers developed methods encompassing all ARIMA models for detection of multiple outliers based on and building upon, Fox's studies. As well as Hilmer (1984), Tsay (1986), Pena (1987), Abraham and Yatawara (1988), Chang, Tiao, and Chen (1988), and Bruce and Martin (1989) contributed to the literature with similar studies [13,16-20].

Besides, Abraham and Yatawara studied the method of Lagrange multipliers and score-based outlier tests in 1988. Pena (1987), Abraham and Chuang (1989), Bruce and Martin (1989) studied and published articles about tests depending on the elimination of outlier observations during outlier detection and effective observations in time series [21].

Initial studies on the effect of outliers in time series were conducted by Box and Tiao in 1975 [22]. Another study on the detection of outliers is the method called Robust Procedure developed by Denby and Martin in 197923. This method was further studied by Martin and Yohai in 1985 [24]. Chang, Tiao, and Chen (1988) revealed in 1988 that incorrectly detected outliers lead to a loss of efficacy of test methods. Monte-Carlo simulations were employed to detect the C value which is the critical value used in outlier detection.

Time series is a serious area of research in statistics. It is also an analytical tool frequently used in quality control procedures, genetic algorithm optimization, fuzzy logic studies, import and export forecasting processes, chemical concentration analyses, and all time-dependent optimizations [25]. Also, predictive models like AR, MA, ARMA, ARIMA, and SARIMA through Box-Jenkins methodology have largely evolved in the second half of the 20. Century [26]. These models were used in different fields like health, economy, technology, transportation, and environmental areas [27-31].

Aydın and Karaarslan proposed a digital twin-based health information system in their study. In that study, image and sound data are obtained by mobile phone. Similarly, information such as body

temperature and saliva samples are obtained through various sensors. Data from different sources are represented by a digital twin created in the cloud, where it is aimed to determine whether the person is Covid-19 by artificial intelligence and machine learning techniques [32].

The COVID-19 outbreak caused radical changes in public life. Various measures are being tried to prevent the spread of the virus. More than 225,000 deaths and 3.2 million cases occurred during the study by Usman and his friends. Early detection of Covid-19 symptoms will contribute to preventing the outbreak from expanding. In this way, sick individuals can be quarantined and prevented from transmitting the disease to others. Usman et al. looked into the possibility of using speech to detect COVID-19 symptoms at an early stage. With this study, a low-cost and ubiquitous solution is proposed with early diagnosis. No complicated and expensive medical devices or specialized medical professionals are required for the preliminary assessment of symptomatic individuals. COVID-19 symptoms can be detected by an application running on a mobile device. Thus, health authorities can be warned [33].

In the past period, online sites and chatbots have been developed to control the symptoms of COVID-19. Since there is no study that statistically evaluates the accuracy of COVID-19 symptom controllers, Munsch et al. conducted a study. In their study, 10 COVID-19 symptom controllers, which are available online for free between 3-9 April 2020, have been selected. Versions of these symptom controllers in this date range were used. Updates after that date were not considered for analysis. They developed two additional simple symptom controllers as a basis for performance evaluation of 10 online COVID-19 symptom controllers. These two controllers evaluate and weigh the presence of COVID-19 symptom frequencies provided by the World Health Organization based on vector distance (SF-DIST) and cosine similarity (SF-COS) [34].

Mackey et al. aim to identify and characterize user-generated conversations that can be addressed in disease recovery using COVID-19 symptoms, test access experiences, and an unattended approach to machine learning. They collected and examined the tweets between 3-20 March 2020 from Twitter. In these tweets, the words related to COVID-19 were filtered. Subject clusters consisting of these words were analysed using an unsupervised machine learning approach called Biterm Topic Model (BTM). The tweets in these clusters were then removed and manually explained for content analysis and evaluated for their statistical and geographical features. They collected a total of 4,492,954 tweets containing terms that could be related to COVID-19 symptoms. They identified 3465 (<1%) tweets with filtering. They analysed these tweets [35].

An application-based self-reporting tool has been created to identify the distribution pattern and possible unreported symptoms by Zens et al. From April 8 to May 15, 2020, they used an app installed on smartphones by 22327 people. Participants are asked to enter information through questionnaires. In this way, they gathered information on both disease histories and symptoms of COVID-19. With this information reported by the participants, it becomes easier to identify new symptoms of COVID-19 disease and to predict the predictive value of some symptoms. In this way, it helps to develop reliable scanning tools. According to the data obtained in this study, they emphasized the necessity of loss of smell and taste as a cardinal symptom and showed that diabetes is a risk factor for the highly symptomatic course of COVID-19 infection [36].

3. Materials and Methods

In recent years there has been considerable interest in the effect of outlying observations in models. Robust techniques have been developed to reduce the effect of such observations. Hence, a large number of tests and procedures have been developed for outlier detection. Most of these procedures operate in the following ways [14]:

(1) Sequentially, examining the most deviant observation first and considering other observations only when the first is beyond the threshold.

(2) Without regard to the differing influence observations may have on the parameter estimates or predicted values which are often the prime focus of the analysis.

When an outlier is detected, the analyst is faced with a number of questions [14]:

(1) Is the measurement process out of control?

(2) Is the model wrong?

(3) Is some transformation required?

(4) Is there an identifiable subset of the observations that is important in its different behavior?

These issues affect the interpretation and confidence in the resulting estimates and/or predictions.

In this study, outlier values were tried to be determined in the evaluation of the data used in the detection of COVID-19 symptoms. For this chemical concentration value known as Box-Jenkins, A series were used to perform error analysis on the data. All systems and details about the materials and methods used are given in the subsections below.

3.1. Information Systems

A system is defined as a whole and a set of associated elements, with inputs and outputs and with predetermined borders, made up of interacting parts put together to achieve a goal or purpose [6].

The definition of system is a general definition likely to also include information systems. Information systems are specific-purpose systems developed to achieve specific goals. Information systems are featured, special-purpose software that transforms data into tangible information.

Data which refers to the input in information systems represent events occurring in the organization or the physical environment. Data does not have the characteristics and qualities of information by itself and cannot be used as information. However, information obtained by association and processing of data attained as a result of an observation or transaction is usable. Data cannot be used as a reference by itself. For instance, a physician uses large amounts of data in disease diagnoses. Blood values, urine values, blood pressure, and heartbeat counts, and if required, X-ray and similar instruments are evaluated together and an opinion is formed on the diagnosis of the disease. Each value mentioned above is unable to go beyond being data only. An opinion built upon the combination of all data is qualified as information and it supports the decision made by the physician.

3.1.1 Information Systems

Information systems are named in accordance with their functions and purposes. In this sense, six different information systems are available as listed below [6].

These information systems are Transaction Processing System (TPS), Management Information System (MIS), Office Automation Systems (OAS), Decision Support Systems (DSS), Executive Information Systems (EIS), Knowledge Work Systems (KWS), and Health Information Systems (HIS).

It is also possible to come across numerous special-purpose information systems other than those mentioned above and developed outside these categories. The common input of all information systems is data [37].

The healthier the data is, the more reliable and accurate the information will be. Data security depends on the attention and experience of individuals obtaining and entering such data into the system and on the reliability of systems. Since it is not always likely to operate a process with individuals doing their jobs properly, it is essential to test whether the data is healthy and ensure that they are reliable. To this end, it is necessary to ensure the compatibility of data forming the basis for modeling with an appropriate model and to operate an algorithm testing the presence of any outliers on the data. If there are any outliers on the data, then it is required to determine their effects and eliminate such effects

(errors) and optimize data. Through this process, the compatibility of data constituting the information can be ensured and consistent results can be achieved.

3.1.2 Strategic Role of Information Systems

Information systems have some significant strategic roles. The first of these roles is to help organizations establish a lasting advantage over their competitors, and the other role is to make technological innovations factors of production in the right place at the right time. Furthermore, the integration of these innovations into the business processes facilitates adaptation to technological changes, enables the transition to automation, and paves the way for obtaining higher quality data at a cheaper price. Although such adaptation is costly and difficult in the initial phase, its gains over time are ample and noteworthy. According to the information systems literature, it is generally regarded that strategic information systems have two types of benefits [38]:

• The first one is information-based gains obtained from a number of technological ideas specific to the organization and earned through creative ideas.

• The second one is already existing benefits that can be acquired by everyone and whose strategic significance is understood through extensive and effective use.

Although the importance of information systems for organizations was not understood in the past, they are becoming increasingly important due to higher competition and unstoppable technological changes.

3.1.3 Advantages of Health Information Systems

Health information systems are software dynamics that are important for an organization at all levels [39]. Given their strategic roles, information systems provide a series of advantages to health institutions. These advantages include:

• Fast access to high-quality information,
• Adaptation to technological changes,
• Cooperation with scientific methods,
• Resistance to compete,
• Opportunity to follow innovations and adapt them to businesses,
• Accurate diagnosis and satisfaction,
• High profits and chance to grow,
• Ease of adaption to changes,
• Remodelling opportunity,
• Setting a basis for research and development activities.

3.2. Statistical Modeling Process

The most frequently used statistical software packages today include SPSS, MINITAB, SAS, STATISTICA, and so on. Model parameters are generated in order to eliminate the potential outliers from data by using these packages which are a kind of information system. In this study, Statistical modeling transactions are performed using MINITAB software package. Data retrieved for this purpose is regarded as time series (ARMA) (Auto Regressive Moving Average Model) data.

3.3. Box-Jenkins and Outlier Forecasting Model

Outlier modeling is a process for eliminating the bias occurring on the data because the result of modeling with biased data is necessarily biased. In this regard, it is necessary to remove the biases occurring on the data and it should be done before modeling. This process is also called data cleaning.

Data Cleaning is the process that consists of detecting and imputing anomalous data1. In this context, two types of outliers are observed in Box-Jenkins time series forecasting models [15]. Type 1

errors (Additive Outlier (AO)) are induced by individuals, devices, or erroneous use of devices. Effects of these outliers which are not data-related must certainly be separated from observations [41]. Type 2 errors (Innovational Outlier (IO)) occurs as a result of natural randomness and affects all observations starting from their emerging with a decreasing trend. There are differing opinions on whether the effect of this second type of error should be separated or not. It is observed that errors in time series can be identified with their sources and reasons [13,15].

In addition, error detection in time series is based on autocorrelation established between residuals (e_t) (ρ: autocorrelation $\varepsilon_t = \rho\varepsilon_{t-1} + \varepsilon_t^*$ $(E(\varepsilon_t, \varepsilon_{t-1}) \neq 0)$ $E(\varepsilon_t) = e_t$), and the Type 1 error detection can be done much more easily by data scanning processes [41].On the other hand, in Type 1 error, the effect on parameter estimation is much higher and is defined as a shock effect [40].

Box-Jenkins time series model is defined as follows:

Assume that $\{x_t\}$ is a time series generated with $ARMA(p,q)$ a model containing no data error. $ARMA(p,q)$ Model is described as:

$$\phi(B)x_t = \theta(B)e_t \tag{1}$$

where, $\phi(B) = 1 - \phi_1 B - ... - \phi_p B^p$, $\theta(B) = 1 - \theta_1 B - ... - \theta_q B^q$, $B^k x_t = x_{t-k}$ $E(x_t) = 0$ $\{e_t\} \rightarrow (0, \sigma^2)$. If $\phi_1, ..., \phi_p$ values which are the roots of $\phi(B)$ function defined in the equation model are outside the unit circle, then the model fulfills the stationary condition; if $\theta_1, ..., \theta_p$ values which are the roots of $\theta(B)$ function are outside the unit circle, then it fulfills the nonstationary condition, and thus, reversibility assumptions [42].

The stationarity of time series simply refers to keeping the correlation between observations and error terms within prescribed limits and to the decrease of partial autocorrelation values of observations in parallel with the increase in lags. In addition, if the series is stationary, the assumptions that are prerequisites for time series modeling will be met. In the Box-Jenkins model, error types can be classified as human-induced errors, data-induced errors, and model-induced errors.

3.4. Human-Induced Error Type

If an observation value is calculated differently than expected due to a human or instrument mistake or as a result of a measurement error, these types of outliers are defined as first type or human-induced errors. Such errors cause shock changes on parameter estimation values [40]. It occurs when normal data is incorrectly entered into the system by individuals or in similar cases. Also, parameter bias is sharper and greater in these types of errors. Effects on such observations must definitely be eliminated. They are defined as Additive Outlier (AO) or A-type outlier models in the literature. Such errors can be detected more accurately through data scanning processes. They were first introduced and modeled by Fox in 1972 [15].

Human-induced outlier model is defined as

$$y_t = z_t + \delta x_t \tag{2}$$

where y_t is the observed value, δ is the size of outlier, x_t is variable valued as 1 at the time of outlier (T = t) and 0 in other times [13].

3.5. Data-Induced Error Type

The Data-induced model affects subsequent observations starting from its emerging position. If the outlier has a persistent or permanent effect on the level and variance process of the series, it is called an innovational outlier. This refers to an illness (anomaly) state with decreasing effect. Such effect

progressively decreases. It was first introduced by Fox in 1972 and modeled as the Innovational Outlier (IO) model. It is also defined as a B-type model in the literature [15].

The data-induced error model is expressed as

$$y_T = \frac{\theta(B)}{\phi(B)}(e_T - \delta x_T) \tag{3}$$

where θ(B) is the *MA* function, ϕ(B) is the *AR* function, e_t is the residual at the time, x_t is the variable with a value of 1 at T = t and 0 at other times [13].

$$\rho^2 = (1 + \pi_1^2 + \pi_2^2 + ... + \pi_{n-T}^2) \tag{4}$$

$$\varpi_I = e_T \tag{5}$$

$$\varpi_A = \rho^2 \pi(F) e_T , \tag{6}$$

$$\pi(F) = (1 - \pi_1 F - \pi_2 F^2 - ... - \pi_{n-T} F^{n-T} \tag{7}$$

$$\lambda_{1.T} = \varpi_I / Var(\varpi_I) \tag{8}$$

$$\lambda_{1.T} = \varpi_A / \rho^2 Var(\varpi_A) \tag{9}$$

In error detection processes, C values are taken as C=3.00 for high-sensitivity detection, as C=3.50 for mid-sensitivity detection, and as C=4.00 for low-sensitivity detection.

3.6. Model-Induced Error Type

Another risk encountered in information systems is the selection of the wrong model equation for the data. In such cases, totally normal observations can become outliers as a result of selecting the wrong model [1]. Furthermore, models established without eliminating the potential error effects on data may be erroneously selected. It is necessary to observe the tendencies of data on the scatter diagram in order to avoid such outliers. Thus, it will be possible to have preliminary information on appropriate models for the data.

3.7. Error Detection Algorithm

Error detection algorithm consists of the following steps:

- Read observations from the defined file.
- Read ARMA parameters obtained by using the program package.
- Calculate π_j's from the estimated model.
- Use $\hat{\sigma}_a^2$ and obtain $\hat{e}_t$'s and find outliers.
- Read critical values C which can be 3.00, 3.50, and 4.00.
- Do;
  1. Calculate $\hat{\sigma}_a^2$ from the $\hat{e}_t$;
  2. Increase the current value by one;
  3. Calculate the $\lambda_{1.T}$, $\lambda_{2.T}$ which define the data effects;
  4. If $\lambda_{1.T} > C$, display outlier position and IO;
  5. If $\lambda_{2.T} > C$, display outlier position and AO.
  6. Otherwise, there is no outlier. Stop.
  7. Calculate the effect of IO and AO and update these effects on observations.

8. Calculate new $\hat{e}_T$'s for updated observations,

- End Do.

Read updated new observations and perform new algorithms again [43].

3.8. Outlier Detection Flowchart

An algorithm flowchart demonstrating the error detection process on datasets is presented in Figure 1. The software for this flowchart is a method called iterative procedure determined to be the most effective method among outlier detection processes. This method is converted into a module with C# programming language and the error outlier detection process is performed [12].

In this method, observational data is read into the statistical program package (MINITAB) and the time series model parameters and residuals for each observation (et) are obtained. Following this transaction, a software program that conducts error detection on data is used and the detection process is initiated. The detection process continues iteratively until no errors are present in the series. When all erroneous observations on the series are eliminated, the software operation is also concluded. As a result of this process, variance and parameter values change and the model is indirectly optimized.

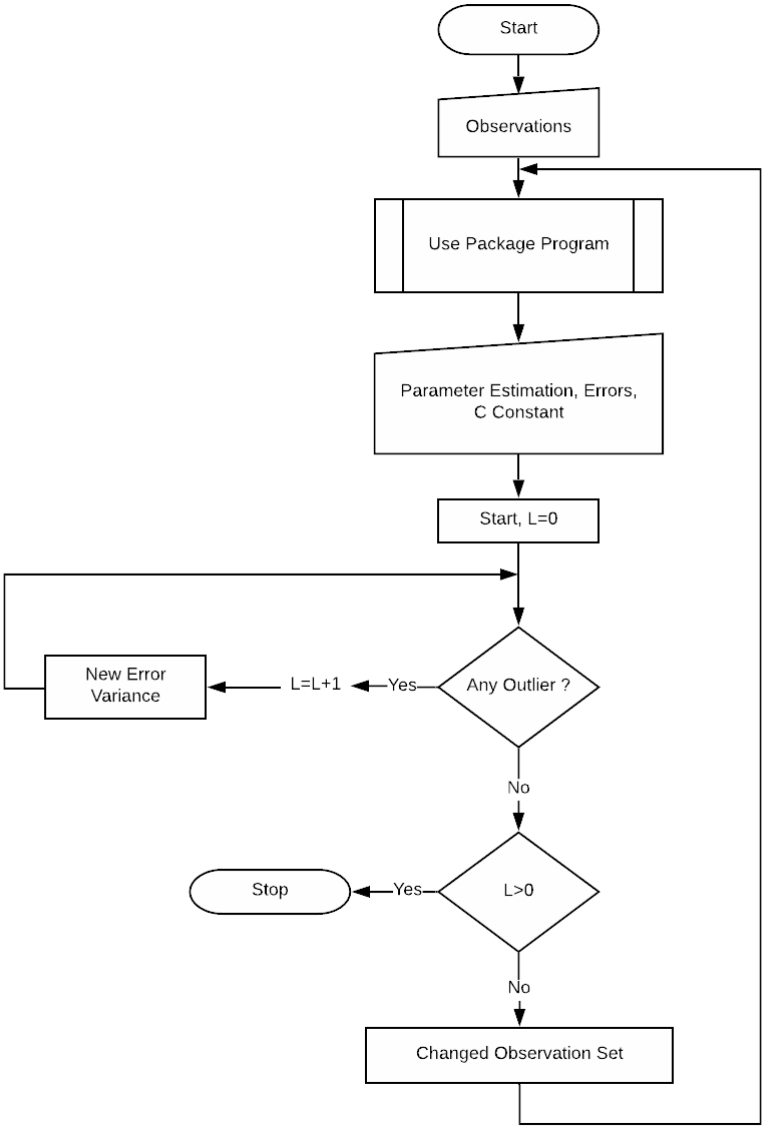

Figure 1. Outlier Detection Algorithm Flowchart

4. Conclusion

By electronic records in hospitals, the most effective and efficient healthcare services are given to the patients within the shortest time. Additionally, hospital staff have less workload and be less likely to make mistakes [44]. On the other hand, there are always risks during the application of information systems. Risks that enable access from abstract datasets to significant information systems are usually data-driven risks. Especially during the COVID-19 pandemic process, the risks that may arise due to the mistakes of health personnel have become very important. Such risks can be eliminated. Thus, a control process on data sets is certainly required. Through these processes, it is possible to attain more minimal variance values, more objective parameter estimations, and more effective models. It will thus be possible to have more effective and accurate datasets by using the results obtained from these models. In addition, even though there are human-induced risks on data, these data can be corrected and rendered more suitable to acquire information. Human-driven or data-driven risks on data may also result in wrong model parameters. Such aberration may be so high that the model format may sometimes entirely change. In this respect, the natural result of human or data-induced errors in data is the selection of wrong models, which appears as model risk. In line with these inferences, it is considered that the following results and suggestions are noteworthy:

• Data-induced errors are natural. The effects of these data are also natural. For example, it occurs when a patient contracts a virus without realizing and some of his/her values are different than expected. Effects on data continue in a decreasing manner until the patient clears the virus from his/her body. According to the scientific literature, it is the researcher's choice to eliminate or not eliminate these effects, because probable natural aberrations in models are inherent in modeling.

• Human-driven risks are easier to detect in data. Such data is called "contaminated", which is "infected", in the literature. They occur when a data entry operator enters the data erroneously while transferring them into the system. Such effects must definitely be estimated and separated from data. Moreover, these effects cause a shock on variance and parameter estimations. In recent studies, outlier detection studies were mostly based on human-induced outliers

• The effect of data-induced risks on the model is normal, while the effect of human-induced risks on the model is abnormal and has to be eliminated.

• Prior to data modeling, data must be observed using graphs called scatter diagrams and an appropriate model must be investigated on graphs. It will thus be possible to obtain healthier results in terms of parameter estimations.

• These kinds of error debugging analyses optimize the parameters and make the models stronger and more dynamic.

• In order to receive the expected benefits from information systems, it must be ensured that data are healthy as it is, so to speak, the nutrients of such systems. It must be remembered that however perfectly a system operates, if it is fed erroneous data, then the results attained will be far from becoming information.

• Informed and qualified personnel must be employed for the achievement of all these goals and the improvement and control of information systems. It is a prerequisite, even though costly, for organizations to achieve a competitive power.

Secure hospital information systems cost high. However, this cost is only for a short period of time. In the long term, their benefits outweigh the costs for organizations.

In the present study, a method based on the statistical time series approach and Box-Jenkins model was implemented to detect the errors in data used in the detection of Covid-19 symptoms. Outlier data was detected with an iterative error detection process which has been developed with C# programming language and is also an information system. An improvement in mean squares of error and a reduction

in variance were observed as a result of replacing outliers with estimated data by using the method. These results depict that the proposed method is successful in detecting the errors in time series data and replacing such data with estimated data. It was determined that problems induced by data outliers can be reduced by applying the proposed method to health information systems such as the detection system of Covid-19 symptoms. In future studies, if there is sufficient data on Covid-19 tests, the method here can be applied to detect and correct outliers.

Conflict of interest:

The authors report no conflicts of interest. The authors alone are responsible for the content and writing of the paper.

The Declaration of Ethics Committee Approval

The author declares that this document does not require an ethics committee approval or any special permission. Our study does not cause any harm to the environment.

Authors' Contributions:

A. K.: Conceptualization, Methodology, Formal analysis, Original draft preparation.
R. G.: Resources, Implementation, Investigation.
Ö. A.: Resources, Implementation, Writing -Original draft preparation, Journal Correspondence.
All authors read and approved the final manuscript.

References

[1] Akouemo, H., Povinelli, R., "Data Improving in Time Series Using ARX and ANN Models". *IEEE PES Transaction on Power Systems*, 32, 3352-3359, 2015.

[2] Ergun, Ü., "Modern Management Accounting Applications by Information Technologies" *Dokuz Eylul University Journal of Faculty of Economics and Administrative Sciences*, 11, 1-17, 1995.

[3] Soyuer, H., İşletmelerde Bilgisayar Destekli Bilgi Sistemi Uygulamaları ve Üretim/İşlemler Yönetiminde Bilgisayara Dayalı Sistemler, Ph. D. thesis, Gazi University Social Sciences Institute, Ankara, TR, 2000

[4] O'Brein, J.A., Introduction to Information Systems. Irwin McGraw Hill, Boston, 1997

[5] Earl, M.J., "Experiences in Strategic Information System Planning", *MIS Quarterly*, 17(1), 1-12, 1993.

[6] Kalıpsız, O., Buharalı, A., Biricik, G., Sistem Analizi ve Tasarımı. [System Analysis and Design], Papatya Yayıncılık Eğitim, İstanbul, TR, 2011

[7] Lucas, H., Information System Concept for Management (5th Edition), McGraw-Hill, New York, NY, 1994

[8] Peppard, J., IT strategy for Business, Pitman Publishing, New York, NY, 1993

[9] Katsikas, S.K., "Health Care Management and Information Systems Security: awareness, training, or education?", *International Journal of Medical Informatics*, 60, 129-135, 2000.

[10] Gritsalis, D.A., "Enhancing Security and Improving Interoperability in Healthcare Information Systems", *Medical Informatics*, 23(4), 309-324, 1998.

[11] Ward, M.J., Self, W.H., Froehle, C.M., "Effects of Common Data Errors in Electronic Health Records on Emergency Department Operational Performance Metrics: A Monte Carlo

Simulation", *Academic emergency medicine: official journal of the Society for Academic Emergency Medicine*, 22(9), 1085-1092, 2015.

[12] Kaya, A., "Modelling for Detection Processes Outliers in Time Series and Its Performance Analysis", *Uludag University Journal of Faculty of Economics and Administrative Sciences*, 22 (1), 271-279, 2003.

[13] Chang, I., Tiao, G.C., Chen, C., "Estimation of Time Series Parameters in the Presence of Outliers", *Technometrics*, 30(2),193-204, 1988. Doi:10.1080/00401706.1988.10488367

[14] Andrews, D., Pregibon, D., "Finding the Outliers that Matter. Journal of the Royal Statistical Society", *Series B (Methodological)*, 40(1), 85-93, 1978.

[15] Fox, A.J., "Outliers in Time Series", *Journal of the Royal Statistical Society Series B*, 34, 350-363, 1972.

[16] Hillmer. S.C., "Monitoring and Adjusting Forecasts in the Presence of Additive Outliers*",* *Journal of Forecasting*, 3, 205-221, 1984.

[17] Tsay, R.S., "Time Series Model Specification in the Presence of Outliers", *Journal of the American Statistical Association*, 81(393), 132-141, 1986.

[18] Pena, D., Measuring the importance of outliers in ARIMA models. New Perspectives in Theoretical and Applied Statistics John Wiley, New York, USA, 1987

[19] Abraham, B., Yatawara, N. A., "Score Test for Detection of Time Series Outliers", *Journal of Time Series Analysis*, 9(2), 109-119, 1988.

[20] Bruce, A.G., Martin, D., "Leave-k-out diagnostics for time series (with discussion)", *Journal of the Royal Statistical Society Series B*, 51, 363-424, 1989.

[21] Abraham. B., Chuang, A., "Outlier Detection and Time Series Modelling", *Technometrics*, 31(2), 241-248, 1989.

[22] Box, G.E.P., Tiao, G.C., "Intervention Analysis with Applications to Economic and Environmental Problems", *Journal of American Statistical Association*, 70(349), 70-79, 1975.

[23] Denby. L., Martin, R.D., "Robust estimation of the first order autoregressive parameter", *The Journal of the American Statistical Association*, 74, 140-146, 1979.

[24] Maronna, R., Martin, R., Yohai, V., Robust Statistics: Theory and Methods, Wiley, New York, USA, 2006.

[25] Firmino, P.R.A., Mattos Neto, P.S.G., "Ferreira TAE. Correcting and combining time series forecasters", *Neural Networks*, 50, 1-11, 2014.

[26] Paulino, J., Gomes, C., Gonçalves Júnior, J., Rodrigues, M., Souza, A., Pimentel, J., Brito, K., Saboia, S., Firmino, P., "Predictive Models and Health Sciences: A Brief Analysis", International Archives of Medicine. 2017. Doi: 10.3823/2487.

[27] Chen, Z., Chen, Y., Li, T., "Port cargo throughput forecasting based on combination model", Proceedings of in Joint International Information Technology. Mechanical and Electronic Engineering Conference (JIMEC 2016). Xi'an, China, 2016,148-154.

[28] Adedia, D., Nanga, S., Appiah, S.K., Lotsi, A., Abaye, D.A., "Box-Jenkins' Methodology in Predicting Maternal Mortality Records from a Public Health Facility in Ghana*", Open Journal of Applied Sciences*, 8, 189-202, 2018. Doi:10.4236/ojapps.2018.86016

[29] Langat, A., Orwa, G., Koima, J., "Cancer Cases in Kenya; Forecasting Incidents Using Box &Jenkins Arima Model", *Biomedical Statistics and Informatics*, 2, 37-48, 2017.

[30] Aboagye-Sarfo, P., Mai, Q., Sanfilippo, F.M., Preen, D.B., Stewart, L.M., Fatovich, D.M., "A comparison of multivariate and univariate time series approaches to modelling and forecasting emergency department demand in Western Australia", *Journal of Biomedical Informatics*, 57, 62-73, 2015. Doi: 10.1016/j.jbi.2015.06.022

[31] Luz, P.M., Mendes, B.V.M., Codeço, C.T., Struchiner, C.J., Galvani, A. P., "Time Series Analysis of Dengue Incidence in Rio de Janeiro, Brazil", *The American Journal of Tropical Medicine and Hygiene*, 79(6), 933-939, 2008. Doi:10.4269/ajtmh.2008.79.933

[32] Aydın, Ö., Karaarslan, E., "Covid-19 Belirtilerinin Tespiti İçin Dijital İkiz Tabanlı Bir Sağlık Bilgi Sistemi". Online International Conference of COVID-19 (CONCOVID), İstanbul, Turkey,2020, pp.8-9.

[33] Usman, M., Wajid, M., Zubair, M., Ahmed, A., "On the possibility of using Speech to detect COVID-19 symptoms: An overview and proof of concept", Researchgate, 2020. Doi:10.13140/RG.2.2.31718.57923

[34] Munsch, N., Martin, A., Gruarin, S., Nateqi, J., Abdarahmane, I., Weingartner-Ortner, R., Knapp, B., "A benchmark of online COVID-19 symptom checkers", *medRxiv* 2020.05.22.20109777, 2020. Doi: 10.1101/2020.05.22.20109777

[35] Mackey, T. K., Purushothaman, V. L., Li, J., Shah, N., Nali, M., Bardier, C., Liang, B., Cai, M., Cuomo, R., "Machine Learning to Detect Self-Reporting of Symptoms, Testing Access, and Recovery Associated with COVID-19 on Twitter: Retrospective Big Data Infoveillance Study", *JMIR Public Health and Surveillance*, 6(2), e19509, 2020. Doi:10.2196/19509.

[36] Zens, M., Brammertz, A., Herpich, J., Suedkamp, N. P., Hinterseer, M., "App-based tracking of self-reported COVID-19 symptoms (Preprint)". ResearchGate, 2020. Doi:10.2196/preprints.21956

[37] Louden, K.C., Laudon, J.P., Management Information Systems: managing the digital firm (8th. edition), Prentice-Hall, New Jersey, USA, 2004.

[38] Kini, R.B., "Strategic Information Systems", *Information Systems Management*, 10(4), 42-50, 1993.

[39] Ammenwerth, E., Graber, S., Herrmann, G., Bürkle, T., König, J., "Evaluation of Health Information Systems-Problems and Challenges". *International Journal of Medical Informatics*, 71, 125-135, 2003.

[40] Ljung, G.M., "On Outlier Detection in Time Series". *Journal of the Royal Statistical Society: Series B*, 55, 559-567, 1993.

[41] Kaya, A., "A Type Outlier in AR (1) Model", *The Journal of Statisticians*, 3, 1-7, 2010.

[42] Box, G.E.P., Jenkins, G.M., Time series analysis: Forecasting and control, Holden-Day, San Francisco, USA, 1976.

[43] Kaya, A., "Outlier Effects on Databases, LNCS 3261, Advancing Information Systems." Proceedings of Third International Conference, ADVIS 2004, İzmir, Turkey, Springer, 2004. p. 88-96.

[44] Kılıç, T., "Digital Hospital; An Example of Best Practice", *International Journal of Health Services Research and Policy*, 1(2), 52-58, 2016. Doi:10.23884/ijhsrp.2016.1.2.04

Middle East Journal of Science

https://dergipark.org.tr/mejs

MEJS

e-ISSN:2618-6136

Research Article

SYNTHESIS, CHARACTERIZATION AND BIOLOGICAL EVALUATION OF ESTER DERIVATIVES OF 4-(DIETHYLAMINO) SALICYLALDEHYDE AS CHOLINESTERASE AND TYROSINASE INHIBITORS

***Reşit ÇAKMAK*[*,1] *Ercan ÇINAR*[2] *Eyüp BAŞARAN*[3] *Mehmet BOĞA*[4]

[1]Medical Laboratory Techniques Program, Vocational School of Health Services, Batman University, Batman, Turkey
[2]Department of Nursing, School of Health Sciences, Batman University, Batman, Turkey
[3]Department of Chemistry and Chemical Processing Technologies, Vocational School of Technical Sciences, Batman University, Batman, Turkey
[4]Department of Analytical Chemistry, Faculty of Pharmacy, Dicle University, Diyarbakır, Turkey
[*] Corresponding author; resit.cakmak@batman.edu.tr

Abstract*:* *Alzheimer's disease, one of the diseases that still has no a specific therapy, has become a major public health issue owing to the increasing population of the elderly, particularly in rich countries. Inhibitory of cholinesterase enzymes (acetylcholinesterase (AChE) and butyrylcholinesterase (BChE), which hydrolyze acetylcholine (ACh) and butyrylcholine (BCh) neurotransmitters, have recently become a choice for the therapy of this disease. Therefore, there is currently a great demand for novel enzyme inhibitors with desirable properties for applying in the treatment of AD. In this study, a series of ester derivatives of 4-(diethylamino)salicylaldehyde (**1-5)** were successfully prepared and structurally illuminated with FT-IR, ^{1}H- and ^{13}C NMR spectroscopy. The inhibitory properties of the synthesized molecules on AChE, BChE, and tyrosinase enzymes were investigated, respectively. Compound **1** indicated potent inhibitory activity against BChE with 87.28±0.87% inhibition better than galanthamine (73.83±0.25 %inhibition) employed as standard. Compound **3** showed significant inhibitory effect against tyrosinase with 87.73±0.22 % inhibition, which is better than kojic acid utilized as standard. The obtained results clearly revealed that some of these molecules have the potential to be used as potent enzyme inhibitor candidates in the future studies.*

Keywords*: Esters, Acetylcholinesterase, Butyrylcholinesterase, Tyrosinase.*

Received: June 4, 2021 Accepted : August 06, 2021

1. Introduction

Alzheimer's disease (AD) is a progressive chronic disease that prevents the continuation of daily living activities [1]. The most important risk factor for AD is age. This disease affects the central nervous system in humans. AD causes cognitive and functional deterioration, neuropsychiatric and behavioral disturbances, visual and spatial skills, impairment in learning new information and remembering learned information, and speech impairment. In addition, AD is an irreversible neurodegenerative disease that causes significant impairment in a person's social and professional life [2,3]. AD is a disease that occurs with the loss of neurons and synapses in some parts of the central nervous system [4,5]. The earliest symptom of the disease is short-term memory loss. The first stages of the disease can be very mild, so this situation may not be noticed by the patient. Dementia is not a natural consequence of aging, but a disease that should be distinguished from the cognitive and

psychological changes seen with normal aging [6]. For its therapy, a treatment method is followed to prevent forgetfulness and related skill losses that reduce the quality of daily life. It is known that a decrease in ACh in the brain is one of the reasons why AD occurs in the elderly. Damage to the cholinergic system in AD is the most prominent neurochemical disorder known [7]. Among the pharmacological approaches developed to heal this damage, the most successful method is the treatment with AChE inhibitors. For the treatment process, AChE inhibitors are used to prevent the reduction of ACh that causes disease progression [8-12].

Melanin is one of the most common pigments in nature [13]. This pigment plays a role in the darkening of fruits and vegetables and also the determination of skin, hair, and eye color in humans and animals [14, 15]. Tyrosinase is the main enzyme responsible for the production of melanin pigment in fungi and vertebrates [16]. In living things, some pigmentation abnormalities can be observed in the skin due to the production of melanin and the activity of the tyrosinase enzyme [17,18]. Low activity of tyrosinase and decreases in melanin synthesis cause hypopigmentation problems in the skin [19]. However, excessive activity of the tyrosinase enzyme increases the amount of melanin synthesis, which leads to hyperpigmentation problems [20,21]. In both conditions, the differences in the parts of the skin that are visible and in contact with the social environment cause social and psychological problems in individuals. Nowadays, many people are interested in skin whitening (hypopigmentation agent) products [22]. In the dermo-cosmetics industry, especially in Asian countries, products with hypopigmentation effect are frequently preferred. The market for these products is growing as tyrosinase inhibitors not only remove pigmentation disorders but also other spots on the skin. Increasing interest from color cosmetics to functional cosmetics increases the investments made in this sector [23]. The molecules used as tyrosinase inhibitors can be obtained by chemical or biological pathways [24]. In some cases, an inhibitor obtained from biological sources is synthetically produced and used; for example, kojic acid [25].

This research was carried out to contribute to the ongoing researches for the discovery and development of effective enzyme inhibitors. In this study, we targeted to search the inhibition effects of the ester derivatives of 4-(diethylamino)salicylaldehyde (**1-5**) on cholinesterase and tyrosinase enzymes *in vitro* conditions. The synthesized molecules were characterized by spectral analysis such as FT-IR, ^{1}H, and ^{13}C NMR.

2. Materials and Methods

2.1. Chemistry and analysis

In the current study, all commercially available chemicals used for the synthesis of the target molecules were received from Turkish representatives of Aldrich, Sigma-Aldrich, and Merck Chemical companies. FTIR spectra of the synthesized molecules were recorded on Agilent Cary 630 FTIR spectrometer with diamond ATR imaging accessory. ^{1}H and ^{13}C NMR spectra were recorded on a Bruker Avance III 400 MHz and 100 MHz (with $CDCl_3$ and DMSO-d_6 as solvent) spectrometer. Melting points of all ester derivatives were detected on a Barnstead IA9100 Electrothermal digital melting points apparatus.

2.2. General procedure for the synthesis of ester derivatives (1-5)

A solution of 4-(diethylamino) salicylaldehyde (10 mmol) and the corresponding benzoyl chloride derivative (10 mmol) in pyridine (25 mL) was heated under reflux for 1 h [26]. This solution was left to cool down and then poured onto ice-cold water (50 mL). Thereafter, it was held for 24 h at 25 °C, and the formed precipitate was filtered, and then rinsed with 50 mL of distilled water; and they

left to dry in the open air overnight. Finally, the residue was crystallized from ethanol to give the target molecule.

2.2.1 5-(Diethylamino)-2-formylphenyl benzoate (1) [27]

Shiny brown solid, yield: 88%, m.p. 90-92 °C. FT-IR, ATR (cm^{-1}): 3065 (C-$H_{arom.}$), 2971 (C-$H_{aliph.}$), 2817, 2712 (C-$H_{aldehyde}$), 1737 (C=O_{ester}), 1670 (C=$O_{aldehyde}$), 1598 (C=$C_{arom.}$). ^{1}H NMR ($CDCl_3$) δ: 1.25 (t, 6H, (2xC***H***$_3$)), 3.46 (q, 4H, (2xC***H***$_2$)), 6.43 (d, 1H, *J*=2.4 Hz, C_6H_3-***H***), 6.62 (dd, 1H, *J* = 8.9, 2.4 Hz, C_6H_3-***H***), 7.55 (t, 2H, *J*=7.7 Hz, C_6H_5-***H***), 7.65–7.70 (m, 1H, C_6H_5-***H***), 7.79 (d, 1H, *J*=8.9 Hz, C_6H_3-***H***), 8.24–8.28 (m, 2H, C_6H_5-***H***), 9.89 (s, 1H, –C***H***=O), ppm. ^{13}C NMR ($CDCl_3$) δ: 12.49 (***C***H_3), 44.85 (***C***H_2), 104.40, 108.79, 116.51, 128.66, 129.25, 130.33, 132.50, 133.75, 153.17, 154.62 (Ar-***C***), 165.09 (***C***=$O_{aldehyde}$), 186.23 (***C***=O_{ester}), ppm.

2.2.2 5-(Diethylamino)-2-formylphenyl 2-nitrobenzoate (2)

Pale yellow solid, yield: 85%, m.p. 86-88°C. FT-IR, ATR (cm^{-1}): 3095 (C-$H_{arom.}$), 2968 (C-$H_{aliph.}$), 2867, 2777 (C-$H_{aldehyde}$), 1747 (C=O_{ester}), 1652 (C=$O_{aldehyde}$), 1592 (C=$C_{arom.}$), 1526 (Ar-$NO_{2asym.}$), 1340 (Ar-$NO_{2sym.}$). ^{1}H NMR ($CDCl_3$) δ: 1.28 (t, 6H, (2xC***H***$_3$)), 3.49 (q, 4H, (2xC***H***$_2$)), 6.54 (d, 1H, *J*=2.4 Hz, C_6H_3-***H***), 6.63 (dd, 1H, *J*=8.9, 2.4 Hz, C_6H_3-***H***), 7.66–7.76 (m, 2H, C_6H_5-***H***), 7.81–7.87 (m, 1H, C_6H_3-***H***), 8.23–8.09 (m, 2H, C_6H_5-***H***), 9.79 (s, 1H, –C***H***=O), ppm. ^{13}C NMR ($CDCl_3$) δ:12.42 (***C***H_3), 44.93 (***C***H_2), 104.37, 108.78, 116.25, 124.10, 128.04, 130.28, 131.67, 134.89, 147.24, 152.66, 153.26 (Ar-***C***), 165.35 (***C***=$O_{aldehyde}$), 186.85 (***C***=O_{ester}), ppm.

2.2.3 5-(Diethylamino)-2-formylphenyl 3-nitrobenzoate (3)

Pale brown solid, yield: 89%, m.p. 106-107°C. FT-IR, ATR (cm^{-1}): 3087 (C-$H_{arom.}$), 2974 (C-$H_{aliph.}$), 2821, 2719 (C-$H_{aldehyde}$), 1752 (C=O_{ester}), 1672 (C=$O_{aldehyde}$), 1600 (C=$C_{arom.}$), 1525 (Ar-$NO_{2asym.}$), 1348 (Ar-$NO_{2sym.}$). ^{1}H NMR (DMSO-d_6) δ: 1.14 (t, 6H, (2xC***H***$_3$)), 3.45 (q, 4H, (2xC***H***$_2$)), 6.68 (d, 1H, *J*=2.4 Hz, C_6H_3-***H***), 6.75 (dd, 1H, *J*=8.9, 2.4 Hz, C_6H_3-***H***), 7.71 (d, 1H, *J*=8.9 Hz, C_6H_3-***H***), 7.92 (t, 1H, *J*=8.0 Hz, C_6H_5-***H***), 8.52–8.60 (m, 2H, C_6H_5-***H***), 8.78–8.80 (m, 1H, C_6H_5-***H***), 9.66 (s, 1H, –C***H***=O), ppm. ^{13}C NMR (DMSO-d_6) δ: 12.75 (***C***H_3), 44.65 (***C***H_2), 105.20, 109.13, 115.87, 122.67, 124.68, 128.66, 131.30, 135.21, 136.39, 148.39, 152.99, 153.33 (Ar-***C***), 163.27 (***C***=$O_{aldehyde}$), 187.15 (***C***=O_{ester}), ppm.

2.2.4 5-(Diethylamino)-2-formylphenyl 4-dinitrobenzoate (4)

Shiny dark yellow solid, yield: 92%, m.p. 131-132 °C. FT-IR, ATR (cm^{-1}): 3106 (C-$H_{arom.}$), 2975 (C-$H_{aliph.}$), 2821, 2717 (C-$H_{aldehyde}$), 1740 (C=O_{ester}), 1665 (C=$O_{aldehyde}$), 1600 (C=$C_{arom.}$), 1525 (Ar-$NO_{2asym.}$), 1344 (Ar-$NO_{2sym.}$). ^{1}H NMR ($CDCl_3$) δ: 1.26 (t, 6H, (2xC***H***$_3$)), 3.47 (q, 4H, (2xC***H***$_2$)), 6.43 (d, 1H, *J*=2.4 Hz, C_6H_3-***H***), 6.65 (dd, 1H, *J*=8.9, 2.4 Hz, C_6H_3-***H***), 7.71 (d, 1H, *J*=8.9 Hz, C_6H_3-***H***), 8.37–8.44 (m, 4H, C_6H_5-***H***), 9.76 (s, 1H, –C***H***=O), ppm. ^{13}C NMR ($CDCl_3$) δ: 12.46 (***C***H_3), 44.91 (***C***H_2), 104.55, 108.72, 115.91, 123.71, 131.48, 135.02, 135.06, 150.84, 152.96, 153.11 (Ar-***C***), 163.36 (***C***=$O_{aldehyde}$), 186.57 (***C***=O_{ester}), ppm.

2.2.5 5-(Diethylamino)-2-formylphenyl 3,5-dinitrobenzoate (5)

Shiny dark yellow solid, yield: 96%, m.p. 149-150°C. FT-IR, ATR (cm^{-1}): 3058 (C-$H_{arom.}$), 2976 (C-$H_{aliph.}$), 2877, 2785 (C-$H_{aldehyde}$), 1749 (C=O_{ester}), 1675 (C=$O_{aldehyde}$), 1601 (C=$C_{arom.}$), 1540 (Ar-$NO_{2asym.}$), 1339 (Ar-$NO_{2sym.}$). ^{1}H NMR ($CDCl_3$) δ: 1.27 (t, 6H, (2xC***H***$_3$)), 3.49 (q, 4H, (2xC***H***$_2$)), 6.46 (d, 1H, *J*=2.4 Hz, C_6H_3-***H***), 6.67 (dd, 1H, *J*=8.8, 2.5 Hz, C_6H_3-***H***), 7.66 (d, 1H, *J*=8.8 Hz, C_6H_3-***H***), 9.32 (t, 1H, *J*=2.1 Hz, C_6H_5-***H***), 9.37 (d, 2H, *J*=2.1 Hz, C_6H_5-***H***), 9.66 (s, 1H, –C***H***=O), ppm. ^{13}C NMR ($CDCl_3$) δ (ppm): 12.42 (***C***H_3), 44.97 (***C***H_2), 104.71, 108.71, 115.41, 122.65, 130.15, 133.75, 136.81, 148.77, 153.13, 155.42 (Ar-***C***), 163.49 (***C***=$O_{aldehyde}$), 186.93 (***C***=O_{ester}), ppm.

2.3. Enzyme inhibition assays

Anticholinesterase assays

The inhibitory effects of synthesized molecules (**1-5)** on AChE and BChE were determined according to the modified spectrophotometric method of Ellman et al., [28]. In this study, the absorbance of each molecule was measured at 412 nm. The final solution of tested molecules was 200 µL. To calculate the percentage of both enzyme inhibitions, the following formula was employed:

$$\text{Inhibition (\%)} = (T_{control}-T_{sample}) / T_{control} \times 100$$

Where T is the absorbance. Galanthamine in this process was employed as a positive control. All tests were repeated three times.

Antityrosinase assay

Anti-tyrosinase activities of synthesized molecules (**1-5)** were determined according to the method designed by Hearing and Jimenez [29]. In this study, the absorbance of each molecule was measured at 475 nm. To calculate the percentage of all enzyme inhibitions, the following formula was employed:

$$\text{Inhibition (\%)} = (T_{control}-T_{sample}) / T_{control} \times 100$$

Where T is absorbance. Kojic acid was utilized as an inhibitor for the positive control. All tests were repeated three times.

Statistical analysis

The results of antityrosinase and anticholinesterase activities of the synthesized molecules were reported as the mean ± standard deviation (SD) of three parallel measurements. The statistical significance was predicted by employing a Student's t-test, where a p-value < 0.05 was considered significant.

3. Results and Discussion

3.1. Synthesis and characterization

In this research, the ester derivatives of 4-(diethylamino)salicylaldehyde (one new, three commercially available, and one known) (**1-5)** as target molecules were successfully attained in one step. These esters were readily prepared by the reaction of 4-(diethylamino)salicylaldehyde with an appropriate non-substituted or nitro-substituted benzoyl chloride derivative in the molar ratio of 1:1 in pyridine as a solvent, which provided excellent yields (**85–96%**). To attain these molecules purely, they were thoroughly purified by crystallization method and their melting points were established. After these processes were performed, their chemical structures were illuminated with ^{1}H and ^{13}C NMR, FT-IR spectroscopic analysis, respectively. The synthetic pathway to obtain the target molecules (**1-5**) is described in Scheme 1.

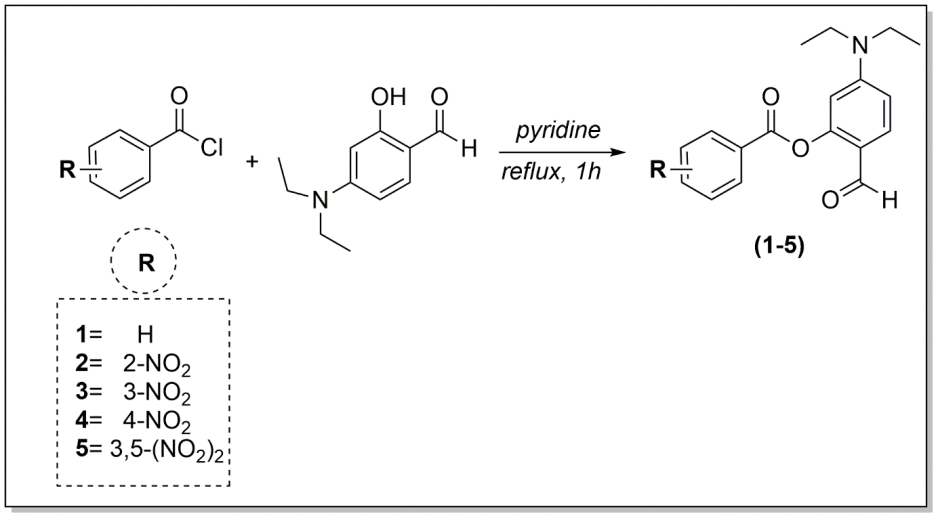

Scheme 1. Synthetic pathway to synthesis of ester derivatives (**1-5**)

IR spectra of all synthesized ester derivatives showed strong absorption peaks in the 1737–1752 cm^{-1} range, representing the presence of the C = O group of the ester, while the C = O band of the aldehyde group was established at 1652–1675 cm^{-1}. A weak two-band signal of the aldehyde group (–CHO) was observed at 2817–2877 cm^{-1} and 2712–2785 cm^{-1}, respectively. Weak absorption bands detected in the ranges of 3058–3106 cm^{-1} and 2976–2968 cm^{-1} correspond to aromatic and aliphatic C–H stretching vibrations, respectively. Also, the symmetrical and asymmetrical stretching bands of the aromatic-nitro group (Ar-NO_2) in the structures of molecules (**2-5**) were observed at 1339–1348 cm^{-1} and 1525–1540 cm^{-1}, respectively. ^1H and ^{13}C NMR spectra of all synthesized target molecules were established in $CDCl_3$ (only compound **3** in DMSO-d_6) as solvent. In ^1H NMR spectra of all synthesized molecules (**1-5)**, the proton peak signal of the aldehyde group (HC = O) was observed as singlet peaks at 9.66–9.89 ppm. The proton peak signals of the aromatic rings were determined as a doublet, doublet of doublet triplet, or multiplet, between 6.43 and 9.37 ppm. Furthermore, the methyl protons (–CH_3) of the diethylamino group (–$N(CH_2CH_3)_2$) resonated as triplet peaks at 1.14–1.28 ppm, while methylene (–CH_2–) protons resonated as quartet peaks at 3.45-3.49 ppm. ^{13}C NMR spectra of all synthesized molecules (**1-5)** were determined to show different resonances in good agreement with the proposed structure. For the molecules (**1-5)**, C = O signals of the ester and aldehyde groups were detected at 186.23–187.15 and 163.27–165.35 ppm, respectively. In the spectra, the signals of the aromatic ring carbons in the aromatic region were observed between 104.37 and 154.62 ppm. Additionally, methyl (–CH_3) carbon atoms belonging to the diethylamino group were detected at 12.42–12.7549 ppm, and the methylene (–CH_2) signal was detected around 44.65–44.97 ppm. Moreover, FT-IR, ^1H, and ^{13}C NMR spectrum of the ester derivatives (**1-5**) were given in the supplementary material (Figures S1-S15).

3.2. Biological evaluation

In this study, the ester derivatives of 4-(diethylamino)salicylaldehyde (**1-5)** were made ready, and then their inhibition properties on AChE, BChE, and tyrosinase enzymes were screened. In inhibition studies, the synthesized molecules (**1-5)** on AChE showed inhibitory activities with IC_{50} values in the range of 24.43-58.46 μM. In AChE assay, galanthamine was employed to be the standard with a 79.40±0.46% inhibition value. Among the tested molecules, compound **4** indicated the best inhibition with a 58.46±0.81 % value in AChE inhibitory activity. Compounds **1**, **3**, and **4** showed moderate anti AChE activities (Table 1). In BChE assay, the tested molecules (**1-5)** on BChE demonstrated inhibitory activities with IC_{50} values in the range of 37.53-87.28 μM. Compound **1** displayed very strong activity against BChE enzyme with 87.28±0.87 inhibition% better than

galanthamine (73.83±0.25 % inhibition) employed as standard. Compounds **2** and **3** were also good anti BChE inhibitory activities (Table 1). On the other hand, these molecules (**1-5)** on tyrosinase enzyme displayed inhibitory activities with IC_{50} values in the range of 20.15-87.73 µM. Kojic acid was utilized as standard molecules in tyrosinase enzyme inhibitory activity with 79.76±0.79 % inhibition. Compound **3** showed quite strong tyrosinase enzyme inhibitory activity, with 87.73±0.22 % inhibition, which is better than kojic acid (Table 1).

Table 1. AChE, BChE and tyrosinase inhibitory results of the synthesized molecules

Inhibitors	AChE	BChE	Tyrosinase
1	46.55±0.65	87.28±0.87	53.08±0.54
2	34.88±0.73	62.22±0.75	26.64±0.50
3	47.50±0.31	70.74±0.22	87.73±0.22
4	58.46±0.81	37.53±0.54	47.51±0.97
5	24.43±0.40	49.01±0.97	20.15±0.30
Galantamine[b]	79.40±0.46	73.83±0.25	-
Kojik acid[b]	-	-	79.76±0.79

[a] 200µM
[b] Standard compounds

4. Conclusion

In this research, five the ester derivatives of 4-(diethylamino)salicylaldehyde were easily synthesized and characterized by by FT-IR, ^{1}H and ^{13}C NMR. In the biological activity studies, the inhibitory properties of all synthesized molecules were examined one by one. All tested molecules demonstrated enzyme inhibition activities against AChE, and the activity ordering of the synthesized molecules on AChE was determined as **4**>**3**>1>**2**>**5**. In AChE assay, compound **4** with an electron-withdrawing nitro group at the *para* position of the phenyl ring showed better activity than others. In BChE assay, the activity ordering of the synthesized molecules on BChE was determined as **1**>**3**>**2**>**5**>**4**. It was determined that compound **1** with a non-substituted phenyl ring had a very high activity even than standard compound. In tyrosinase assay, the activity ordering of the synthesized molecules on tyrosinase enzyme was established as **3**>**1**>**4**>**2**>**5**. It was found out that compound **3** with an electron-withdrawing nitro group at the *meta* position of the phenyl ring had a very high activity even than standard compound. When the structure-activity relationships of the tested molecules were investigated, we concluded that both non-substituted and nitro-substituted inhibitors generally had enzyme inhibition activities, although at different rates. Finally, we can easily say that compounds **1** and **3** are of great importance as potential agents for BChE and tyrosinase inhibitors, respectively.

Conflict of interest:

The article's authors declare that there is no conflict of interest between them.

The Declaration of Ethics Committee Approval

The author declares that this document does not require an ethics committee approval or any special permission. Our study does not cause any harm to the environment.

Authors' Contributions:

R. Ç: Conceptualization, Methodology, Validation, Formal analysis, Investigation, Writing-original draft preparation, Writing - review&editing (%30)

E. Ç: Conceptualization, Validation, Investigation, Writing-original draft preparation (%25)

E. B: Conceptualization, Methodology, Validation, Formal analysis, Investigation, Writing-original draft preparation, Writing - review&editing (%25)

M. B: Validation, Writing-original draft preparation (%20)

The compliance to Research and Publication Ethics

This work was carried out by obeying research and ethics rules.

References

[1] Yokeş, M. B., "Molecular genetics of Alzheimer's Disease", *Journal of Cellular and Molecular Medicine*, 6, 73-97, 2007.

[2] Mesulam, M. M., *Principles of behavioral and cognitive neurology*. Oxford University Press, Oxford 2000.

[3] Lleo, A., Greenberg, S. M., Growdon, J. H., "Current pharmacotherapy for Alzheimer's disease", *Annual Review of Medicine*, 57, 513-533, 2006.

[4] Flynn, B. L., Ranno, A. E., "Pharmacologic management of Alzheimer disease part II: Antioxidants, antihypertensives, and ergoloid derivatives", *Annals of Pharmacotherapy*, 33, 188-197, 1999.

[5] Yaari, R., Corey-Bloom, J., "Alzheimer's disease", *Seminars in Neurology*, 27, 32-41, 2007.

[6] Hanağası, H. A., "Demans kavramı ve hastaya yaklaşım. Klinik Gelişim, 23, 44-47 2010.

[7] Özkay, Ü. D., The effect of some benzothiazole derivatives on the learning and memory parameters of streptozotocin model of alzheimer's disease in rats, Ph. D. thesis, Anadolu University, Eskişehir, TR, Eskişehir, 2009.

[8] Kazancioglu, E. A., Senturk, M., "Synthesis of *N*-phenylsulfonamide derivatives and investigation of some esterase enzymes inhibiting properties", *Bioorganic Chemistry*, 104, 104279, 2020.

[9] Arslan, T., Ceylan, M. B., Baş, H., Biyiklioglu, Z., Senturk, M., "Design, synthesis, characterization of peripherally tetra-pyridine-triazole-substituted phthalocyanines and their inhibitory effects on cholinesterases (AChE/BChE) and carbonic anhydrases (hCA I, II and IX)", *Dalton Transactions*, 49, 203-209, 2020.

[10] Telpoukhovskaia, M. A., Patrick, B. O., Rodríguez-Rodríguez, C., Orvig, C., "*In silico* to *in vitro* screening of hydroxypyridinones as acetylcholinesterase inhibitors", *Bioorganic and Medicinal Chemistry Letters*, 26, 1624-1628, 2016.

[11] Bajda, M., Więckowska, A., Hebda, M., Guzior, N., Sotriffer, C. A., Malawska, B., "Structure-based search for new inhibitors of cholinesterases", *International Journal of Molecular Sciences*, 14, 5608-5632, 2013.

[12] Özil, M., Balaydın, H. T., Şentürk, M., "Synthesis of 5-methyl-2, 4-dihydro-3H-1, 2, 4-triazole-3-one's aryl Schiff base derivatives and investigation of carbonic anhydrase and cholinesterase (AChE, BuChE) inhibitory properties", *Bioorganic Chemistry*, 86, 705-713, 2019.

[13] Rescigno, A., Sollai, F., Pisu, B., Rinaldi, A., Sanjust, E., "Tyrosinase inhibition: general and applied aspects", *Journal of Enzyme Inhibition and Medicinal Chemistry*, 17, 207-218. 2002.

[14] Loizzo, M. R., Tundis, R., Menichini, F., "Natural and synthetic tyrosinase inhibitors as antibrowning agents: an update", *Comprehensive Reviews in Food Science and Food Safety*, 11(4), 378-398, 2012.

[15] Różanowska, M., Sarna, T., Land, E. J., Truscott, T. G., "Free radical scavenging properties of melanin: interaction of eu-and pheo-melanin models with reducing and oxidising radicals" *Free Radical Biology and Medicine*, 26, 518-525, 1999.

[16] Zolghadri, S., Bahrami, A., Hassan Khan, M. T., Munoz-Munoz, J., Garcia-Molina, F., Garcia-Canovas, F., Saboury, A. A., "A comprehensive review on tyrosinase inhibitors", *Journal of Enzyme Inhibition and Medicinal Chemistry*, 34, 279-309, 2019.

[17] Gillbro, J. M., Olsson, M. J., "The melanogenesis and mechanisms of skin- lightening agents–existing and new approaches" *International Journal of Cosmetic Science*, 33, 210-221, 2011.

[18] Plensdorf, S., Livieratos, M., Dada, N., "Pigmentation disorders: diagnosis and management" *American Family Physician*, 96, 797-804, 2017.

[19] Kim, H., Choi, H. R., Kim, D. S., Park, K. C., Topical hypopigmenting agents for pigmentary disorders and their mechanisms of action. *Annals of Dermatology*, 24, 1, 2012.

[20] Nicolaidou, E., Katsambas, A. D., "Pigmentation disorders: hyperpigmentation and hypopigmentation", *Clinics in Dermatology*, 32, 66-72, 2014.

[21] Pillaiyar, T., Manickam, M., Jung, S. H., "Recent development of signaling pathways inhibitors of melanogenesis", *Cellular Signaling*, 40, 99-115, 2017.

[22] Pillaiyar, T., Manickam, M., Jung, S. H., "Downregulation of melanogenesis: drug discovery and therapeutic options", *Drug Discovery Today*, 22, 282-298, 2017.

[23] Pillaiyar, T., Namasivayam, V., Manickam, M., Jung, S. H., "Inhibitors of melanogenesis: an updated review", *Journal of Medicinal Chemistry*, 61, 7395-7418, 2018.

[24] Smit, N., Vicanova, J., Pavel, S., "The hunt for natural skin whitening agents", *International Journal of Molecular Sciences*, 10, 5326-5349, 2009.

[25] Kwak, S. Y., Choi, H. R., Park, K. C., Lee, Y. S., "Kojic acid–amino acid amide metal complexes and their melanogenesis inhibitory activities", *Journal of Peptide Science*, 17, 791-797, 2011.

[26] Topal, G., Tombak, A., Yigitalp, E., Batibay, D., Kilicoglu, T., Ocak, Y. S. (2017). Diester molecules for organic-based electrical and photoelectrical devices", *Journal of Electronic Materials*, 46(7), 3958-3964.

[27] Takahashi, T., Hijikuro, I., Sugimoto, H., Kihara, T., Shimmyo, Y., Niidome, T.. "Preparation of novel curcumin derivatives as βsecretase inhibitors", *PCT Int Appl*, WO 2008066151 A1, 2008.

[28] Ellman, G. L., Courtney, K. D., Andres Jr, V., Featherstone, R. M., "A new and rapid colorimetric determination of acetylcholinesterase activity", *Biochemical Pharmacology*, 7, 88-95, 1961.

[29] Hearing, V. J., Jiménez, M. Mammalian tyrosinase-the critical regulatory control point in melanocyte pigmentation. *International Journal of Biochemistry*, 19, 1141-1147, 1987.

Middle East Journal of Science

https://dergipark.org.tr/mejs **MEJS**

e-ISSN:2618-6136

Research Article

IN-VITRO INVESTIGATION OF DONKEY MILK EFFICACY AGAINST STANDARD STAPHYLOCOCCUS AUREUS STRAINS

Akın YİĞİN [1*] ***Mehmet DEMİRCİ*** [2] ***Serap KILIÇ ALTUN*** [3] ***Bekir Sami KOCAZEYBEK*** [4]

[1*]Harran University, Faculty of Veterinary, Department of Genetics, Şanlıurfa, Turkey
[2*]Kırklareli University, Faculty of Medicine, Department of Medical Microbiology, Kırklareli, Turkey
[3*]Harran University, Faculty of Veterinary, Department of Food Hygiene and Technology, Şanlıurfa, Turkey
[4*]İstanbul Cerrahpaşa University, Faculty of Medicine, Department of Medical Microbiology, İstanbul, Turkey
* Corresponding author; skilicaltun@harran.edu.tr

Abstract: *Donkey milk, which is very similar to breast milk in terms of protein profile and lactose content, has been used for therapeutic purposes since ancient times. Different studies report its antimicrobial activity against an important human pathogen such as S. aureus. Therefore, in our study, we aimed to examine the antimicrobial efficacy of donkey milk against standard MRSA and MSSA strains in-vitro environment. In our study, in-vitro antimicrobial efficacy of donkey milk obtained from 53 different donkeys against S. aureus ATCC 43300 (MRSA) and S. aureus ATCC 29213 (MSSA) was investigated by broth microdilution method. Donkey milk mixed with TSB medium at different serial dilution rates was studied in 96 microwell plates. When the effectiveness of different concentrations of donkey milk added to TSB medium in vitro against ATCC MRSA and MSSA strains was examined, no suppression was observed, and growth was found to be higher than the control results after 24 hours of incubation at high milk concentrations. In conclusion, according to the results of our study, no antimicrobial effect of donkey milk was observed in-vitro against standard MRSA and MSSA strains. This situation may be caused by the fact that S. aureus strains may have different virulence abilities, as well as the differences in protein structure in milk between species.*

Keywords: *MRSA, MSSA, Donkey milk*

Received: October 26, 2021 Accepted: December 20, 2021

1. Introduction

Milk has also been an essential component of human nutrition since the domestication of animals, as it provides important nutrients to all mammals and plays a critical role in health. In recent years, the number of individuals suffering from intolerances and allergic reactions arising from cow's milk ingestion has increased, leading to the search for alternative foods [1, 2]. The donkey is a member of the Equidae family and has become widespread in Africa, Asia, South America, and Europe with the domestication process that started in 6000 BC. It has been used for lifetimes ranging from 30 to 50 years as a pack animal for transport or riding. The donkey is also an animal serving humanity in the fields of milk production (in the food and cosmetic industry), meat production, ecotourism, and onotherapy.

Donkey milk is known for its therapeutic properties and has been used since ancient times in the treatment of various diseases such as wound healing, bronchitis, asthma, joint pain, and gastritis. Today, it is also available as a commercial product for people allergic to cow's milk proteins, newborns, and the elderly [1]. The donkey milk used by Hippocrates and Avicenna as a remedy for different diseases or by the Egyptian Queen Cleopatra in her bath to keep her skin soft and moist has been found to be very

similar to breast milk, especially in terms of protein profile and lactose content. Thanks to this structure, it stimulates the absorption of calcium from the intestine and thus provides the development of intestinal flora in humans. In addition, it is thought that high lysozyme content selectively creates antibacterial properties against pathogenic microorganisms [2, 3].

Staphylococcus aureus (*S. aureus*) is an important zoonosis responsible for a wide range of diseases and is a commensal microorganism [4, 5]. Prior to the use of methicillin, methicillin-sensitive *S. aureus* (MSSA) strains were almost the only cause of both serious and uncomplicated *S. aureus* infections in healthy individuals [6]. But shortly after methicillin became available in clinics, strains of methicillin-resistant *S. aureus* (MRSA) were reported and, since then, MRSA outbreaks have been observed worldwide. Control of MRSA is still an important problem in hospitals [5]. In some studies, it has been reported that donkey milk have different levels of antimicrobial activity against *S. aureus* strains [7, 8]. Therefore, we aimed to examine the effectiveness of different dilution rates of donkey milk against *S. aureus* strains, which is an important problem all over the world, and to determine the antimicrobial effect of standard MRSA and MSSA strains in-vitro [8, 9].

2. Material Method

2.1. Bacterial origins

S. aureus ATCC 43300 (MRSA) and *S. aureus* ATCC 29213 (MSSA) strains were used in our study. *S. aureus* strains were incubated in 5% sheep blood agar (Oxoid, UK) at 37ºC in an environment with 5% CO2 for 24 hours. After incubation, 0.5 McFarland suspensions prepared in sterile saline were used from colonies of S. aureus ATCC 43300 (MRSA) taken from blood agar medium [9].

2.2. Donkey Milk samples

In our study, 53 different donkey milk offered for sale in different regions of Turkey were purchased raw and these milks were used for in-vitro treatment with MRSA and MSSA strains [10].

2.3. Determination of MIC and MBC values by examining the antimicrobial effect

The effect of donkey milk on *S. aureus* ATCC 43300 (MRSA) and *S. aureus* ATCC 29213 (MSSA) strains were examined and the liquid microdilution method was used to define the minimal inhibitory concentration (MIC) and minimal bactericidal concentration (MBC) levels [11]. 5, 10, 20, 40, 80, 160, 320, 640 µL (0.5%, 1%, 2%, 4%, 8%) of donkey milk into a tube containing tryptic soy broth broth (Oxoid, UK) , 16%, 32%, 64%) were added and serial dilutions were made in a total volume of 1 mL. 180 µL of liquid TSB medium containing donkey milk was added to 96-well plates and 20 µL of 0.5 McFarland bacterial suspensions were added on top. Data obtained from 200 µL of milk-free TSB medium for negative control and 180 µL of non-milk-free TSB medium for positive control and 20 µL of bacterial suspensions were considered. After inoculations, 96-well plates were incubated at 37ºC for 24 hours. Bacterial growth in each well was measured at 600 nm using an Epoch spectrophotometer (Biotek, Germany) according to the manufacturer's instructions. The values at which growth was suppressed 100% were accepted as the MIC value. In order to determine the MBC value, the samples with MIC value were incubated in 5% sheep blood agar (Oxoid, UK) at 37ºC in an environment with 5% CO_2 for 48 hours and the values without growth were accepted as MBC [11, 12].

3. Results and Discussion

When the effectiveness of different concentrations of donkey milk added to TSB medium in-vitro against ATCC MRSA and MSSA strains was examined, it was found that there was no suppression

and that even at high milk concentrations, the growth was higher than the control group after 24 hours of incubation. The results are given in Table 1.

It was determined that the reproduction of MSSA strains was less affected by donkey milk than MRSA strains and MRSA strains were able to grow more in this medium at all dilution ratios. Since 100% suppression was not observed in all dilution ratios, MIC value and related MBC value were not determined.

Table 1. Growth percentages and standard deviation data of MRSA and MSSA strains in-vitro in donkey milk added to TSB medium

Donkey milk concentration in TSB medium	**0.5%**	**1%**	**2%**	**4%**
S. aureus ATCC 29213 (MSSA)%	97.22±1.5	95.78±2.4	98.43±1.4	105.72±1.8
S. aureus ATCC 43300 (MRSA)%	98.68±1.9	98.3±2.6	99.41±1.7	108.62±2.2
Donkey milk concentration in TSB medium	**%8**	**%16**	**%32**	**%64**
S. aureus ATCC 29213 (MSSA)%	112.41±1.1	114.74±1.7	121.56±2.7	128.3±3.2
S. aureus ATCC 43300 (MRSA)%	121.36±1.4	128.3±1.8	129.71±2.1	131.4±2.9

Donkey milk is traditionally consumed in Asia, Eastern Europe, and Africa, however, when the positive effect on human health became widespread, took its place in developed country markets with increasing consumer awareness [13]. The antimicrobial activity in donkey milk is mainly due to lactoferrin, lysozyme, immunoglobulins, and lactoperoxidase. It is thought to originate from some small whey protein structures such as ingredients. It can vary greatly between species, races, and individuals due to genetic or reproductive variants [14].

When the studies examining the antimicrobial activity of donkey milk against *S. aureus* were checked; In a study conducted by Yirmibeşoğlu and Öztürk in 2020 they examined the zone diameters of donkey milk-impregnated discs against *S. aureus*, they found this zone diameter to be 11,5 mm, and the ampicillin zone diameter they added for control purposes was 22 mm [7]. In Koutb et al.'s study in 2016, they found that donkey milk-impregnated discs formed a zone diameter of 18 mm against *S. aureus* ATCC 8095, and the minimum lethal concentration was 64 when they examined it [8]. In Saric et al.'s study in 2014, they reported that the antibacterial effect of donkey milk against *L. monocytogenes* and *S. aureus* increased especially during the bacterial lag phase, and inhibited the growth of bacteria in this period. In this study, *S. aureus* was inhibited after 8 hours. It was stated that there was not even a 1 log increase in reproduction compared to the control [15]. Contrary to the studies of Koutb et al. (8) and Yirmibeşoğlu and Öztürk [7], our results were similar to Saric's study, no value that would show a minimum inhibitory concentration was observed in the in-vitro environment. Since we did not examine the lag phase and different durations in our study as in Saric's study [15], we did not find the antimicrobial effect of donkey milk at different points. Similar to the data in our study, Pilla et al. reported that they found the presence of *S. aureus* in donkey milk samples when they examined the hygienic status of donkey milk in 2010 [16]. Their results also support the data in our study. Although different enzymes are mentioned in its content, milk does not show this effect despite *S. aureus* origins. We think that the reason for this may be due to the rich protein structure in its content.

4. Conclusion

In conclusion, according to the results of our study, no antimicrobial effect of donkey milk was observed against standard MRSA and MSSA strains in-vitro. The reason for this situation may be due

to the fact that the protein content of the milk obtained from different donkey species is different, as well as the ability of *S. aureus* to adapt to different environments and produce different virulence factors that can live there. We believe that comprehensive studies should be conducted on donkey milk, which is close to breast milk.

Conflict of interest

No conflict of interest or common interest has been declared by the author.

The Compliance to Research and Publication Ethics

This work was carried out by obeying research and ethics rules.

The Declaration of Ethics Committee Approval

The author declares that this document does not require an ethics committee approval or any special permission. Our study does not cause any harm to the environment.

Authors' Contributions

A.Y.: Conceptualization, Methodology, Formal analysis, Writing

M.D.: Conceptualization, Methodology, Resources, Investigation

S.K.A.: Methodology, Writing - Original draft preparation

B.S.K..: Methodology, Writing - Original draft preparation

References

[1] Derdak R, Sakoui S, Pop OL, et al. "Insights on Health and Food Applications of Equus asinus (Donkey) Milk Bioactive Proteins and Peptides-An Overview". *Foods*. 9(9), 1302-? 2020. doi:10.3390/foods9091302

[2] Martini M., Altomonte I., Licitra R., Salari F. "Nutritional and Nutraceutical Quality of Donkey Milk". *J. Equine Vet. Sci.*, 65, 33–37, 2018. doi: 10.1016/j.jevs.2017.10.020

[3] Osman Swar M. "Donkey milk-based formula: A substitute for patients with cow's milk protein allergy". *Sudan J Paediatr*., 11(2), 21-24, 2011.

[4] Gordon RJ, Lowy FD. "Pathogenesis of methicillin-resistant Staphylococcus aureus infection". *Clin Infect Dis.*, 46 Suppl 5(Suppl 5), 350-359, 2008. doi:10.1086/533591

[5] Branger C, Gardye C, Galdbart JO, Deschamps C, Lambert N. "Genetic relationship between methicillin-sensitive and methicillin-resistant Staphylococcus aureus strains from France and from international sources: delineation of genomic groups". *J Clin Microbiol.* 41(7), 2946-2951, 2003. doi:10.1128/jcm.41.7.2946-2951.2003

[6] David MZ, Boyle-Vavra S, Zychowski DL, Daum RS. "Methicillin-susceptible Staphylococcus aureus as a predominantly healthcare-associated pathogen: a possible reversal of roles? ". *PLoS One.*, 6(4), e18217, 2011. doi:10.1371/journal.pone.0018217

[7] Yirmibeşoğlu SSS, Öztürk BET. "Comparing microbiological profiles, bioactivities, and physicochemical and sensory properties of donkey milk kefir and cow milk kefir". *Turkish Journal of Veterinary and Animal Sciences*, 44 (4), 774-781, 2020.

[8] Koutb M, Khider M, Ali EH et al. "Antimicrobial Activity of Donkey Milk Against Dermatomycotic Fungi and Foodborne Bacteria". *International Journal of Biomedical Materials Research*., 4, 11-17, 2016. doi: 10.11648/j.ijbmr.20160403.11

[9] Dinç H, Demirci M, Yiğin A. "*Lactobacillus acidophilus* ve *Lactobacillus casei*'nin, metisilin dirençli ve metisilin duyarlı *Staphylococcus aureus* biyofilm genlerine in-vitro etkisinin incelenmesi". *Eurasian Journal of Veterinary Sciences*, *35*(1), 44-48, 2019.

[10] Demirci M, Yigin A, Altun SK, Uysal HK, Saribas S, Kocazeybek BS. "*Salmonella* Spp. and *Shigella Spp*. detection via multiplex real-time PCR and discrimination via MALDI-TOF MS in different animal raw milk samples". *Niger J Clin Pract*., 22(8), 1083-1090, 2019. doi: 10.4103/njcp.njcp_596_18.

[11] Kesici S, Demırci M, Kesici U. "Efeitos antimicrobianos do fentanil e da bupivacaína: estudo in vitro [Antimicrobial effects of fentanyl and bupivacaine]", *Rev Bras Anestesiol*., 70(4), 357-363, 2020. doi: 10.1016/j.bjan.2020.04.010.

[12] Assiri AMA, Elbanna K, Al-Thubiani A. et al. "Cold-pressed oregano (Origanum vulgare) oil: a rich source of bioactive lipids with novel antioxidant and antimicrobial properties", *Eur Food Res Technol*., 242, 1013–1023 (2016). doi:10.1007/s00217-015-2607-7

[13] Šarić, L., Pezo, L., Šarić, B. et al. "Calcium-dependent antibacterial activity of donkey's milk against Salmonella", *Ann Microbiol.,* 67, 185–194, (2017). doi:10.1007/s13213-016-1250-2

[14] Brumini, D., Criscione, A., Bordonaro, S. et al. "Whey proteins and their antimicrobial properties in donkey milk: a brief review", *Dairy Sci. & Technol.,* 96, 1–14, (2016). doi:10.1007/s13594-015-0246-1

[15] Ljubiša Šarić et al., "Antibacterial activity of Domestic Balkan donkey milk toward Listeria monocytogenes and Staphylococcus aureus", *Food and Feed Research*, 41(1), 47-54, 2014.

[16] Pilla, R., Daprà, V., Zecconi, A., Piccinini, R., "Hygienic and health characteristics of donkey milk during a follow-up study", *J Dairy Res*, 77(4), 392-7, 2010. doi: 10.1017/S0022029910000221.

Middle East Journal of Science

https://dergipark.org.tr/mejs **MEJS**

e-ISSN:2618-6136

Research Article

INVESTIGATION OF PLACENTAL HOFBAUER CELLS BY IMMUNOHISTOCHEMISTRY METHODS IN COMPLICATED PREGNANCIES

Yusuf Nergiz [*1] ***Şebnem Nergiz*** [2] ***Fırat Aşır*** [3] ***Ayşe Şahin*** [4] ***Elif Ağaçayak*** [5]

[1]University of Dicle, Faculty of Medicine, Dept. of Histology and Embryology, Diyarbakır
[2]University of Dicle, Atatürk Health School, Department of Microbiology, Diyarbakır. , Diyarbakır
[3]University of Dicle, Faculty of Medicine, Dept. of Histology and Embryology, Diyarbakır
[4] Hospital of Obstetrics and Gynecology and Children, Diyarbakır
[5]University of Dicle, Faculty of Medicine, Dept. of Obstetrics and Gynecology, Diyarbakır
[*] Corresponding author; yusufnergiz21@gmail.com

Abstract: *Development of the placenta without any complication is essential for normal pregnancy. The placenta is a multifunctional organ that plays a vital role in fetal development. Hofbauer cells are one of the most important groups of placental cells. These cells are placental macrophages and have a role in many placental events. The aim of this study is to investigate the placental distribution and density of Hofbauer cells and to contribute to the understanding of the causes and pathogenesis of complicated pregnancies. In this study, 60 full-term placentas were divided into 4 equal groups: control, preeclampsia, gestational diabetes (GDM), and (hemolysis, elevated liver enzymes, low platelet) HELLP group. The placenta was dissected and the samples were fixed 10% neutral buffered formalin. Following routine paraffin wax procedure, 5 µm sections were stained with CD68 for marking Hofbauer cells. In immunohistochemical evaluation, Hofbauer cells in villous stroma showed positive CD68 expression. Immunostaining Findings: CD68 showed a granular staining pattern in the cytoplasm of Hofbauer cells. The group with the highest CD68 positive cell number was HELLP group and the number of cells per cell (1.46 ± 0.25) was significantly different from all groups. CD68 positive cell count in the placental villus was the highest in HELLP group and the number of Hofbauer cells per villus was significantly different from the other groups.*

Keywords: *Hofbauer cells, CD68, preeclampsia, HELLP syndrome, gestational diabetes*

Received: October 05, 2021 Accepted : December 21, 2021

1. Introduction

Preeclampsia (PE) is characterized by proteinuria >300 mg/24 hours, spot urine protein/creatinine >0.3≥1, high liver enzymes, thrombocytopenia, and hypertension >160/110 mmHg.The etiology of preeclampsia is still unknown. Vascular lesions in various organ systems, vasospasm, increased platelet activation, and platelet degeneration, and subsequent activation of the intravascular coagulation system are essential causes that induce preeclampsia. Preeclampsia is a quite popular topic since it causes complications at a rate of 6-8% after the 24th week of pregnancy and is responsible for 20-25% of all perinatal deaths [1].

Gestational diabetes mellitus (GDM) is a type of diabetes observed in the second or third trimester of pregnancy. Gestational diabetes developed due to the metabolic and hormonal changes in pregnancy, leading to carbohydrate intolerance; high blood sugar with insulin resistance after the 24th week of pregnancy. GDM is one of the prediabetes conditions that pose a risk for the development of type 2 diabetes in future life. GDM is one of the most common pregnancy problems with macrosomia,

birth injuries, cesarean section, hydramnios to various maternal and fetal complications. GDM may trigger preeclampsia, neonatal metabolic disorders, and Type 2 DM development after birth [2].

The formation of the placenta is highly complicated and mediated through fetal extraembryonic tissues and the endometrial tissues during pregnancy. During early pregnancy (approximately 10th day), numerous macrophages invade placental tissue. A full-term placenta without any complications is essential for a normal pregnancy. The placenta plays a vital role in fetal development. Hofbauer cells are one of the most important groups of placental cells. These cells are placental macrophages and have a role in many placental events [3].

There have been many studies indicating the presence of stromal large cells of the human chorionic villi since the 19th century. These villous stromal cells were identified by Kastchenko in 1884, while Virchow and later Chaletzky-Neumann were reporting large cells with clear cytoplasm isolated in the pregnancies with mole hydatid [4].

Previously, the term "Chalatezky-Neumann cells" has been used by many researchers. However, at the beginning of the 20th century, the morphological and functional definition of these cells in normal villi was described by Hofbauer [5].

After this definition, the term Hofbauer cells (HBCs) was widely used in the literature. Round, fusiform, or star-like Hofbauer cells are localized in the villous stroma and are pleomorphic. Their size depends on the length of their process with a diameter of 10-30 μm. In the first studies, the most striking feature of Hofbauer cells is that they have a granular cytoplasm with vacuoles [6].

In later studies, electron-lucent vacuoles of different volumes surrounded by numerous membranes were observed in the cytoplasm of these cells. In addition, lysosomes containing granules of varying density and short endoplasmic reticulum profiles were noted [7-11).

Many theories have been proposed about the origin of Hofbauer cells. Chaletzky suggested that these cells originate from the maternal decidua; Neumann stated they were from the syncytium, whereas other researchers have suggested that they originate from the endothelium [5]. The most important finding in this regard is that these cells, which Wynn claims based on sex chromatin staining, are of fetal origin [12]. Thus, most researchers believe that Hofbauer cells are of chorionic mesenchymal origin. These cells can be identified in the placental villi in early development (after the 18th day of pregnancy). In the placentas of uncomplicated pregnancies, Hofbauer cells either disappear or are found singlet after the fourth month of pregnancy. On the other hand, there is an increase in the density of these cells in pathological placental cases such as intrauterine growth retardation and gestational diabetes [8, 10, 13].

These cells are capable of both immune and non-immune phagocytosis in addition to their essential functions. They can capture maternal antibodies that pass into placental tissue. They are also an important source of thromboxane, prostaglandins, and cytokines in the placenta [14-16]. High levels of phagocytosis confirm the functions of these cells [17]. Recently, there have been reports that Hofbauer cells express "sprout" proteins and thus play an important role in the branching of the villous tree and the development of the placenta [18-19].

The aim of this study is to investigate the placental distribution and density of Hofbauer cells and to contribute to the understanding of the causes and pathogenesis of complicated pregnancies.

2. Materials and Methods

This study was approved by the Dicle University Medical School Non-interventional Ethical Committee with the record number of 2016/194. 60 full-term placentas were divided into 4 equal groups: control, preeclampsia, gestational diabetes, and HELLP group.

Group I: Control group

Group II: Preeclampsia group.

Group III: Gestational diabetic group.

Group IV: HELLP group.

a)Histological procedure: Placentas were dissected and the samples were fixed 10% neutral buffered formalin. Following routine paraffin wax procedure, 5 µm sections were stained with CD68 (Abcam, CAT No: ab133386) for marking Hofbauer cells. 5 µm sections from paraffin blocks were taken on positively charged slides. For Hofbauer cells, immunostaining was performed by streptavidin-biotin immunoperoxidase method using CD68 antibody (Neomarkers. prediluted).

CD68 Staining Protocol

Paraffin sections were kept in an oven at 56°C overnight, and then deparaffinized by keeping them in xylol for 2x15 minutes.

For cleaning, sections were kept in xylene, later in descending alcohol series (100%, 100%, 96%, 90%, 80%, 70%), and finally brought to distilled water for 5 minutes.

Sections were washed in PBS and confined in a circle with a hydrophobic pen.

Afterward, 3% hydrogen peroxide was dropped on the sections, and the endogenous peroxidase activity was blocked after waiting for 5 minutes.

The sections were washed in buffered phosphate saline (PBS) solution for 3x minutes.

The sections were placed in a special container containing citrate solution and boiled in a microwave oven for 10 minutes to release the antigen.

Sections were left to cool at room temperatures and later 100 microliters of CD68 primary antibody(1:750) were dropped on the sections for 45 minutes.

Sections were washed in PBS and then, the same amount of biotinylated secondary antibody (1:750) was added for 20 minutes.

Sections were incubated for enzyme binding with streptavidin peroxidase (Thermo, cat no: TS-125-HR) for 30 minutes at room temperature.

After incubation with streptavidin peroxidase, it was washed 3x5 minutes with PBS

Sections were reacted with 3,3'diaminobenzidine (DAB) chromogen (Thermo, cat no: TA-125-HD).

The reaction was observed under the microscope and then transferred to PBS to terminate the reaction.

Sections were counterstained with Mayer hematoxylin for 40 seconds.

Sections were washed under tap water for about 5 minutes.

Sections were kept in increasing alcohol series for 5 minutes.

Sections were kept in Xylol for 2x15 minutes and cleared.

The sections were then mounted with medium, and the sections were left to dry at room temperature.

Brown cytoplasmic staining was evaluated as positive in Hofbauer cells detected in villous stroma by CD68. The sections were examined with Zeiss Imager A2 light microscope and micrographs were taken.

b) Statistical analysis: Placenta sections in all groups were stained with CD68 in order to see placental Hofbauer cells accumulation. 10 placenta sections of each group were randomly selected and 100 villi were counted in each section in order to evaluate Hofbauer cells.

Syncytial layer, villus stroma, and /or Hofbauer cells were positively stained, and the mean of groups was calculated. The data were evaluated by One-Way Anova and Post-Hoc Tukey tests with SPSS 24 (IBM, USA). Results were analyzed by multiple comparisons and $p<0.05$ was considered significant.

Ethical statement:

This study was carried out in accordance with the rules of research and publication ethics. The study was approved by the Dicle University Medical School Non-Interventional Ethics Committee (5/5/2016/194.).

3. Results

a) CD 68 Immunostaining results

We would like to emphasize that the placental Hofbauer cells were stained quite intensively with CD68 and that this staining shows a gradual increase in the control, preeclampsia, gestational diabetes, and HELLP groups (Figure 1-4). CD68 showed a granular staining pattern in the cytoplasm of Hofbauer cells. The reason for this particular staining is that the CD68 antibody is activated by the lysosomal granules of Hofbauer cells.

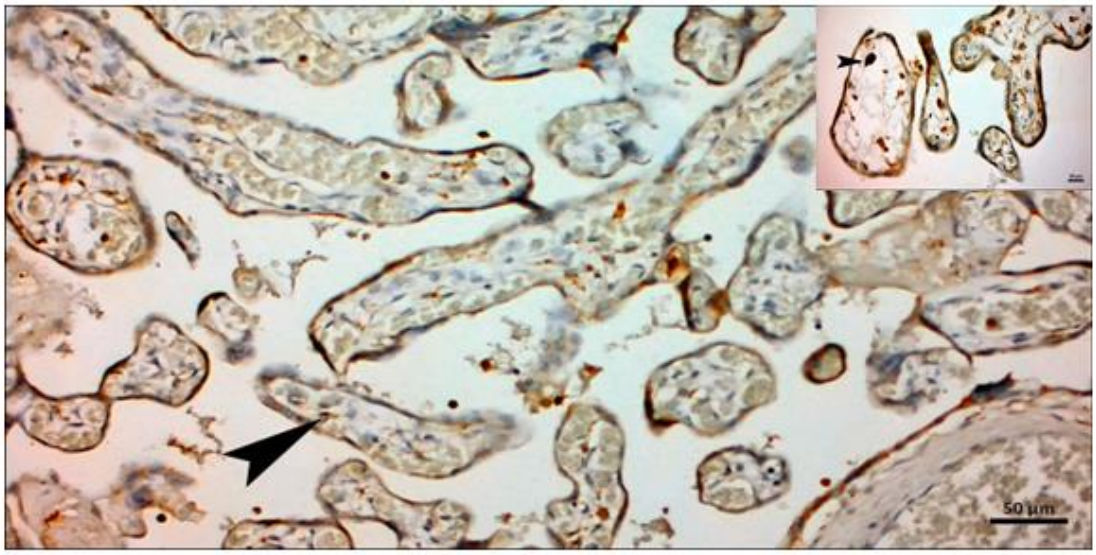

Figure 1. CD68 immunoreactivity in Hofbauer cells in placental tissue of the control group. Hofbauer cells show a small number of CD68 immunopositive reactions in mature villi. The inset shows some of Hofbauer cells (Black arrow) at higher magnification.

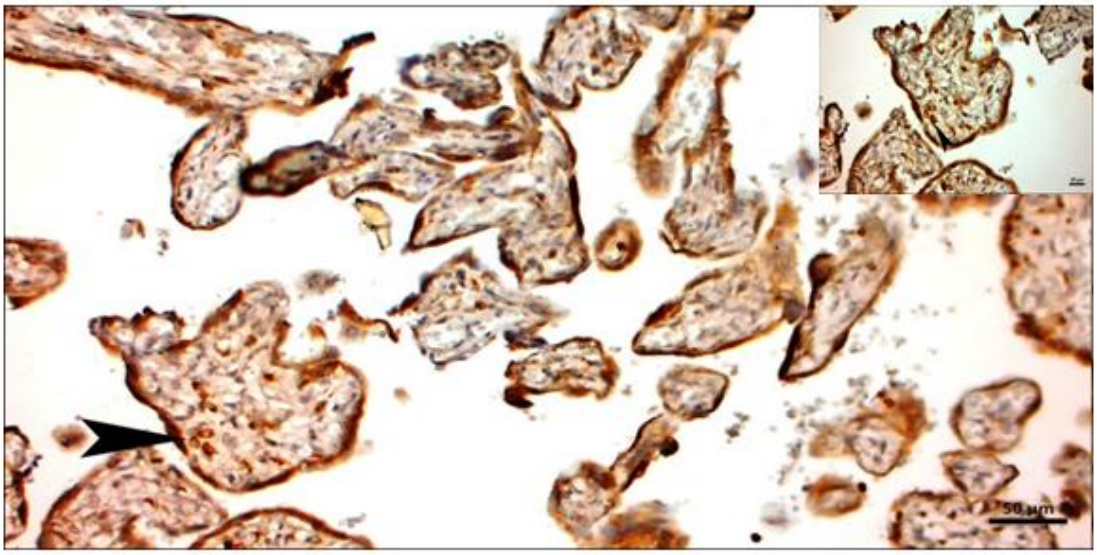

Figure 2. CD68 immunoreactivity in Hofbauer cells in placental tissue belonging to the group of gestational diabetes mellitus. CD68 immunopositive Hofbauer cells (black arrow) showed a relative increase in mature villi in the gestational diabetes mellitus group compared to the control group, (CD68, Bar: 50 μm). The inset shows a high magnification Hofbauer cells in high density.

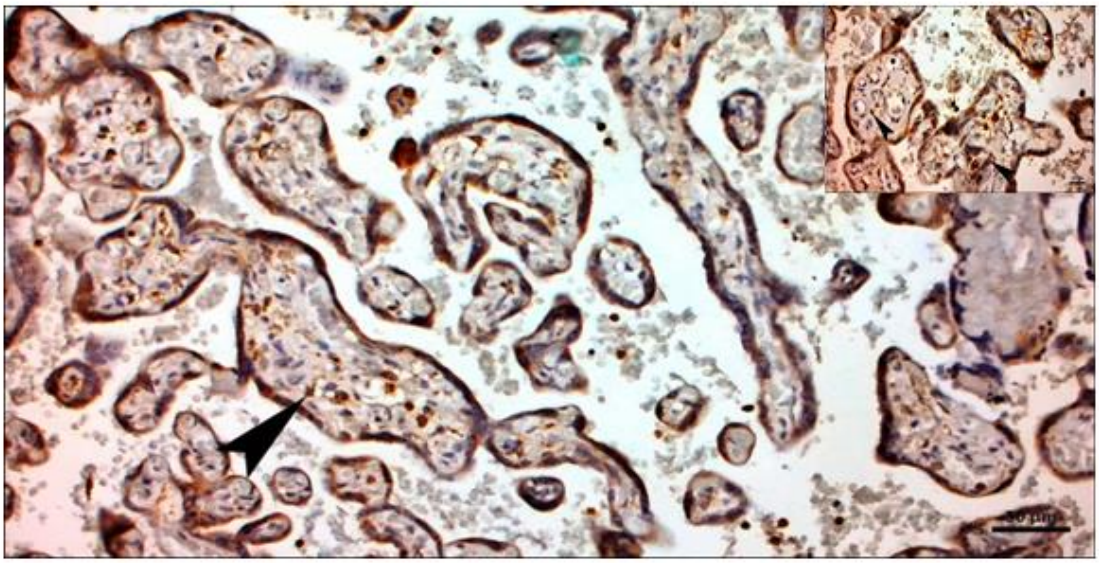

Figure 3. CD68 immunoreactivity in Hofbauer cells in placental tissue belonging to the preeclampsia group. CD68 immunopositive Hofbauer cells (black arrow) increased in the preeclamptic group compared to the control group (CD68, Bar: 50 μm). Hofbauer cells are seen in the histological section of the intermediate villi at high magnification.

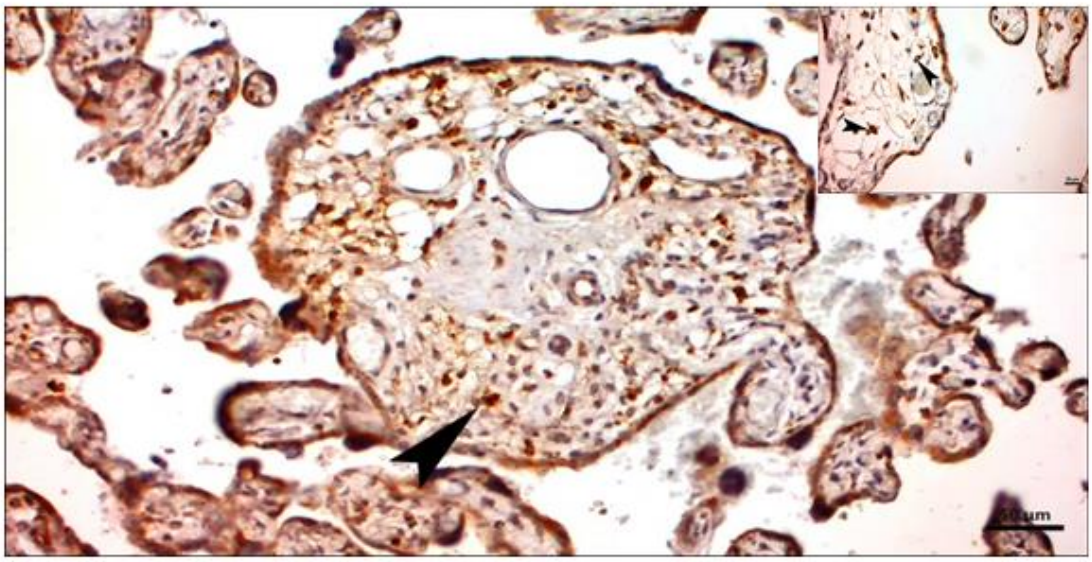

Figure 4. CD68 immunoreactivity in Hofbauer cells in placental tissue belonging to the HELLP group. In HELLP group placental sections, CD68 immunopositive Hofbauer cells (black arrow) showed a marked increase compared to the control group (CD68, Bar: 50 μm). The inset shows A large number of Hofbauer cells are seen in the stroma of the intermediate villus.

b) Statistical analysis results: It was found that the number of Hofbauer cells was 0,88 ± 0,21 in the preeclamptic group where the number of CD68 positive Hofbauer cells per villus was 0,46 ± 0,09 in the control group and this increase was significant compared to the control group ($p<0.05$). The number of cells per villus in the gestational diabetes group was 0.96 ± 0.15 and this increase was significant compared to the control group ($p <0.01$), but there was no significant difference between the preeclampsia group and the Gestational diabetes groups (0.05). The group with the highest CD68 positive cell number was HELLP group and the number of cells per villus (1.46 ± 0.25) was significantly different from all groups (Table 1).

Table 1. CD 68 positive Hofbauer Cells count in each villus

Groups	CD68+ cells (mean±sd)
Control group	0.46±0.09
Preeclampsia group	0.88±0.21
Gestational Diabetes group	0.96±0.15
HELLP group	1.46±0.25

4. Discussion

The placenta is a temporary organ necessary for the development of the embryo and fetus. There are many cells in the placenta. The most important of these are Hofbauer cells. There are limited studies on Hofbauer cells related to preterm birth. This is particularly the case in chorioamnionitis, which causes HELLP syndrome, severe preeclampsia, and spontaneous preterm delivery. In two independent studies, the number of CD68+ Hofbauer cells in the chorioamnionitis was found to be significantly lower [7, 20].

The mechanism of the low number of Hofbauer cells in chorioamnionitis is unknown, but it is estimated that these cells go to apoptosis. These cells especially transform into multinucleated giant cells in the placenta with chorioamnionitis. These cells have reduced immunological abilities when compared to Hofbauer cells in normal pregnancy [20].

Although HELLP is commonly observed with preeclampsia, it is actually a separate syndrome. The clinical presentation of preeclampsia and HELLP are different [21-22]. Preeclampsia is typically characterized by hypertension and proteinuria, while HELLP is mostly associated with the coagulation system.

HELLP and preeclamptic placentas show clinical differences in pathological aspects [22]. Although events such as infarction and intervillous thrombosis are very common in the placentas of patients with preeclampsia, this situation is less common in the placentas of patients with HELLP [21]. Generally, Hofbauer cell count and IL-10 are clearly low in patients with severe preeclampsia [23-24]. In preeclampsia, the scarcity of Hofbauer cells promotes inflammatory damage. On the other hand, the number of CD68+ Hofbauer cells is high in patients with HELLP. This excess of cells may be due to increased inflammation and the resulting response [22].

Hofbauer cells, one of the cell types in the placenta, are placental macrophages. Although there are many studies related to these cells, their possible roles in vasculogenesis and angiogenesis processes in the placenta have not been studied much. In a study conducted for this purpose, it was stated that the location and number of Hofbauer cells may be related to the vascular structures in the center of the villus, and thus these cells may play a role in vasculogenesis and angiogenesis. Curettage materials taken in the first trimester were used as placental tissue for the study.

Double immunohistochemical staining was performed with CD68 (macrophage marker) and CD31 (endothelial marker) to show the relationship of Hofbauer cells with primitive vessel formation. As a result, Hofbauer cells are thought to be involved in vasculogenesis and angiogenesis times, since they correlate with vascular structures [18]. In our study, we examined the change in the presence of gestational diabetes, preeclampsia, and HELLP syndrome in Hofbauer cells, which are thought to be involved in this process, which is very important for the development and functionality of the placenta, such as vascularization. We found that the placentas of pregnant women in the diabetic group and the preeclamptic group in our study, especially in pregnant placentas with HELLP syndrome, had more immunopositive Hofbauer cells in the villus stroma than in healthy pregnant women.

In another study, the number and functions of Hofbauer cells in the placenta were evaluated by examining pregnant placentas with complications of gestational diabetes. Tissue samples were taken for PCR and immunohistochemical evaluations from the placentas of 15 pregnant women with GDM and 10 healthy pregnant women for the study. CD68 and CD14 were selected as Hofbauer markers and IL-6 and TNF-alpha for inflammatory cytokines. As a result of immunohistochemistry staining, it was determined that CD68+ or CD14+ cells were significantly increased in the GDM group compared to the control group. According to these results, it is reported that Hofbauer cells increase in GDM pathology. In our study, we determined that CD68 immunopositive cells were higher in the GDM group than in healthy pregnant women.

As a result of our study, it was shown that there is macrophage accumulation in placentas with GDM and that the expression of pre-inflammatory mediators is higher than the control group, and it was concluded that these factors play an important role in the etiology of gestational diabetes. The data obtained as a result of this study and the findings obtained as a result of our study support each other [25]. It has been shown that Hofbauer cells may be important in the pathogenesis of early fetal losses.

5. Conclusion

In our study with diabetic, preeclamptic, and HELLP syndrome pregnant women, we found that the number of Hofbauer cells in the villus stroma increased in different pathological conditions.

Ethical statement

This study was carried out in accordance with the rules of research and publication ethics. The study was approved by the Dicle University Medical School Non-Interventional Ethics Committee (5/5/2016/194.).

Acknowledgment

This study was supported by the Scientific Research Projects of Dicle University with project number: TIP.16.017.

Conflict of interest

The authors declare no conflict of interest.

Authors' Contributions

All authors read and approved the final manuscript. All authors mentioned in the paper have significantly contributed to the research:

Y. N: Conceptualization, Formal analysis, Funding acquisition, Investigation, Project administration, Supervision, Writing – review, and editing (%30)

Ş. N: Formal analysis, Funding acquisition, Investigation, Methodology, Validation, Visualization, Writing – original draft (%15)

F. A: Data curation, Software, Validation, Visualization, Writing – original draft, Writing – review and editing (%20)

A. Ş: Formal analysis, Funding acquisition, Methodology, Visualization, Writing – original draft, Writing – review and editing (%20)

E. A: Conceptualization, Formal analysis, Funding acquisition, Investigation, Methodology, Resources, Supervision (%15)

References

[1] MacGillivray I: "*Pleeclampsia: the hypertensive disease of pregnancy* ", Phidalphia. WB Saunder, 1983.

[2] Di Cianni G., Miccoli R., Volpe L., Lencioni C., Del Prato S. " Intermediate metabolism in normal pregnancy and in gestational diabetes ", *Diabetes Metab. Res.* 19, 259–270, 2003.

[3] Chang, M.D.Y., Pollard, J.W., et al. "Mouse placental macrophages have a decreased ability to present antigen", *Proceedings of the National Academy of Sciences*, 90, 462-466, 1993.

[4] Fox, H. "The incidence and significance of Hofbauer cells in the mature human placenta", *Journal of Pathology and Bacteriology,* 93, 710-717, 1997.

[5] Hofbauer, J. "The function of the Hofbauer cells of the chorionic villus, particularly in relation to acute infection and syphilis", *Am J Obstet Gynecol*, 10(1), 1-14,1975.

[6] Enders, AC., King, BF. "The cytology of Hofbauer cells". *Anat Rec*, 167(2), 231-6,1975.

[7] Vinnars, MT., Rindsjo, E., Ghazi, S., Sundberg, A., Papadogiannakis, N. " The number of CD68(+) (Hofbauer) cells is decreased in placentas with chorioamnionitis and with advancing gestational age", *Pediatr Dev Pathol*, 13(4), 300-4, 2010.

[8] Demir, R., Erbengi, T. "Some new findings about Hofbauer cells in the chorionic villi of the human placenta", *Acta Anat (Basel*), 119(1), 18-26,1984.

[9] Castellucci, M., Zaccheo, D., Pescetto, G. "A three-dimensional study of the normal human placenta villous core. I. The Hofbauer cells", *Cell Tissue Res*, 210(2), 235-47, 1980.

[10] Kondi-Pafiti, A., Grigoriadis, C., Samiotaki, D., Filippidou-Giannopoulou, A., Kleanthis, C., Hassiakos, D. "Immunohistochemical study of inhibin A and B expression in placentas from normal and pathological gestations", *Clin Exp Obstet Gynecol*, 40(1), 109-12, 2013.

[11] King, BF. "Ultrastructural differentiation of stromal and vascular components in early macaque placental villi", *Am J Anat.*, 178(1), 30-44, 1987.

[12] Wynn, RM. "Derivation and ultrastructure of the so-called Hofbauer cell", *Am J Obstet Gynecol*, 97(2), 235-48, 1967.

[13] Martinoli, C., Castellucci, M., Zaccheo, D., Kaufmann, P. "Scanning electron microscopy of stromal cells of human placental villi throughout pregnancy". *Cell Tissue Res.* 235(3), 647-55, 1984.

[14] Hauguel-de Mouzon, S., Guerre-Millo, M. "The placenta cytokine network and inflammatory signals", *Placenta*, 27(8):794-82006.

[15] Wood, GW., King, GR Jr. "Trapping antigen-antibody complexes within the human placenta", *Cell Immunol*, 69(2), 347-62, 1982.

[16] Wetzka, B., Clark, DE., Charnock-Jones, DS., Zahradnik, HP., Smith, SK. "Isolation of macrophages (Hofbauer cells) from human term placenta and their prostaglandin E2 and thromboxane production", *Hum Reprod*, 12(4), 847-52, 1997.

[17] Tang, Z., Tadesse, S., Norwitz, E, Mor, G, Abrahams, VM., Guller, S. "Isolation of Hofbauer cells from human term placentas with high yield and purity", *Am J Reprod Immunol*, 66(4), 336-48, 2011.

[18] Seval, Y., Korgun, E.T., et al."Hofbauer cells in early human placenta: possible implications in vasculogenesis and angiogenesis", *Placenta*, 28, 841-845, 2007.

[19] Anteby, EY., Natanson-Yaron, S., Greenfield, C., Goldman-Wohl, D., Haimov-Kochman, R., Holzer, H., et al. "Human placental Hofbauer cells express sprouty proteins: a possible modulating mechanism of villous branching", *Placenta*, 26(6), 476-83, 2005

[20] Ben Amara, A., Gorvel, L., Baulan, K., Derain-Court, J., Buffat, C., Verollet, C.et al. "Placental macrophages are impaired in chorioamnionitis, an infectious pathology of the placenta", *J Immunol.*, 191, 5501–5514, 2013.

[21] Vinnars, M.T., Wijnaendts, L.C., Westgren, M., Bolte, A.C. Papadogiannakis, N., Nasiell, J. "Severe preeclampsia with and without HELLP differ with regard to placental pathology", *Hypertension*, 51, 1295–1299, 2008.

[22] Evsen, M.S., Kalkanli, S., Deveci, E., Sak, ME., Ozler., A, Baran, O. et al. "Human placental macrophages (Hofbauer cells) in severe preeclampsia complicated by HELLP syndrome:v immunohistochemistry of chorionic vill", *Anal Quant Cytopathol Histpathol*, 35, 283–288, 2013.

[23] Yang, S.W., Cho, E.H., Choi, S.Y., Lee, Y.K., Park, J.H., Kim, M.K. et al. "expression in Hofbauer cells may play an important role in immune tolerance in fetal chorionic villi during the development of preeclampsia", *J Reprod Immunol*., 124, 30–37, 2017.

[24] Tang, Z., Buhimschi, I.A., Buhimschi, C.S., Tadesse, S., Norwit, E., Niven-Fairchild, T.et al. "Decreased levels of folate receptor-beta and reduced numbers of fetal macrophages

(Hofbauer cells) in placentas from pregnancies with severe pre-eclampsia", *Am J Reprod Immunol*., 70, 104–115, 2013.

[25] Demir, R., Kayisli, UA., Seval, Y., Celik-Ozenci, C., Korgun, ET., Demir-Weusten, AY., et al. Sequential expression of VEGF and its receptors in human placental villi during very early pregnancy: differences between placental vasculogenesis and angiogenesis", *Placenta*, 25, 560–572, 2004.

Middle East Journal of Science

https://dergipark.org.tr/mejs **MEJS**

e-ISSN:2618-6136

Research Article

ESTIMATION OF NEUTRONS OCCURRING IN THE LINAC ROOM AT DIFFERENT PHOTON ENERGIES

***Taylan TUĞRUL*[1*]**

[1] Department of Radiation Oncology, Medicine Faculty, Van Yüzüncü Yıl University, Van, TURKEY

[*] Corresponding author; taylantugrul@gmail.com

Abstract: *The high-energy photons produced by the Linear accelerator (Linac) induce some nuclear reactions in the materials in the Linac room and Linac head. Neutrons formed as a result of the interaction of photons with materials are called photoneutrons. The aim of the study is to examine the neutron doses formed in the environment for 6 different photon energies. In the study, the components in the Linac head and the Linac chamber are modeled with the help of the Monte Carlo N-Particle (MCNP) program. Then, the flux and dose of photoneutrons formed at 8 different points as a result of 6 different photon energies obtained from the Linac head were measured. as can be seen from the results, as the photon energy used in the Linac increases, the resulting dose, and flux of photoneutron increase. It can be understood from the results that the amount of neutron dose to be received by the organs in the treatment field may be higher than the other organs. Especially in the treatments where the patient is lying in the prone position, there may be a possibility of neutrons reaching the patient spinal cord. Since photoneutrons with high radiobiological ability may pose a risk of secondary cancer for patients, the photon energy chosen for patient treatments should be chosen appropriately and the use of unnecessary high photon energy should be avoided.*

Keywords*: Photoneutron, MCNP, Linac, Neutron Flux.*

Received: October 10, 2021 Accepted: December 25, 2021

1. Introduction

Although there are many methods used for cancer treatment, the method of radiotherapy utilizing photons and electrons is the most commonly used technique [1]. Electron energies from 6 MeV to 25 MeV can be generated in Linear accelerator (Linac) devices, which have been used in radiotherapy [2,3]. Because tungsten is a good material used to reduce the energy of photons, the important components of Linac consist of tungsten. The primary collimator, jaws, and multi-leaf collimator (MLC), which are possessed in Linac, are these components. The flattening filter affecting the photon beam is usually made of steel [4].

Although the use of high-energy photons is a good method for cancer treatment, it has a downside. During the radiotherapy treatment applied to the patient, some nuclear reactions that can generate neutrons occur in the Linac room due to the high energy radiation obtained in the Linac devices [2,4,5,6]. The photon energy directly affects neutron production [4].

The photons created by the Linac cause undesirable neutron formation in the environment after a certain threshold value [7,8,9,10]. These undesirable neutrons, which are demonstrated a high linear

energy transfer (LET) ability, indicate secondary cancer risk for the patients and can ever reach staff outside the room [6,11,12,13].

The atomic number (Z) of the environment in which the radiation is emitted directly affects the threshold value of the photon energy for the formation of nuclear reactions. While this threshold value is 7 MeV for the nuclear reaction that may occur in materials with a high Z value such as tungsten, this value is 16 MeV for oxygen with a low Z value [14,15]. The process from primary electron generation to the transport of all radiation and all nuclear reactions that may occur can be modeled with the Monte Carlo (MC) method [14].

The neutron created by the photon is called photoneutron. The high-density head components of the Linac are associated with the photoneutrons produced. In addition, these photoneutrons can also be produced from the wall concrete in the room of Linac and the patient body [12,16,17,18,19]. The main cause of the photoneutrons formation is nuclear reactions between tungsten and photon. Photoneutrons are also formed in the environment due to other materials (flatting filter, source thickness, etc.) but they are neglected because their ratio is low [6]. It has been stated in previous studies that most of the neutrons formed (87%) are due to tungsten components [12,20].

The photoneutrons formed in the Linac head and Linac room are obtained as direct reaction neutrons (knock-on) and evaporation neutrons [4]. When photons interact with a nucleus, their energy is dispersed among nucleons. When a neutron near the nucleus surface achieves enough energy, that neutron is emitted from the nucleus as an evaporation neutron. Photoneutron, known as a knock-on neutron, occurs when the photon gives all of its energy to a single neutron. In addition, this neutron spreads mainly in the direction of the incoming photon [2,6,21]. Photoneutrons produced by nuclear reactions as a result of the use of Linac is roughly 100 to 200 times larger than electron-neutron production, so studies have focused on photoneutrons [6,8,19].

This study aims to examine the neutron flux and neutron dose that can occur in the environment at different photon energies obtained from Linac. Measurement results were obtained at eight different points.

2. Materials and Methods

In the study, the simple model of the head of Linac was simulated by MCNPX2.6 MC code [22]. The Monte Carlo N-Particle (MCNP) code is a common code for examining neutron, photon, and electron transport. A protective shield made of lead covering the head of the Linac is also included in the modeling. The simulations were implemented for six different photon energies and 10x10 cm^2 field sizes. In the modeling, detectors in the eight different points were defined to measure neutrons. The detectors were employed to calculate the flux (Particle x cm^{-2} x s^{-1}) and neutron dose (mrem/hour). Some measurement points were selected from regions that may be critical to the patient. If we define the target position as (0,0,0) on the x, y and z axes, detector positions; (0,0,-90) for Point 1, (0,0,-50) for Point 2, (-40,0,-100) for Point 3, (-80,0,-100) for Point 4, (0,-40,-100) for Point 5, (0,-80,-100) for Point 6, (-240,-180, -100) for Point 7 and (-145,-400,-100) for Point 8. The created simulation is shown in Figure 1 and Figure 2.

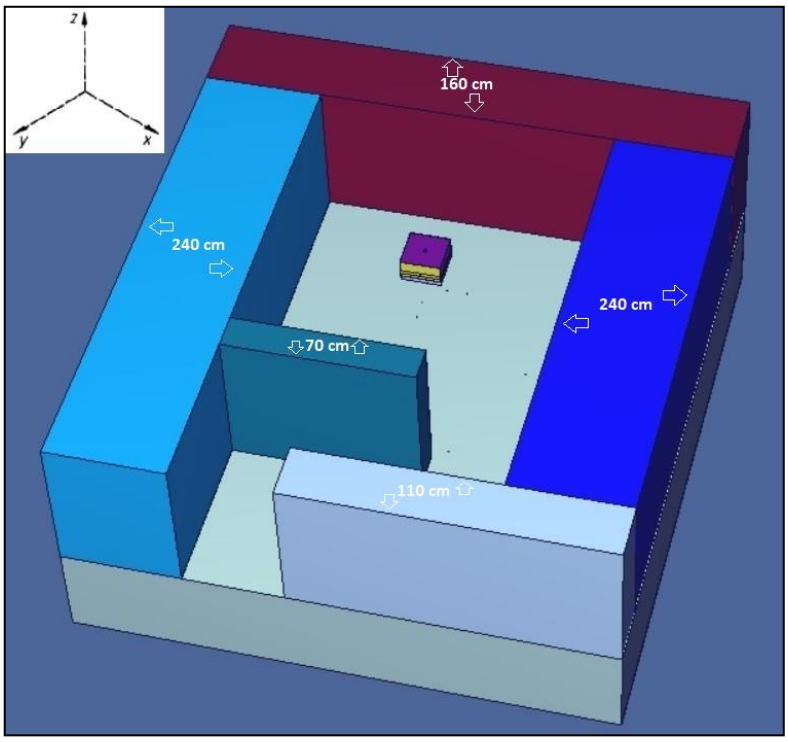

Figure 1. Simulation image of Linac room and Linac head created in MCNP

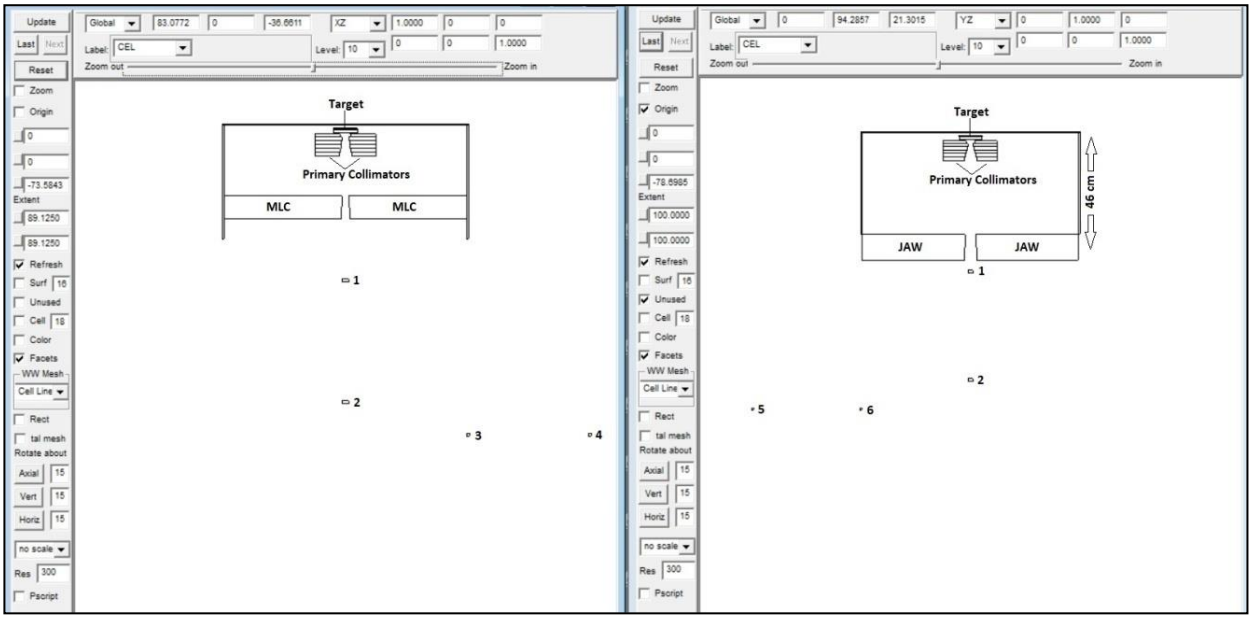

Figure 2. Simulation image of some detectors and Linac head created in MCNP

The geometric structure of the Linac room, which includes all its components and thickness, has been taken into account. In addition, the target, flattening filter, primary collimator, jaws, and MLC components of the Linac head are also considered. Agosteo et al. and Carinou et al. have pointed out that there was no significant difference in comparing a simple MC model and a detailed MC model [23,24]. The walls of the Linac room were simulated with a 2.35 gr/cm3 density concrete type containing 50.0% O, 31.5% Si, 8.3% Ca, 4.8% Al, 1.9% K, 1.7% Na, 1.2% Fe and 0.6% H [2,25].

In MCNP, the F5 tally was used to measure the flux and neutron dose. It was utilized the variance reduction technique was to reduce the computation time and focus on the desired result in modeling. In MCNP, the F5 tally was modified with the help of DE/DF dose factors, and the dose values at the desired points were obtained as "mrem/hour" [22,26]. The results were acquired using e/ɣ/n mode in MCNP and run for 109 histories. The statistical uncertainties obtained for all results were below 1%.

3. Results

As a result of 6 different photon energies produced in the Linac head, the flux and dose of photoneutrons occurring in different positions of the Linac chamber were investigated. Photoneutrons formed in the Linac room are made up of knock-on and evaporation contributions. Contributions from other reactions are quite small [6]. Some of the locations where photoneutrons are measured have been attempted to be chosen similarly to places where the patient's surface may be exposed during treatment. The results at the points where flux and dose were measured for the photoneutron are shown in Table 1 and Table 2.

Table 1. The obtained flux values for 6 different photon energies.

	Flux (Particle x cm^{-2} x s^{-1})							
	Point 1	**Point 2**	**Point 3**	**Point 4**	**Point 5**	**Point 6**	**Point 7**	**Point 8**
6 MV	N/A	N/A	N/A	N/A	N/A	N/A	N/A	N/A
8 MV	1,23E-08	5,27E-08	7,62E-10	5,52E-09	2,25E-09	4,80E-09	2,17E-09	6,13E-10
10 MV	6,08E-07	5,66E-06	6,04E-08	1,80E-07	1,33E-07	1,76E-07	7,34E-08	2,01E-08
12 MV	3,55E-06	2,15E-05	3,54E-07	9,66E-07	6,18E-07	9,90E-07	3,85E-07	1,05E-07
15 MV	2,18E-05	1,24E-04	1,51E-06	5,88E-06	3,02E-06	6,55E-06	2,32E-06	6,15E-07
18 MV	7,55E-05	4,14E-04	4,41E-06	1,99E-05	8,78E-06	2,36E-05	7,79E-06	2,03E-06

Table 2. The obtained neutron dose values for 6 different photon energies.

	Dose (mrem/hour)							
	Point 1	**Point 2**	**Point 3**	**Point 4**	**Point 5**	**Point 6**	**Point 7**	**Point 8**
6 MV	N/A	N/A	N/A	N/A	N/A	N/A	N/A	N/A
8 MV	1,14E-12	4,73E-12	4,55E-14	3,93E-13	1,68E-13	3,54E-13	1,51E-13	4,34E-14
10 MV	6,88E-11	6,88E-10	6,81E-12	1,94E-11	1,50E-11	1,92E-11	7,89E-12	2,16E-12
12 MV	3,96E-10	2,40E-09	3,91E-11	1,05E-10	7,10E-11	1,08E-10	4,21E-11	1,16E-11
15 MV	2,55E-09	1,46E-08	1,76E-10	6,81E-10	3,53E-10	7,57E-10	2,68E-10	7,11E-11
18 MV	9,18E-09	4,96E-08	5,26E-10	2,41E-09	1,05E-09	2,86E-09	9,38E-10	2,44E-10

Khaledi et al. stated that the threshold value of tungsten for the formation of photoneutrons is 7.42 MeV in their study [12]. In our study, we also did not observe flux and neutron dose values for the photoneutron at 6 MV photon energy.

As expected, as the photon energy increased, the photoneutrons formed in the medium also increased. We obtained the highest photoneutron value at point 2, 50 cm from the source. The second highest value was measured at 90 cm (Source-skin distance (SSD)=90) from the source. As the measurement points moved away from the central photon axis, the photoneutron flux and dose began to decrease. This is a result of the same trend as other studies [2,21,27]. It can be understood from this result that the amount of neutron dose to be received by the organs in the treatment field may be higher than the other organs. As seen in Table 2, when the photoneutrons formed at a distance of SSD=90 cm are examined, there is an approximately 8 thousand-fold difference between 8 MV and 18 MV.

The lowest flux and dose values were measured at the farthest point from the source. The photoneutron dose and flux values at Points 3-5 and 4-6, which are equidistant from the source, were found to be close to each other. The differences between them can be attributed to the axis positions of the MLC and jaws. Photoneutrons measured in the study also include contaminated neutrons produced by the interaction of photons with concrete.

4. Conclusion

Since photoneutrons, which are harmful to normal tissues, formed during radiotherapy treatment may lead to the risk of secondary cancer, their behavior in the environment should be carefully examined. As can be seen from the results, as the photon energy used in the Linac devices increases, the resulting photoneutron dose, and flux increase. Photoneutrons reaching critical organs may cause some complications and secondary cancer risk in the patient. Furthermore, photoneutrons can reach the spinal cord, especially when the patient is in a prone position. Photon energy selected for patient treatments should be chosen appropriately, unnecessary high photon energy use should be avoided.

Ethical statement

Ethical approval is not required for this study, as no patient or animal data were used in the study.

Conflict of interest

The authors must notify any conflicts of interest.

Authors' Contributions

T. T: Measurement, Literature review, Simulation, Modelling, Writing - Original draft preparation
The author reads and approved the final manuscript.

References

[1] Mesbahi, A., Keshtkar, A., Mohammadi, E., Mohammadzadeh, M., "Effect of wedge filter and field size on photoneutron dose equivalent for an 18MV photon beam of a medical linear accelerator", *Applied Radiation and Isotopes*, 68, 84–89, 2010.

[2] Khabaz, R., Boodaghi, R., Benam, M.R., Zanganeh, V., "Estimation of photoneutron dosimetric characteristics in tissues/organs using an improved simple model of linac head", *Applied Radiation and Isotopes*, 133, 88–94, 2018.

[3] Vega-Carrillo, H.R., Hernandez-Almaraz, B., Hernandez-Da´vila, V.M., Ortiz-Hernandez, A., "Neutron spectrum and doses in an 18MV LINAC", *Journal of Radioanalytical and Nuclear Chemistry*, 283, 261–265, 2009.

[4] Khabaz, R., "Effect of each component of a LINAC therapy head on neutron and photon Spectra", *Applied Radiation and Isotopes*, 139, 40-45, 2018.

[5] Naseri, A., Mesbahi, A., "A review on photoneutrons characteristics in radiation therapy with high-energy photon beams", *Reports of Practical Oncology and Radiotherapy*, 15, 138–144, 2010.

[6] Vega-Carrillo, H.R., Martı´nez-Ovalle, S.A., Lallena, A.M., Mercado, G.A., Benites- Rengifo, J.L., "Neutron and photon spectra in LINACs", *Applied Radiation and Isotopes*, 71, 75–80, 2012.

[7] Followill, D.S., Nüsslin, F., Orton, C.G., "IMRT should not be administered at photon energies greater than 10 MV", *Medical Physics*, 34, 1877–1879, 2007.

[8] Lin, J.P., Chu, T.C., Lin, S.Y., Liu, M.T., "The measurement of photoneutrons in the vicinity of a Siemens Primus linear accelerator", *Applied Radiation and Isotopes*, 55, 315–321, 2001.

[9] Vega-Carrillo, H.R., Baltazar-Raigosa, A., "Photoneutron spectra around an 18 MV LINAC", *Journal of Radioanalytical and Nuclear Chemistry*, 287, 323–327, 2011.

[10] Zanini, A., Durisi, E., Fasolo, F., Ongaro, C., Visca, L., Nastasi, U., Burn, K.W., Scielzo, G., Adler, J.O., Annand, J.R.M., Rosner, G., "Monte Carlo simulation of the photoneutron field in linac radiotherapy treatments with different collimation systems", *Physics in Medicine and Biology*, 49, 571-582, 2004.

[11] Benites-Rengifo, J.L., Vega-Carrillo, H.R., "Neutron Dosimetry in Solid Water Phantom", AIP Conference Proceedings 1626, 114-116, 2014.

[12] Khaledi, N., Dabaghi, M., Sardari, D., Samiei, F., Ahmadabad, F.G., Jahanfarnia, G., Saadi, M.K., Wang, X., "Investigation of photoneutron production by Siemens artiste linac: A Monte Carlo Study", *Radiation Physics and Chemistry*, 153, 98–103, 2018

[13] Agosteo, S., FoglioPara, A., "Energy and spatial dependence of neutron fluxes in radiotherapy rooms for a simple dose estimate method", *Nuclear Instruments and Methods in Physics Research Section B: Beam Interactions with Materials and Atoms*, 93, 362–369, 1994.

[14] Sumini, M., Isolan, L., Cucchi, G., Sghedoni, R., Iori, M., "A Monte Carlo model for photoneutron generation by a medical LINAC", *Radiation Physics and Chemistry*, 140, 345–348, 2017.

[15] Burn, K.W., Ongaro, C., Photoneutron production and dose evaluation in medical accelerators, Cern Libraries, Geneva, 2002.

[16] d'Errico, F., Nath, R., Tana, L., Curzio, G., Alberts, W.G., "In-phantom dosimetry and spectrometry of photoneutrons from an 18 MV linear accelerator", *Medical Physics*, 25, 1717–1724, 1998.

[17] Hall, E.J., Martin, S.G., Almols, H., Hei, T.K., "Photoneutrons from medical linac accelerators radiobiological measurements and risk estimates", *International Journal of Radiation Oncology - Biology - Physics*, 33, 225–230, 1995.

[18] IAEA, Handbook on Photonuclear Data for Applications. Cross-Sections and Spectra, International Atomic Energy Agency IAEA-TECDOC-1178, Vienna, 2000.

[19] Martinez-Ovalle, S.A., Barquero, R., Gomez-Ros, J.M., Lallena, A.M., "Neutron dose equivalent and neutron spectra in tissue for clinical linacs operating at 15, 18 and 20 MV", *Radiation Protection Dosimetry*, 147, 498–511, 2011.

[20] Pena, J., Franco, L., Gomez, F., Iglesias, A., Pardo, J., Pombar, M., "Monte Carlo study of Siemens PRIMUS photoneutron production", *Physics in Medicine and Biology*, 50, 5921-5933, 2005.

[21] Mohammadi, N., Miri-Hakimabad, S.H., Rafat-Motavalli, L., "A monte carlo study for photoneutron dose estimation around the high-energy linacs", *Journal of Biomedical Physics & Engineering*, 4, 127–139, 2014.

[22] MCNP Version 2.6.0, MCNPX USER'S MANUAL. Los Alamos National Laboratory, USA, 2008.

[23] Agosteo, S., FoglioPara, A., Maggioni, B., Sangiust, V., Terrani, S., Borasi, G., "Radiation transport in a radiotherapy room", *Health Physics*, 68, 27–34, 1995.

[24] Carinou, E., Kamenopoulou, V., Stamatelatos, I.E., "Evaluation of neutron dose in the maze of medical electron accelerators", *Medical Physics*, 26, 2520–2525, 1999.

[25] Khabaz, R., "Analysis of neutron scattering components inside a room with concrete walls", *Applied Radiation and Isotopes*, 95, 1–7, 2015.

[26] White, D.R, Griffith, R.V., Wilson I.J., Photon, Electron, Proton, and Neutron Interaction Data for Body Tissues ICRU Report 46, International Committee on Radiation Units and Measurements, USA, 1992.

[27] Ghiasi, H., Mesbahi, A., "Monte Carlo characterization of photoneutrons in the radiation therapy with high-energy photons: a comparison between simplified and full Monte Carlo models", *Iranian journal of radiation research*, 8, 187–193, 2010.

Middle East Journal of Science

https://dergipark.org.tr/mejs **MEJS**

e-ISSN:2618-6136

Research Article

INCUBATION SHARING OF NORTHERN BALD IBIS (*Geronticus eremita*) PARTNERS

***Ahmet KILIÇ*[1] *Ersin UYSAL*[2]**

[1]Dicle University Science FacultyDepartment of Biology TR-21280 Diyarbakır Turkey
[2] DicleUniversity, Vocational School of Technical Sciences, Department of Computer Technologies, Diyarbakır Turkey
ahmetk@dicle.edu.tr

Abstract: *This study related out during the incubation period of northern bald ibises. Northern bald ibises in Birecik are free-living in nature during the breeding period (February–June) in 2013-2015. Pairs share the incubation between the two sexes. Females were incubated for 177.08 minutes per day on average while males were incubated for 240.99 minutes per day. This incubation period is statistically different (P< 0.0001) with males staying 23-32% longer than females. Females and males stayed in incubation together for only a short time. According to observations made (n=79), couples stay together on nests for 20.52 minutes on average. During the observations made all day long it was realized that eggs are left alone for only 0.40 minutes on average. Incubation periods did not vary according to years. According to the observations made in 2013 (n=100) period for staying in the nest was not different than observations of years 2014 and 2015 statistically (P>0.05). According to 2014 (n=128) and 2015 (n=88) results no statistical difference could be observed between incubation periods (P >0.05).The excess eggs during incubation are protected by northern bald ibises which do not have any nest (altruism). From time to time-synchronized behaviors can be observed in the population.*

Keywords: *female sitting time, male sitting time, breeding, Geronticus eremita, synchronized behavior*

Received: October 2, 2021 Accepted: December 29, 2021

1. Introduction

The aim of this study is to reveal the incubation sharing periods of the partners. It was aimed to contribute to the rescue of the northern bald ibis, which is endangered.

Although the Northern Bald Ibis *Geronticus eremita* (Linnaeus, 1758), was listed as a critically endangered (CR) species, globally, by IUCN; recently changes as endangered (EN) in 2018[1]. The number of those living freely in nature is less than 1000. The northern bald ibis in different zoos and stations has been originated from Morocco [1- 4].

The northern bald ibis population living in the cliff in the Atlantic Ocean coasts in North Africa (Morocco) is the greatest one [5, 6]. A total of 262 chicks hatched in 2013 in Souss-Massa National Park and Tamri in Morocco and only 148 chickens have reached the maturity to be able to leave the nest by flying. According to the evaluation in 2014, there is a population consisting of 524 individuals in the Souss-Massa region. 192 chickens were raised in the incubation sustained by 115 couples in this region in 2014. It has been determined that 1.6chickenson averages have been raised in these nests participating in reproduction [7].

The second population takes place in Turkey. The interest in the northern bald ibis in Anatolia shows a difference from other regions of the world. Northern bald ibis is seen as holy in Birecik and they are not hunted. Also those from Birecik have always been helpful in the issue of the protection and reproduction of them since before [8 - 12]. The population living in Birecik (Şanlıurfa) for centuries is accepted as semi-natural today [1, 13]; because the population sustains its existence thanks to the contributions made by the people. Northern bald ibis spending the winter in cages is set free in the reproduction periods (March-June) [14]. 185 Northern bald ibises have been set free from cages in 2015 [13]. The number of Northern bald ibises taken to the cages at the end of the reproduction period has risen to 209.52fledgling attended to the population reproducing in 2015 [13].

A northern bald ibis colony accustomed to migration with the help of the people has been formed in Europe. The adults that have spent the winter in Toscana (Laguna di Orbetello) in Italy migrate to Germany and Austria for reproduction [15]. This colony consists over of 100 individuals – in the year 2016[1].

Knowing the route of migration is realized in the birds via instinct and learning. As in storks, it is known that northern bald ibises are also known to migrate to the south at the end of the reproduction period. They fly to Africa (Somali, Ethiopia) in which they will spend the winter [11]. In a study conducted with storks in North Europe; it has been observed that the young storks not knowing the routes of migration migrate from north to south instinctively. However, the experienced individuals migrate through South Eastern (Anatolia) as different from this route [16]. As in storks, it has been detected that the young individuals head towards the south in the absence of the experienced northern bald ibises knowing the routes of migration. It has also been determined that although the adult northern bald ibises know the places where they will spend the winter head towards Africa (Somali, Ethiopia), young northern bald ibises head towards Saudi Arabia [17].

It has been revealed in the observations conducted in cages that the experienced individuals of the northern bald ibises are more successful in incubations. It has been determined that whether there is loyalty to the spouse does not affect the number of offspring breeding [18].

The loyalties of the northern bald ibises to their partners could not be completely determined in the ones living freely. It has been estimated that the northern bald ibises living freely may show seasonal loose monogamy. It is specified that monogamy is observed in the northern bald ibises living in cages [19].

The mating behaviors are observed in northern bald ibises during the reproduction period. These behaviors rapidly decrease together with the making of the last egg [20]. Mating is carried out mostly (65%) after the mutual feather cleaning of the couples. Male and female northern bald ibis stand side by side after mating and they erect their beaks upwards simultaneously. Female ones get on the back of the males and show mating trials [20].

Material is carried instead of the nest while the nest owners sustain their partner relations until the beginning of the incubation. Carrying the material is under the responsibility of the males. The female sits in the nesting place and ensures the establishment of the brought material. 98% of the materials carried to the nest are brought by the male. The carried materials are herbal materials such as thick and thin branches, grass, and straw. In addition; plastic bags, paper, and different packing materials are also carried to the nest out of the rubbish thrown by the people [21].

Finding and carrying the nest material is an effort necessary to be spent. Males are responsible for finding and bringing the material. Stealing materials from neighbor nests during and after the establishment of the nest is an observed behavior. Nest owners do not leave the nest alone before and after incubation so much. It has been determined during the day-long observations conducted before incubation that the nest is left alone for only 19 minutes in total. The material in the nests left alone for a few minutes is pillaged at that moment by the neighbors [21].

It has been determined that incubation lasts for 27-28 days for the bald ibises living freely. The offspring of the same nest hatch from the egg at intervals of 2-3 days. Hatching of the offspring from the egg may take two days [22]. Female and male northern bald ibises share tasks and grow the offspring together. The offspring leave the nest after they are 45-50 days old [23].

2. Materials and Methods

The northern bald ibises living in the Birecik district of Şanlıurfa province (37.0197 N, 37.9759 E) have formed our study material. The population conducting their mating (March-June) in nature is kept in "Northern BaldIbis Production Station" for eight months. Food supply is also during the period they are in nature. The northern bald ibises set free from cages at the beginning of the reproduction period (end of February- early March) proceed to the prepared and naturally existent nest places and start reproduction acts.

Observations have been carried out two days per week during the reproduction period of the northern bald ibises. The studies were carried out between the years 2012-2015. Observations have been sustained without any interval for 6-10 hours during the day (Table 1). No night observations. Observations have been carried out at a distance of 50-100 m to the nests in the Station of Production. Observations were made from outside the breeding station so that the northern bald ibises would not be affected by the researcher. Five nests neighbor to one another has been regularly observed.

Table 1. Time of observations

Year	Date(hour)	Time of observations (minutes)	Number of nest / incubation observed (n)
2013	04April2013(08.27-17.00) 10 April 2013(09.00-17.00) 11 April 2013(06.55-17.00) 17 April 2013(09.30-17.00) 18 April 2013(07.08-15.55)	513 480 605 450 527	5
2014	05 March 2014(09.20-17.00) 06 March 2014(07.15-16.30) 12 March 2014(09.47-15.45) 13 March 2014(06.55-16.00) 19 March 2014(09.36-17.00) 20 March 2014(06.47-16.00) 26 March 2014(09.50-17.00) 27 March 2014(06.40-16.00)	460 555 358 545 444 553 430 560	5
2015	12 March 2015(07.12-15.00) 18 March 2015(09.55-17.00) 19 March 2015(07.05-15.00) 25 March 2015(09.17-17.00) 26 March 2015(07.03-15.00) 01 April 2015(09.48-17.00) 02 April 2015(07.08-15.00) 08 April 2015(09.15-15.00)	468 425 475 463 477 432 472 345	3

Northern bald ibises are taken to cages at the end of the breeding season (June - July). Brooding station interested-Veterinarians wear colorful plastic rings on the feet of northern bald ibis. In addition, blood is taken from northern bald ibises (for genetic studies and gender determination at Department of Biology of the Middle East Technical University, Ankara-Turkey) [24].

When determining the sex of the northern bald ibises (four years, 2012 - 2015) always the same individuals were observed): First, sexual behavior is investigated (for example, the position in copulation). Second, head patterns of northern bald ibis were examined [25 - 27]. Thirdly, take into account the colored rings on their feet.

We compared our results for sex determination with the blood analysis of northern bald ibises (see Acknowledgement). The results of both studies were the same.

Our sex determination studies were compared to the studies by Yeniyurt [28] and Özkınacı and Yeniyurt [29]. Our results of sex determination matched theirs.

The reproduction activities realized in nests have been recorded via binoculars, telescope (Nikon FIELD SCOPE ED), camera (Fujifilm FinePix S2Pro), and Digital video camera (Canon MVX150i). Evaluation and statistical studies have been conducted afterward.

Mean and standard error values were given as descriptive statistics in the analysis of the data. Two-Way analysis of variance and Bonferroni Multiple Comparison tests were used in statistical evaluations of parameters. The results were considered statistically significant for $P<0.05$.

This research article can be evaluated with the article below. "Assessment of the incubation period for each sex of Turkish semi-wild northern bald ibis (*Geronticus eremita*)" [30].

3. Results

The northern bald ibises lay 1-3 eggs. Incubation lasts 28 days. As before the incubation, partners share tasks in the incubation. Incubation periods have been compared to the observations belonging to the three years (2013-2015). The start of incubation takes place on different dates in March. It is seen that environmental temperature is the determining factor in this change. During the cold March, incubation starts late. The incubation start date is affected by two factors. Average incubation periods in 2013 showed significant change according to the weeks in incubation and the parameter of sex interaction ($F=4.538$; $P<0.001$). These changes are statistically meaningful changes.

The comparative change of the incubation periods in the nests observed in 2013 according to the sex of the nest owner and the number of weeks incubation has lasted are seen in Table 2. It could be comparatively seen in this table that males remain in incubation for a longer time. According to the average of all incubations, males have remained in incubation for a minimum of 115.00 minutes and a maximum of 295.70 minutes. Females have remained in incubation for a minimum of 99.57 minutes and a maximum of 255.00 minutes on average. The period in which spouses have remained in incubation together has been a minimum of 3.71 minutes and a maximum of 13.13 minutes (Table 2). Leaving the nest alone during the incubation is too rare.

Table 2. Time of partner staying in the incubation (minutes) (in the day)

Year	Week	Sex	n (number of observations)	Mean	Standard deviation	Standard Error
2013	1.	Female	7	99.57	126.166	47.686
		Male	7	115.00	144.903	54.768
		Female + Male	7	3.71	5.219	1.973
		Empty	7	0.29	.756	.286
	2.	Female	8	255.00	84.834	29.993
		Male	8	290.38	77.772	27.497
		Female + Male	8	13.13	7.882	2.787
		Empty	8	0.00	.000	.000
	3.	Female	10	180.70	88.282	27.917
		Male	10	295.70	66.014	20.875
		Female + Male	10	12.10	7.520	2.378
		Empty	10	0.00	.000	.000
	4.	No data	-	-	-	

Table 2. Continued

Year	Week	Sex	n (number of observations)	Mean	Standard deviation	Standard Error
2014	1.	Female	8	125.13	110.755	39.158
		Male	8	176.00	174.515	61.700
		Female + Male	8	14.88	26.680	9.433
		Empty	8	0.50	.926	.327
	2.	Female	8	193.88	62.670	22.157
		Male	8	250.88	100.249	35.443
		Female + Male	8	5.00	5.880	2.079
		Empty	8	1.75	1.389	.491
	3.	Female	8	227.75	79.857	28.234
		Male	8	266.00	90.571	32.022
		Female + Male	8	1.00	1.414	.500
		Empty	8	0.75	.707	.250
	4.	Female	8	205.50	78.733	27.836
		Male	8	283.63	95.169	33.647
		Female + Male	8	4.38	4.809	1.700
		Empty	8	1.50	1.309	.463
2015	1.	Female	7	120.14	46.820	17.696
		Male	7	237.29	63.269	23.913
		Female + Male	7	93.71	87.112	32.925
		Empty	7	0.00	.000	.000
	2.	Female	6	174.17	46.808	19.109
		Male	6	285.17	42.410	17.314
		Female + Male	6	10.67	4.633	1.892
		Empty	6	0.00	.000	.000
	3.	Female	6	210.67	63.143	25.778
		Male	6	232.83	58.742	23.981
		Female + Male	6	8.50	9.160	3.739
		Empty	6	0.00	.000	.000
	4.	Female	3	133.67	75.182	43.406
		Male	3	137.00	56.027	32.347
		Female + Male	3	74.33	118.424	68.372
		Empty	3	0.0	.000	.000

The average periods of remaining in nests during incubation in 2014 did not show any significant change when compared to the parameter of weeks and sex interaction (F=1.195; P=0.305).

The comparative change of the incubation periods in the nests observed in 2014 according to the sex of the nest owner and the number of weeks incubation has lasted are seen in Table 2. Male has undertaken the maintenance of incubation for a minimum of 176.00 minutes and a maximum of 283.63 minutes in different weeks. On the other hand, females have remained in the incubation for a minimum of 125.13 minutes and a maximum of 227.75 minutes. Female + male have remained in the incubation together for a minimum of 1.00 minutes and a maximum of 14.88 minutes. Leaving the eggs alone in the incubation is too short. This period has changed between 0.50 – 1.75 minutes.

When the average periods for remaining in incubation in 2015 have been examined, it has been observed that the parameters of weeks and sex interaction (F=4.278; P <0.001) have significantly changed.

Periods of remaining in incubation belonging to the three years (2013-2015) are comparatively seen in Table 2. The comparative change of the periods of remaining in incubation when compared to the sex of the nest owner and the number of weeks the incubation has lasted takes place in Table 2. The average period of the males remaining in the incubation in the nests in different weeks has been a

minimum of 137.00 minutes and a maximum of 285.17 minutes in 2015. The Female has remained in the incubation alone for a minimum of 120.14 minutes and a maximum of 210.67 minutes. Female + male have remained together in the incubation for a minimum of 8.50 minutes and a maximum of 93.71 minutes. It has been detected that the eggs were not left alone in the incubation in 2015 (Table 2).

The distribution of the periods for remaining in the incubations according to the weeks in 2013 on average takes place in Figure 1 comparatively. Females take place in the incubation less than males. It is seen that the periods of the males remaining in the incubation are close to each other in the second and third weeks of the incubation. However, it has been detected that females remain in the incubation longer in the second week when compared to other weeks. The periods (min.) of the female and male for remaining in the incubation together are too few. Incubation is left alone rarely (Figure 1).

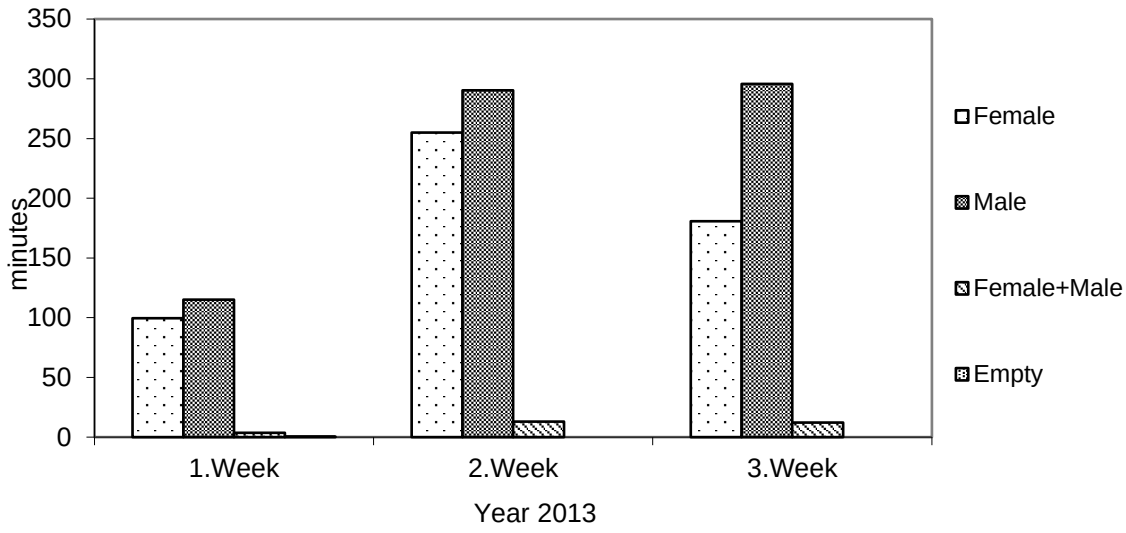

Figure 1. The year 2013 - histogram of the weekly average periods (minutes) of the partners for remaining in the incubation.

The weekly distribution of the average periods of the partners for remaining in the incubation in 2014 takes place in Figure 2 comparatively. Males remain in the incubation more when compared to their partners. Females and males and have remained in the incubation for longer periods in the proceeding incubation weeks. The periods of the partners for remaining in the nest together are too little when compared to the female and male remaining in the incubation alone. Incubation is left alone rarely. The difference of period for remaining in the incubation between females and males has also been observed in various weeks (Figure 2).

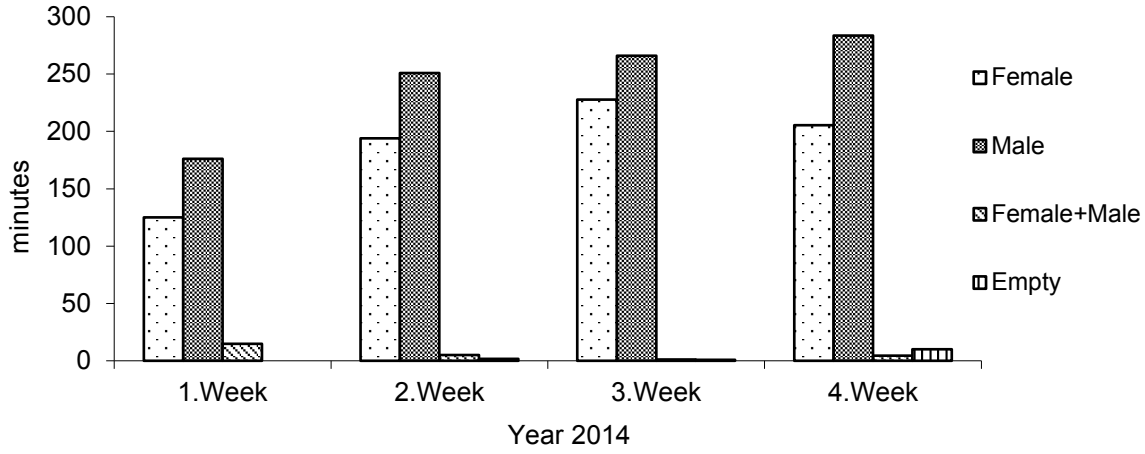

Figure 2. The year 2014 - histogram of the weekly average periods (minutes) of the partners for remaining in the incubation.

The weekly distribution of the average periods of the partners for remaining in the incubation in 2015 takes place comparatively in Figure 3. Males remain in the incubation more when compared to their partners. It is seen that the periods of the males remaining in the incubation decrease as of the second week. Females have increased their periods for remaining in the incubation for the first three weeks. The periods of the partners for remaining in the incubation together are too little when compared to the female remaining in the incubation alone and male remaining in the incubation alone. According to the previous years (2013-2014), it has been detected that females + males remained in the incubation for a longer time in 2015. It has been observed that the eggs have not been left alone (Figure 3).

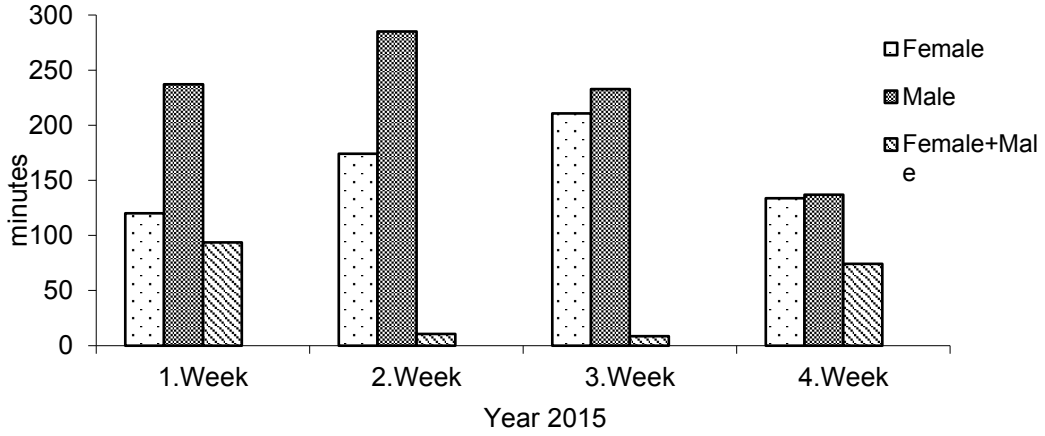

Figure 3. Year2015– histogram of the weekly average periods (minutes) of the partners for remaining in the incubation

3.1. Comparison of the Average Periods for Remaining in the Incubation According to Sex and Years

Average periods ($F=193.565$, $P<0.001$) of remaining in the incubation according to sex have shown a significant change and this is a statistically meaningful change. According to the parameters

of years (F=0.0125; P =0.988) and the interaction of sex and years (F=0.988; P =0.434); average periods for remaining in the incubation have not shown a statistically meaningful change (Average periods for remaining in the incubation has shown similarity with each other according to these parameters).

Descriptive statistical values are given below according to the parameters of sex (Table 3), years (Table 5), and the interaction of years according to sex (Table 7).

When the average of the data attained during the three years (2013-2015) in which observation has been conducted has been calculated, it has been seen that males remain in the incubation longer than their partners. Females have remained in the incubation for 177.08 minutes per day according to the results of the conducted observation (n=79). This value is 26% less than that of males. Males have remained in the incubation for 240.99 minutes per day. This value is clearly longer than that of females. It is rare for the male and female to remain in the incubation together; because there has not been any need for remaining together. Partners are seen in the incubation together for 20.52 minutes on average (n=79) during the day. The nest is not seen empty very much (Table 3).

Table 3. The time of staying in the incubation in 2013-2015 (minutes)

Sex	n	Mean	Standard Error
Female	79	177.08	8.47
Male	79	240.99	8.47
Female + Male	79	20.52	8.47
Empty	79	0.0	8.47

(n: Number of observations) (in the day)

The difference is meaningful (P < 0.0001) when the periods of the females and males for remaining in the incubation are compared. The period of the female for remaining in the incubation alone is much longer than the period for remaining in the incubation together (female + male) and the period for the emptiness of the nest and the difference is meaningful (P <0.0001) (Table 4). The average period of the male for remaining in the incubation is much longer than the period for remaining in the incubation together (female + male) and the period for the emptiness of the nest. The period of the male for remaining in the incubation is meaningfully different from the period for remaining in the incubation together (female + male) and the period for the emptiness of the nest (P <0.0001) (Table 4). It has been detected that the period for remaining in the incubation together (female + male) is not different from the period for the emptiness of the nest (P =0.5643) (Table 4).

Table 4. Multiple comparisons of the period for remaining in the incubation

Sex	Male	Female + Male	Empty
Female	P < 0.0001	P < 0.0001	P < 0.0001
Male		P < 0.0001	P < 0.0001
Female + Male			P = 0.5643

The periods of the northern bald ibises for remaining in the incubation could be seen in Table 5 in three different years (2013-2015). The average of the total of the values "female only" + "male-only" + "male and female together" + "nest empty" has been calculated while calculating the average value. The values of the averages of remaining in the incubation are close to one another among the years. The period of remaining in the incubation in 2013-2015 has changed between 108.83-110.51 (min.) (Table 5).

Table 5. Period of remaining in incubation (minute)

Years	n	Mean	Standard Error
2013	100	108.83	7.44
2014	128	109.91	6.58
2015	88	110.51	7.93

It could be seen in Table 6 with multiple comparisons that the difference between the periods of remaining in incubation in 2013-2015 (according to Table 5) is not meaningful (P > 0.05) (Table 6).

Table 6. Multiple comparisons of the period of remaining in the incubation

Years	2014	2015
2013	ns	ns
2014		ns
ns (non-significant); P > 0.05		

The average of the period of remaining in incubation according to the interaction of years and sex has been comparatively calculated in Table 7. Females remained in incubation between 2013-2015 minimum 161.41 minutes and maximum 188.06 minutes. Males remained in incubation alone minimum 235.45 – maximum 244.13 minutes per day. According to these periods, the male has remained in incubation 23-32% longer than his partner. Sometimes female + male remains in incubation together. It has been observed that the partners remain in incubation together generally during the shift changes. Remaining in incubation together has changed between minimum 6.31 – maximum 45.18 minutes. There is only a single individual in the nest except for the shift changes. It has been determined that the eggs remain alone so rarely during the incubation in the nests monitored in 2013-2015. Nest has been left alone for 0.00-1.13 minutes on average and the eggs have remained alone (Table 7).

Table 7. Periods of remaining in incubation in terms of year and sex (minute)

Sex	Years	N	Mean	Standard deviation	Standard Error
Female	2013	25	181.76	112.960	22.592
	2014	32	188.06	89.512	15.824
	2015	22	161.41	63.663	13.573
Male	2013	25	243.40	123.820	24.764
	2014	32	244.13	121.571	21.491
	2015	22	235.45	69.183	14.750
Female + Male	2013	25	10.08	7.921	1.584
	2014	32	6.31	14.207	2.511
	2015	22	45.18	71.835	15.315
Empty	2013	25	0.08	.400	.080
	2014	32	1.13	1.185	.209
	2015	22	0.00	.000	.000

The average of remaining in incubation belonging to the three years has been dealt with comparatively as a histogram in Figure 4. Females remained in incubation with periods close to each

other in three years (2013-2015). Females remained in incubation at the least in 2015 on average. Males remained in incubation as the least on average in 2015 and as the longest in 2014 (Figure 4). The period of the males remaining in incubation is close to each other although they are in different years. Male and female have remained in the nest together in restricted periods during the shift changes. It is seen in Figure 4 that the incubations have been left alone too rarely (Figure 4).

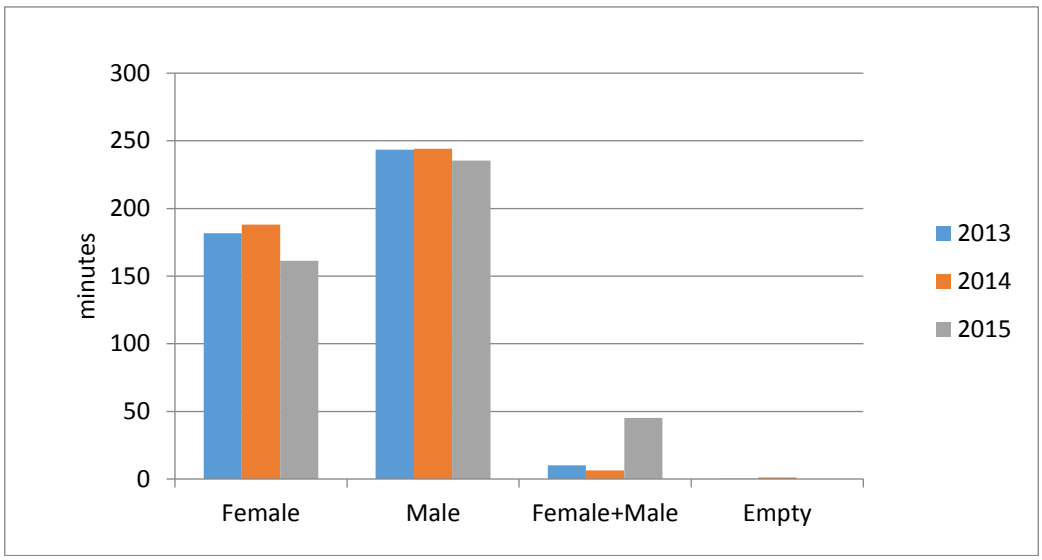

Figure 4. Comparison of the averages of the periods of remaining in incubation (by years)

3.2. Synchronized Behaviors

Northern bald ibises show similar behaviors at the same time before and during the incubation. Mating of the partners to each other in different nests, reproductions, carrying the nest material and the behaviors of starting a family occur within the same period. Shift changes are conducted simultaneously in incubation. At the same time, males or females undertake the mission of incubation from their partners. Shift changes are realized with similar behaviors such as "greeting", "hugging" and "giving a gift". Similar behaviors are observed in different nests at the same time.

4. Discussion

The division of labor for incubation between the two sexes has not previously been studied for the free-flying sex of northern bald ibis. Although northern bald ibises living in cages are marked, a study related to the incubation period of the partners has not been detected. In our study, the partners of northern bald ibises in Birecik reproducing in nature perform the incubation in turns. Males remain in the incubation longer. According to the three years observation average (n=79), males remained in the incubation for 240.99 minutes per day. Females remained in incubation for 177.08 minutes on average (n=79). According to Cramp&Simmons[31], males participated in incubation 26% more.

Partners are rarely together in incubation. The period of remaining in incubation together is 20.52minutes on average according to the observations in three years. It has been detected that eggs have been rarely left alone in incubation. According to the observations between the years 2013-2015 (n=79), eggs were left alone for 0.0 minutes on average (Table 3).

Partners owning nests remain on eggs in turns by sharing the tasks. According to the observations in 2013, the parameter of incubation weeks and sex interaction ($F=4.538$; $P<0,001$) showed dramatic change. In fact, a meaningful change has not been seen when the parameters of incubation weeks and sex interaction ($F=1.195$; $P=0.305$) in 2014 were examined. The parameter of

the interaction of the incubation weeks and sex ($F=4.278$; $P<0.001$) showed a drastic change in 2015. The period of remaining in incubation changed in 2013 and 2015 in different weeks depending on sex. However, the period of remaining in incubation for males or females did not show any difference in 2014 in different incubation weeks. The necessity for the sustainment of the studies in different years occurs for this situation to be able to be clarified.

It is expressed that the female is dominant in the nest during the making of the eggs, she makes show mating (getting on the back of male), she protects her nest against other individuals of the colony and she rarely leaves the nest alone [25]. According to our detections; the expression that female is dominant is considered regarding the female getting on her partner's back. It has been determined that males sometimes encourage and direct their partners to get on their backs with their own wishes. This situation could be considered as the sharing of dominance. Moreover, it is also thought that this stems from the wishes of the males for establishing and sustaining relations; because it has been detected that the nest owner males do not have any female partners establish partner relations with other males. It has been observed during this period that he encourages his partner to get on his back. It has also been recorded that this male tries to get on the back of his partner afterward and show reproduction activities. For this reason, the behavior of getting on the back of partners is considered as a tool for the establishment and sustainment of relations.

Pegoraro [25] specifies that female northern bald ibis protects her nest. According to the observations conducted between 2012 and 2015; the protection of the nest is seen as an action conducted by the male rather than female [32].

The partners coming to undertake the shift remains at the side of the nest for a while before and after the shift change. This situation has been evaluated as remaining in the incubation together. The individual coming to undertake the shift to wait at the side of the nest is related to preparing his/her remaining partner to stand up. The individual remaining in the outer side of the nest after the shift change has been assessed as the wish for not leaving the nest. There is no need for remaining in the nest together; because the nest to be small is not convenient for the partners to remain together. If they remain in the nest together, the partners trying to pull the eggs to their own bottom may give harm to the eggs. Partners act very carefully and slowly during the shift change. This care they show is for the prevention of the negativities possible to occur for the eggs. The partners remaining in the nest together may cause the congeners to pay attention to the nest. Controversies with foreigners may occur in this situation.

Male spending so much time in the incubation ensures the female to wander around freely. Female does not spend time near the nest. She gains more time to be able to go to faraway places for the purpose of searching for food. Males remain in the incubation and decrease the controversies with the neighbor males; because threats and controversies generally occur among males.

It is seen that synchronized behaviors provide various benefits for individuals. Synchronized behaviors are frequently observed in the northern bald ibises showing the property of living gregariously. Synchronization contributes to the social togetherness of the northern bald ibises showing a gregarious lifestyle. Collective flights may prevent enemy attacks. Synchronized flights of lots of northern bald ibises make a dissuasive impact on the predators. Finding the food becomes easy during the search for food together. It also ensures easier finding of the nest materials. Searching for food collectively provides benefits with advantages in hunting. Starting to take food during the food time in northern bald ibis Production Station provides opportunities for the simultaneous benefit of all individuals from restricted food. Synchronized shift change may terminate the controversies possible to occur among the neighbors. The behaviors of the synchronized search for nest material provide an easier finding of nest materials. It is necessary to study how the neighbors or the groups are affected

by one another in synchronized behaviors (shift change, incubation, collective flight, and searching for food together).

Eggs remaining alone in the incubation for 1-4 minutes are considered a dangerous period. The non-incubating individuals come by themselves and remain on the alone eggs. In this way; eggs remain open for a little period and the damage of embryos is prevented. These behaviors could also be considered as the behaviors of self-devotion. It has been detected in 4-year observations that other non-incubating northern bald ibises do not give any harm to the eggs. In addition; the open eggs have been protected by other northern bald ibises. No hunter attach has been observed to the eggs and those in the incubation during the observations between the years 2012-2015. "Curious" youngsters coming to the roofs of the nests worry those in the incubation. However, the existence of other individuals that could not participate in reproduction may dissuade the predators that may come to the incubations. This may be considered as a behavior of self-devotion (altruism). Behaviors of self-devotion have been observed during the periods in which the eggs and offspring have been left alone in the nest. The northern bald ibis not having any nest protects the eggs and chicken belonging to others with self-devotion. Utilization is seen as single-sided. However; in the event of detailed assessment, it could be said that the individual showing behaviors of self-devotion will also get benefit from this situation; because, the experiences it has lived will help her/him be more successful when s/he owns his/her own eggs and offspring.

Şahin [11] has detected that incubation starts with the making of the first egg in the northern bald ibises reproducing freely in nature. The same situation is also observed in the northern bald ibises in Birecik northern bald ibis Production Station during the reproduction periods (2012-2015).

It has not been observed that the partners feed each other in the incubation [25]. Partner feeding could not be detected in incubation times or other times during the studies in Birecik.

The partner that is not in incubation takes place near the nest [25]. Sex is not specified in this detection. Females remain near the nest rarely in the northern bald ibises in Birecik reproducing freely. Males have more tasks in the protection of the nest. The nest owner female firstly tries to expel the foreigner when a foreign male comes to the nest during the times when the female is in incubation. She escapes if she cannot be successful in this fight [32]. The nest owner male comes in a few minutes and expels the foreigner. This situation is an indication of the fact that males are around their nests. However, females show such kinds of behaviors rarely.

The activities which do not provide direct benefit to the individual and which are even harmful, but which are an advantage for their congeners are defined as behaviors of self-devotion (altruism) [33]. Such kinds of behaviors also observed in different animal species are called altruism [34-35]. Northern bald irises show altruistic behavior as well.

5. Conclusion

The northern bald ibis partners cooperate and divide the labor at incubation. During the day, the male sits more in the nest than his partner. There is no difference between incubation weeks. In three different years (2013-2015), the period of sitting at the incubation is close to each other. In incubation, partners stay together for a short time. Eggs are not left alone.

Acknowledgments

We thank our instructor, M. Sadullah ÖZTÜRK, the pioneer of the northern bald ibis rescue project, a true nature lover who helped us greatly. We would like to thank Christopher G. R. Bowden (RSPB-Royal Society for the Protection of Birds) for their scientific contributions. Thanks to the northern bald ibises Brooding station workers and volunteers (General Directorate of Nature Conservation National Parks, Turkey). Thanks to the wardens who feed them. We would like to thank

the team for the individual ringing of the northern bald ibises every year and the collection of blood samples. We thank Dr. E. Çakmak for sharing his knowledge of sex identification with DNA analysis (Department of Biology, Middle East Technical University, Ankara-Turkey). This study was supported by Dicle University (DÜBAP-14-FF-73).

Conflict of interest

The authors declare no conflict of interest.

Authors' Contributions

Statistical evaluations (100%) were carried out by Ersin UYSAL.

Observations and preparation of the article (100%) were carried out by Ahmet KILIÇ.

Ethical Statements

The author declares that this document does not require an ethics committee approval or any special permission. Our study does not cause any harm to the environment.

References

[1] Böhm, C., Bowden C.G.R., Seddon, P.J., Hatipoğlu, T., Oubrou, W., El Bekkay, M., Quevedo, M.A., Fritz, J., Yeniyurt, C., Lopez, J.M., Orueta, J.F., Didone, F., Unsöld, M., "The northern bald ibis *Geronticus eremita*: history, current status and future perspectives", *Oryx*, 55(6), 1-13, 2020.

[2] Böhm, C., "The Northern bald ibis EEP – an overview."(In: Eds. Böhm, C., Bowden, C., Jordan, M.)Northern bald ibisconservation and reintroduction workshop. *IAGNBI Meeting Innsbruck 2003*), 2003, pp.33-35

[3] Böhm, C.,"Der Waldrapp – eine (un)endliche Geschichte? Aktueller Status im Freiland und in Zoos, Schutzprojekte – eine aktuelle Übersicht", *Zeitschrift des Kölner Zoos*., 62(2), 107-123, 2019.

[4] Unsöld, M., Fritz, J., "Methodik der Wiederansiedlung von sedentären und Migrierenden Waldrapp-Populationen", *Vogelwarte* 56, 402-403, 2018.

[5] Bowden, C.G.R., Aghnaj, A., Smith, K.W., Ribi, M., "The status and recent breeding performance of the critically endangered Northern Bald Ibis *Geronticus eremita* population on the Atlantic coast of Morocco", *Ibis*, 145, 419-431, 2003

[6] Bowden, C.G.R., Smith, K.W., El Bekkay, M., Oubrou, W., Aghnaj, A.,Jimenez-Armesto, M., "Contribution of research to conservation action for the Northern bald ibis *Geronticus eremita* in Morocco", *Bird Conservation International*, 18, 74-90, 2008.

[7] Sikli, L., Oubrou, O., El Bekkay, M., "Morocco wild population update" (in eds. Böhm, C., Bowden, C.G.R.:Northern Bald Ibis Conservation and TranslocationWorkshop. *Report of 4th. International Advisory Group for the Northern Bald Ibis (IAGNBI) meeting Seekirchen, Austria, August 2016,* pp 29-30

[8] Akçakaya, H.R., "Bald Ibis *Geronticus eremita* population in Turkey: an evaluation of the captive breeding project for reintroduction", *Biological Conservation*, 51, 225-237, 1990.

[9] Akçakaya, H.R., Akçakaya, R., Barış, Y.S., "Birecik'teki Kelaynak (*Geronticus eremita*) populasyonunun yok olma nedenleri ve koruma çalışmalarının değerlendirilmesi.," *Doğa-Turkish Journal of Zoology*, 16, 1–12, 1992.

[10] Arıhan, O., "Recent information on the occurrence of the Northern Bald Ibis *Geronticus eremita* in Turkey", *Turna*, 1(1), 10-15, 1998.

[11] Şahin, R., "Kelaynak Kuşlarının (*Geronticus eremita*) Davranış ve Biyolojileri" Habilitation. Dicle University, Diyarbakır, Turkey. 1980.

[12] Şahin, R., "Erfolgreiche Volierenbrut der Waldrappen in der Türkei", *Ornithologische Mitteilungen, 32*, 72-74, 1980.

[13] Kılıç, A., "Kelaynak Kuşunun (*Geronticus eremita*) Türkiye'deki Durumu" (oral presentation). In, *Biyoçeşitlilik Sempozyumu, 22-23 May Şanlıurfa, Turkey, 2015*, pp.63.

[14] Kılıç, A., "Reproduction Success in the Birecik Northern Bald Ibis (*Geronticus eremita*)", *Journal of Applied Biological Sciences*, 9 (1), 6-10, 2015.

[15] Unsöld, M.,Fritz,J.,"Die Rückkehr des Waldrapps", *Falke*, 61(7), 27–29, 2014.

[16] Chernetsov. N., Berthold, P.,Querner, U., "Migratory orientation of first-year white Storks (*Ciconia ciconia*): inherited information and social interactions", *Journal Experimental Biology*, 207, 937-943, 2004.

[17] Serra, G., Lindsell, J.A., Peske, L., Fritz, J., Bowden, C.G.R., Bruschini, C., Welch, G., Tavares, J., Wondafrash, M., "Accounting for the low survival of the Critically Endangered northern bald ibis *Geronticus eremita* on a majör migratory flyway", *Oryx*, 49(2), 312-320, 2015.

[18] Holleis, A., Böhm, C., Landmann, A., "Treu sein oder nicht?-Partnerwahl und Partner Treue beim Waldrapp *Geronticus eremita*", *Vogelwarte*, 47(4), 316-317, 2009.

[19] Şahin,R., "Zum Form der Ehe freilebender Waldrappen (*Geronticus eremita*) in Birecik (Türkei)", *Ornithologische Mitteilungen*, 34, 162-163, 1982.

[20] Şahin, R., „Beitrag zum Fortpflanzungsverhalten der freilebenden Waldrappe (*Geronticus eremita*) in der Türkei, 2.Mitteilung: Paarung", *Ökologie der Vögel,* 5, 63-72, 1983.

[21] Kılıç, A.,Uysal, E., Yüksel, F.M."Kelaynak Kuşlarında Kuluçka Paylaşımı." *2. Ulusal Zooloji Kongresi*, 28-31 Ağustos, Afyonkarahisar –Turkey, 2015, pp.3.

[22] Şahin, R., "Beitrag zum Fortpflanzungsverhalten der freilebenden Waldrappe (*Geronticus eremita*) in der Türkei. 3. Mitteilung: Eiablage, Brüten und Schlüpfen", *Ökologie der Vögel*., 5, 255-262, 1983.

[23] Şahin, R., "Eltern-Kind-Beziehungen der freilebenden Waldrappe (*Geronticus eremita*) in Birecik (Türkei)", *Ökologie der Vögel,* 4, 1-7, 1982.

[24] Çakmak, E., Akın Pekşen, Ç, Bilgin, C.C., "Comparison of three different primer sets for sexing birds", *Journal of Veterinary Diagnostic Investigation*, 29, 59-63, 2017.

[25] Pegoraro, K.,"*Der Waldrapp: vom Ibis, den man für einen Raben hielt*."AULA.Wiesbaden, Germany, 1996.

[26] Pegoraro, K., Föger, M., "Individuality in the Northern bald ibis or Waldrapp Ibis *Geronticus eremita*– key features for a complex social system", *Acrocephalus*, 22, 73-79, 2001.

[27] Böhm,C., Pegoraro, K., "*Der Waldrapp Geronticus eremita, Ein Glatzkopf in Turbulenzen*." Verlags KG Wolf, 1. Auflage. Die Neue Brehm- Bücherei Bd 659, Westrap Wissenschaften Hohenwarsleben. Leipzig, Germany, 2011.

[28] Yeniyurt, C.,"Kelaynakların (*Geronticus eremita*) Birecik'teki 2013 Yılı Üreme Başarıları." *22. Ulusal Biyoloji Kongresi, 23-27 June, Eskişehir, Turkey, 2014*, pp. 976.

[29] Özkınacı, G., Yeniyurt, C., "Kelaynakların (*Geronticus eremita*) Birecik'teki 2015 Yılı Üreme Başarıları." *XII. Ulusal Ekoloji ve Çevre Kongresi 14-17 September 2015, Muğla Turkey*, pp.375.

[30] Kılıç, A., Uysal, E**., "**Assessment of the incubation period for each sex of Turkish semi-wild Northern Bald Ibis (*Geronticus eremita*)", *Turkish Journal of Zoology*, 43, 617-627, 2019.

[31] Cramp, S., Simmons, K.E.L., *The Complete Birds of the Western Palearctic*, Oxford University Press CD-Rom, Oxford, UK. 1998.

[32] Kılıç, A., Uysal, E., Yüksel, F., "Kelaynak Kuşlarında (*Geronticus eremita*) Kuluçka Öncesi ve Yuva Kurma Davranışları", *Anadolu Doğa Bilimler Dergisi*, 6(2), 175-183, 2015.

[33] Şahin, R., Biricik, M., *Etoloji. Karşılaştırmalı Hayvan Davranışı Bilimi*. Dicle Üniversitesi Basımevi, Diyarbakır, Türkiye, 1997.

[34] Immelmann, K., *Wörterbuch der Verhaltensforschung*, Parey, Berlin, Hamburg, 1982.

[35] Immelmann, K., *Einführung in die Verhaltensforschung*, Parey.3, neubearb.u.erw.Aufl. Berlin, Hamburg, 1983.